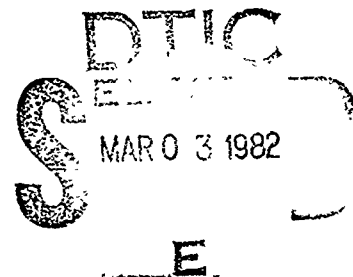AFWAL-TR-81-2099

HEAT TRANSFER IN TURBINES

J. F. Louis
Massachusetts Institute of Technology
Cambridge, Massachusetts 02139

DTIC
MAR 0 3 1982

E

October, 1981

Final Report for Period 1 January 1976 – 31 December 1980
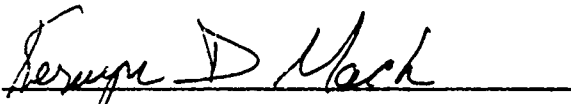
Approved for public release; distribution unlimited

AERO PROPULSION LABORATORY
AIR FORCE WRIGHT AERONAUTICAL LABORATORIES
AIR FORCE SYSTEMS COMMAND
WRIGHT-PATTERSON AIR FORCE BASE, OHIO 45433
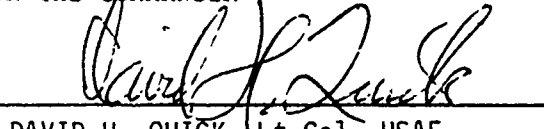
This report has been reviewed by the Office of Public Affairs (ASD/PA) and is releasable to the National Technical Information Service (NTIS). At NTIS, it will be available to the general public, including foreign nations.

This technical report has been reviewed and is approved for publication.

KERVYN D. MACH
Project Engineer

CHARLES E. BENTZ, Tech Area Manager
Hot Section Technology Group

FOR THE COMMANDER

DAVID H. QUICK, Lt Col, USAF
Deputy Director
Turbine Engine Division

SECURITY CLASSIFICATION OF THIS PAGE *(When Data Entered)*

REPORT DOCUMENTATION PAGE		READ INSTRUCTIONS BEFORE COMPLETING FORM
1 REPORT NUMBER AFWAL-TR-81-2099	2. GOVT ACCESSION NO. *AD-A111 584*	3. RECIPIENT'S CATALOG NUMBER
4. TITLE *(and Subtitle)* Heat Transfer in Turbines		5. TYPE OF REPORT & PERIOD COVERED Final Report 1 Jan 76 – 31 Dec 80
		6. PERFORMING ORG. REPORT NUMBER
7. AUTHOR*(s)* J.F. Louis		8. CONTRACT OR GRANT NUMBER*(s)* F33615-76-C-2018
9 PERFORMING ORGANIZATION NAME AND ADDRESS Massachusetts Institute of Technology Cambridge, Massachusetts 02139		10. PROGRAM ELEMENT, PROJECT, TASK AREA & WORK UNIT NUMBERS 62203F 30660615
11. CONTROLLING OFFICE NAME AND ADDRESS Aero Propulsion Laboratory (AFWAL/POTC) AF Wright Aeronautical Laboratories Wright-Patterson Air Force Base, OH 45433		12. REPORT DATE October 1981
		13. NUMBER OF PAGES 116
14 MONITORING AGENCY NAME & ADDRESS*(if different from Controlling Office)*		15. SECURITY CLASS. *(of this report)* Unclassified
		15a. DECLASSIFICATION/DOWNGRADING SCHEDULE N/A

16 DISTRIBUTION STATEMENT *(of this Report)*

Approved for Public Release; Distribution Unlimited

17. DISTRIBUTION STATEMENT *(of the abstract entered in Block 20, if different from Report)*

18 SUPPLEMENTARY NOTES

19 KEY WORDS *(Continue on reverse side if necessary and identify by block number)*

Heat Transfer, Film Cooling, Boundary Layer Theory

20. ABSTRACT *(Continue on reverse side if necessary and identify by block number)*

This report summarizes the studies in heat transfer and film cooling effectiveness performed under Contract F33615-76-C-2018. The purpose of these experimental and theoretical studies is to develop an indepth understanding of heat transfer and film cooling in gas turbines. A common experimental procedure is described for heat transfer measurements under isothermal wall conditions using fast response heat transfer gauges in tests conducted in a shock tunnel and a blowdown facility. The tests were conducted at flow and thermodynamic conditions modeling the operating conditions of advanced gas turbines. The configuration

DD FORM 1473
1 JAN 73

SECURITY CLASSIFICATION OF THIS PAGE *(When Data Entered)*

under study were single slot, single line of holes, double row of holes on a
flat and curved plates, and double lines on an airfoil located in a cascade.
The experimental technique was validated by long duration high temperature tests
of an air cooled flat plate. Also described is an analytical study of the
thermal and fluid mechanical evolution of a cooling film injected from a single
line of inclined holes.

Foreword

This report summarizes the work carried out at the MIT Gas Turbine Laboratory from October 1975 to July 1979.

The work was administered under the direction of the Air Force Aero Propulsion Laboratory, Air Force Systems Command, United States Air Force. The principal investigator is Professor Jean F. Louis. The Gas Turbine personnel who have participated in the research effort include:

Jean F. Louis	Professor of Aeronautics and Astronautics
A.E. Sotak	Research Support Staff, Energy Laboratory
A. Berenfeld	Graduate Research Assistant, Aeronautics and Astronautics
P.H. Ramette	Graduate Research Assistant, Aeronautics and Astronautics
M. Ortiz	Graduate Research Assistant, Aeronautics and Astronautics
A. Gominho	Graduate Research Assistant, Mechanical Engineering

iii

TABLE OF CONTENTS

Table of Contents (Cont'd)   PAGE

LIST OF FIGURES

SECTION 1

INTRODUCTION

High performance gas turbines require high turbine inlet temperatures while the skin of exposed components has to be maintained at a lower temperature for long life expectancy.

This lower skin temperature can be obtained by a combined use of internal convection cooling and of an external thermal barrier in the form of a film of cool air, covering the skin of exposed components. The design of such turbines requires detailed information on the heat transfer distribution and aerodynamics of highly-loaded stages, and on the effectiveness of the film thermal barrier. This film can be obtained by blowing air through a porous surface, a slot, or an array of holes. The first technique, transpiration cooling, requires relatively small cooling flows. The momentum of the blown air is negligible compared to the main stream momentum, and the boundary layer theory can be applied to determine the thermal effectiveness of the film. However, the technological implementation of transpiration cooling has met severe difficulties, and the second technique of film cooling has found many applications in advanced gas turbines. Since the air is injected through a limited number of orifices, often at an angle to the wall, momentum of the injected flow is not negligible compared to the main flow, and the boundary layer theory cannot be applied to this case. New analytical and experimental information is therefore needed to determine the effectiveness of the film thermal barrier obtained by a wide variety of injection configurations.

The critical information needed for film cooling deals with coolant penetration into the main flow and with the generation of streamwise vorticity in the vicinity of the injection point. Further downstream, information is needed to understand the coupled turbulent and vortical mixing of the coolant with the mainstream.

Engine performance optimization depends critically on the selection of an effective cooling configuration and a detailed understanding of heat transfer to turbine components. A systematic study of relevant heat transfer and film cooling effectiveness is described in this report, which covers: (1) analytical and experimental studies of a wide variety of film cooling configurations, (2) experimental and analytical predictions of heat transfer over highly-loaded profiles, and (3) film cooling effectiveness over a subsonic profile. Short duration studies using a shock tunnel and hot blow-down facilities[1] provide a practical and flexible means to acquire the necessary experimental information while providing good modeling of the flow and temperature fields. These short duration studies are validated by long duration high temperature tests of an air cooled flat plate.

SECTION 2

2. Experimental Approach

2.1 Adiabatic and Isothermal Wall Heat Transfer

Heat transfer measurements are conventionally referred to as adiabatic conditions. The determination of heat transfer rate requires the knowledge of film coefficient and of an adiabatic wall temperature (T_{ad}). The heat transfer coefficient is determined for the case of no injection and a well-developed boundary layer. An adiabatic wall effectiveness is defined as

$$n_{ad} = \frac{T_{ad} - T_\infty}{T_c - T_\infty}$$

where T_∞ and T_c are the main stream and coolant temperatures. This adiabatic approach is correct when the ratio of the main stream to film temperatures is close to unity. In advanced gas turbines, heat diffusion brings metal temperatures closer to an isothermal temperature distribution rather than an adiabatic one. In the presence of angular injection and high main flow to coolant temperature ratios, and in close vicinity to the injection point where large gradients of flow properties exist, the validity of using adiabatic wall information to determine heat loads to the cooled surfaces is in doubt, thus requiring the investigation of heat transfer phenomena by directly measuring heat transfer under correctly modeled turbine conditions. This need provides the justification to refer the data to isothermal conditions. Under these conditions, the heat transfer rate is

$$Q/A = h(T_w - T_\infty)$$

where T_w is the temperature of the isothermal wall and the isothermal effectiveness is defined

3

$$n_{iso} = 1 - Q_c/Q_o$$

where Q_c is the heat transfer with cooling and Q_o is the heat transfer at the same condition without cooling. The isothermal effectiveness represents the capacity of the thermal barrier provided by the film to reduce the heat transfer.

Adiabatic and isothermal effectivenesses are related by

$$n_{iso} = 1 - h_c/h_o \ (1 + n_{ad} \frac{T_c - T_\infty}{T_\infty - T_w})$$

when h_c and h_o are the film coefficients with and without cooling.

2.2 Experimental Techniques

Unsteady heat transfer measurements under steady flow conditions provide the advantages of relatively simple heat transfer measurements of short duration, and of flexibility in modeling actual gas turbine operating conditions. To model gas turbines, one needs a high enthalpy flow for the mainstream and a low enthalpy flow for the coolant. By scaling the temperatures of these flows and the skin temperature from the actual turbine conditions and matching Reynolds, Mach and Prandtl numbers, a fairly representative model can be obtained for the heat transfer and cooling problems.

The experimental technique used is to establish the high and low temperature flows concurrently in a stepwise fashion for a duration short enough to render wall temperature changes minimal so that heat fluxes can be measured on a quasi-isothermal surface.

The short duration necessitates the use of fast response instrumentation such as thin-film gauges, calorimetric gauges, and Kistler pressure transducers.

4

2.3 Experimental Facilities

A shock tunnel and a blow-down facility[1] are used for these tests. The shock tunnel is used to obtain basic data on film cooling effectiveness over flat and curved plates. The blow-down facility can be used either in conjunction with a cascade or with a rotating turbine rig to determine distribution of heat transfer rates and film cooling effectiveness over blade profiles, end walls, and turbine shrouds.

2.3.1 The shock tunnel[1] (Figure 1) is attached to a 3" shock tube through an accelerating nozzle. At the downstream end of the plexiglass, constant area (2 in. x 7/8 in.) tunnel, a choked nozzle controls the Mach number. The steady flow test time is approximately 10 ms, whereas the time to establish flow is 1 ms. For those short durations, tests of the order of 10 ms, the plexiglass walls have large enough thermal inertia to limit their temperature rise to less than $7^{\circ}F$, thus not offsetting the isothermal wall boundary. Various configurations of coolant holes (or slots) on the tunnel walls are connected to a coolant flow supply plenum. The location of the holes (or slots) provides a local flow Reynolds of 3×10^5. The coolant flow is prepurified nitrogen, which is cooled by passing it through a copper coil immersed in a bath of liquid nitrogen. The introduction of the coolant is synchronized with the rupture of the shock tube diaphragm. Arrays of thin-film gauges are located downstream of the injection point to determine the heat transfer rate as a function of distance.

2.3.2 <u>The Hot Blow-down Facility</u>[1] (Figure 2) consists of air supply
system storing 400 lbs of air at 2400 psi, dome-loading type pressure reg-
ulators, a 6 ft long and 1.5 ft diameter pebble bed heater filled with 3500
lbs of stainless steel balls and a filter trap. The facility has two
branches, each consisting of a diaphragm section, a metering throat, a
pressure reducing section utilizing a supersonic nozzle and diffuser, and a
transitional piece leading in one branch to the turbine rig and in the
other branch to the cascade. The tests are typically less than 1 s,
whereas steady flow is established after 0.15s - 0.25s. The heat transfer
rate is measured by calorimetric gauges, a thin aluminum or copper disc
(0.5 mm thick) embedded in a teflon cap with a thermocouple joined to its
back.

2.4 Similarity Laws

The flow modeling used in the above facilities can easily be deter-
mined. The short operating time makes it reasonable, first, to assume an
isothermal wall model, and, second, to scale down the operational tempera-
ture of the metal surface, T_{op}, to room temperature, T_R, by the temperature
scaling factor, $S = T_{op}/T_R$.

Matching up experimental Reynolds and Mach numbers to those of the
actual engine conditions, one obtains

$$\frac{\rho_R V_R L_R}{\mu_R} = \frac{\rho_{op} V_{op} L_{op}}{\mu_{op}}$$

where L is the scale length, and

$$V_R/(\gamma_R R_R T_R)^{1/2} = V_{op}/(\gamma_{op} R_{op} T_{op})^{1/2}$$

if the Prandtl numbers of the two conditions are the same.

Assuming

$$\frac{\mu_{op}}{\mu_R} \frac{\gamma_R}{\gamma_{op}} \cdot \frac{R_{op}}{R_R}^{1/2} = \frac{T_{op}}{T_R}^{\eta}$$

where η is a number like 0.5 to 0.7, one obtains

$$\frac{P_{op}}{P_R} \cdot \frac{L_{op}}{L_R} = \frac{T_{op}}{T_R}^{\eta + 1/2} = (S)^{\eta + 1/2}$$

The scaling implies that if room temperature is used to model turbine components temperatures which are as high as $1650^{\circ}F$, the temperature scaling factor would be 4. If the length scale is kept the same and $\eta = 0.64$, the pressure would be reduced by the ratio, $p_{op}/p_r = S^{1.14} = 4.86$. For the tests with film cooling, the temperature of the coolant is reduced by the ratio $S = 4$.

3. Film Cooling Effectiveness

As mentioned before, engine designs geared to long life do not presently use transpiration cooling, seldom use injection parallel to the mainstream and, in most cases, use injection at an angle to the mainstream. As a reference, however, the state of understanding of parallel injection will be reviewed briefly.

3.1 Parallel Injection

When the film is injected parallel to the main flow, turbulent mixing dominates the interaction between the two streams. Downstream, the mixed layer is dominated by the wall shear stress, therefore, by suitable balance of both energy and mass for the mixed streams, Stollery and El Ehwany[2], and Leontev and Kutateladze[3] have derived the following relation:

$$\frac{T_{ad} - T_{\infty}}{T_{\infty} - T_{c}} = A\left(\frac{ms}{x}\right)^{0.8} \quad R_{ec} \frac{\mu_{c}}{\mu_{o}}^{0.2}$$

applicable for $x \gg s$, where s is the slot height, with $A = 3.03$ in reference 2, and $A = 3.1$ in reference 3, where R_{ec} is the Reynolds number based on coolant conditions.

This theoretical relationship compares favorably with the test results[4][5][6] for data obtained far downstream, but the scatter becomes appreciable in the region closer to the injection point. In the vicinity of the injection point, the mixing is dominated by the local vorticity field which is not included in the above theoretical formulation.

3.2 Film Cooling with Angular Injection

When a film is injected at an angle to the mainstream from a well to provide a thermal barrier over a section of wall, it undergoes two determining processes: a viscous interaction and a pressure interaction. The viscous interaction results in the turbulent mixing of the two streams. The pressure interaction exists since the momentum of the injected flow normal to the wall is commensurable with the main stream momentum. The pressure gradient normal to the wall near the injection point is significant and boundary layer theories are no longer applicable.

The pressure interaction determines the penetration of the coolant into the boundary layer and in the mainstream, and also the formation of streamwise vorticity. The viscous interaction determines the rate of entrainment of the mainstream fluid by the coolant and the rate of mixing of the two streams.

Further, the pressure interaction for injection parameters commonly used leads to a separation of the coolant and boundary layer at the injection point and leads to the formation of a separation bubble just downstream of the injection point. The evidence for the existence of the boundary layer separation at the injection point and the formation of a separation bubble are several:

3.2.1 This separation is theoretically expected when the criterion determined by Kutateladze and Leontev[7] is applied to the conditions of film cooling with angular injection. This criterion indicates that separation will occur when the normal mass injection parameter

$$m_y = \frac{(\rho_c U_c)y}{\rho_\infty U_\infty} \geq 2\ C_{fo}$$

where C_{f_0} is the skin friction coefficient in the absence of coolant, and y refers to the direction normal to the wall. For a flow Reynolds number at the injection point of $R_e = 3 \times 10^5$, $C_{f_0} = 2.5 \times 10^{-3}$, and this criterion would indicate that separation is likely to occur when $m_y \gg 5 \times 10^{-3}$, i.e., for a typical angle of injection of $30°$, separation would occur for a value of the total mass injection parameter.

$$m = \frac{\rho_c U_c}{\rho_\infty \rho_\infty} \geq 0.1$$

Practical values of the injection parameter are generally appreciably larger than $m = 0.1$.

3.2.2 The existence of a separation bubble downstream of $30°$ slot was demonstrated by dye and hydrogen bubble visualization techniques in a water tunnel[8]. The study indicated that the length of the separation bubble was proportional to the momentum ratio

$$K_o^2 = \frac{\rho_c U_c^2}{\rho_\infty U_\infty^2}$$

The flow visualization also indicated the appearance of streamwise vortices having consecutive opposite directions of rotation. This vorticity results from the coupling between the injected flow and its streamwise velocity. The vortical motion has the effect of enhancing the mixing of the coolant with the mainstream as evidenced by the presence of fluid elements in the separation bubble. The study also indicated that the vortices persisted far downstream.

3.2.3 Measurements of heat transfer coefficient (Figure 3) downstream of a 30° injection slot on a curved wall indicated that the heat transfer coefficient goes through a maximum close to the injection for a given value of the injection parameter. This maximum can be explained by the existence of the separation bubble in which hot gas is being entrained.

3.2.4 Measurements of heat transfer rate at the trailing edge of a plate indicate[9] that the isothermal effectiveness measured at the trailing edge can be severely reduced (Figure 4) by locating the coolant injection slot at a distance shorter than the reattachment point of the separation bubble (Figure 5). The separation bubble is observed in the range of mass injection up to values of m, for which complete separation of the boundary layer occurs.

In the case of injection through inclined holes, the separation downstream of the injection point is mitigated by the formation of counter rotation vortices which persist far downstream and contribute to the downstream mixing of the two streams.

As it will be described below, streamwise vorticity is also generated when slot injection is used.

3.3 Film-Cooling Effectiveness with Angular Injection

A comprehensive experimental program[10][11][12] has been undertaken to investigate different film cooling configurations of slots, single and double line holes for different streamwise and crosswise angular injection.

Figure 6a is a representative layout of the flat plate used in the shock tunnel for the evaluation of film-cooling effectiveness. The injection scheme uses a double line of holes which make an angle α_1, with the

11

streamwise direction and α_2 with the crosswise direction. Thin-film heat transfer gauges are located at different distances corresponding to different values of the ratio of the streamwise distance (x) to the hole diameter. These gauges provide an average local heat transfer rate, whereas the gauges located at $x/D = 27$ are used to measure the crosswise variation of effectiveness. Most of the tests were conducted at a stagnation temperatue of $1000^\circ R$ and 10 psia stagnation pressure, which simulated the inlet conditions $4000^\circ R$ and 175 psia of an advanced gas turbine. The Mach number was typically $M = 0.5$ and the coolant temperatures were $220^\circ R$, $310^\circ R$, $400^\circ R$ and $500^\circ R$. The mass injection parameter was varied between 0.1 to 1.6. The streamwise angles used were 10°, 20° and 30° and the crosswise angles used were 0°, 30°, 50°, 70°, and 90°.

The influence of the different configuration parameters can be assessed.

3.3.1 Effect of the Crosswise Angle for Holes

The cross-stream injection angle does not effect the film cooling effectiveness over a flat plate to any great degree. Its influence is limited to the area just downstream of the injection point as indicated by the film effectiveness footprints[11], e.g., (Figure 6b), measured for $\alpha_2 = 30^\circ$ and for different values of the mass injection parameter. In the region close to the hole, the coverage increases with the crosswise width of the hole.

3.3.2 Influence of the Distribution of Holes

Data of film effectiveness were correlated by using the concept of equivalent slot width, which is the width of a slot which would pass the same amount injection mass flow as the single or double line of holes.

12

Figure 7 gives the general correlation found for single and double lines of holes with α_2 varying from $0°$ to $90°$ using the concept of equivalent slot width in the parameter

$$A_o^* = K_o^{-1.35} R_{es}^{-.25} x/s_{eq}$$

where K_o is the square root of the momentum ratio and R_{es} is the Reynolds number based on the injection conditions.

3.3.3 Slot versus Hole Injection

As seen in Figure 8, the film cooling effectiveness of hole injection is sharply lower than injection through a slot, corrected for equivalent coolant mass flow introduced to form the film. By observing that the mixing area for a circular jet is π times larger per unit length of slot, the correlation parameter A_o^* was corrected by this amount for data related to holes. In other words $\pi^x = 1.0$ for a slot and $\pi^x = \pi$ for hole injection. With this change in the correlation parameter, the hole data aligned with the slot data quite well (Figure 9). The best overall agreement is, however, obtained when the factor π^x is raised to the power 1.41.

3.3.4 Overall Correlation

With the incorporation of this parameter and the temperature ratio $\theta = T_c/T_\infty$, the best correlation[12] is obtained for both holes and slots, with the group $m^{-1.35} \cdot \theta^{-0.68}$, which reduces to $K_o^{-1.35}$.

The best overall correlation of slot and holes data obtained for $\alpha_1 = 20°$ (Figure 10) is, therefore, obtained against the group

$$A_2 = \pi^{*1.41} K_o^{-1.35} x/s_{eq}$$

13

Previous film cooling data for values of $\alpha_1 = 10, 20, 30^{\circ}$ have indicated a dependence of the effectiveness on the parameter $(K_o \cos^2 \alpha_1)^{-1.35}$. However, more data (over a wider angular range) are needed to validate this correlation fully.

3.3.5. Tests and Correlations for Slot-Injection over Curved Surfaces

The test channels utilized in this investigation were made of plexiglass, and have curbed test surfaces scaled to the following dimensions: Test Channel: A 3" convex radius, 3 7/8" concave radius. Test Channel B: 7 "convex radius, 7 7/8" concave radius. Both channels have a uniform 2" x 7/8" rectangular cross-section and are equipped at the downstream end with a choking nozzle. The nozzle has a 1 1/2" x 7/8" rectangular throat, which produces a Mach number of 0.5 under choked flow conditions. A schematic of the test channel is shown in Figure 11. The injection slots which pass the coolant from the plenum chamber to the channel are 2" long and 0.03" wide. The angle of injection is 20° relative to the surface. The injection slots are located at bend angles of 30° in Channel A, and 17° in Channel B from the channel entrance. These locations assure that the injection is made in region of nea constant static pressure when referred to Figure 12.

Downstream of the injection slot, each curved plate is instrumented with 14 thin film gauges: 8 along the centerline to measure the isothermal effectiveness, and 6 across the plate at a downstream locations $x/s = 34$. To verify the flow uniformity a map of the distribution of the gauges is shown in Figure 13. Each channel has in addition a Kistler piezoelectric transducer located in the middle of the side wall. Figure 14 gives the isothermal effectiveness profile on the 3" suction surface for different

14

blowing factors which shows the actual increase of effectiveness with
increasing m and the usual decrease with x. Figure 15 summarizes all the
results as a function of the parameter $\bar{\bar{x}} = \dfrac{x}{SK_o^2}$.

These results show clearly that a smaller radius results in a decrease
of effectiveness on the concave side and an increase on the convex surface.
The values of the effectiveness on the convex surface exceed that on the
concave surface.

These results are quite expected since turbulent mixing spreads across
the entire boundary layer on the concave side.[13] Further, the concave
side promotes the formation of the longitudinal vortices[13,14] which
increase the mixing process.

On the convex surface, the thinner boundary layer works to suppress
radial mixing. The shear stress appears to decrease rapidly from the near
wall region to the edge of the boundary layer. As a result, the turbulent
heat flux tends to be low and cooling effectiveness high. When the effec-
tiveness data are plotted against the correlating parameter A_2 used for
flat plate data, the data cluster well but they show scatter particularly
for the data obtained in the channel with a short radius of curvature.

A new correlation is proposed for curved walls. It includes the
effect of curvature and it has the general form

$$Y_A = K_o^{-2} \left[\cos^2\alpha \pm \lambda \frac{Ds}{R} \sin^2\alpha\right] \frac{x}{S}$$

Where R is the radius of curvature of the wall, λ is an empirical non-
dimensional constant, D_s is the equivalent slot diameter 4A/P; the positive
sign applies to suction (convex) surface data and the negative sign to
pressure (concave) surface data. Figure 16 shows the data plotted against

15

Y_A for $\lambda = 92$. The data cluster well but a small divergence exists for the data obtained on the concave wall of the channel with a small radius of curvature.

3.3.6 Steady State Experiments on a Flat Plate. A Validation of the Short Duration Technique

The correlations developed above have been obtained in short duration tests taking great care to obtain steady state conditions and to use proper scaling. In the scaling, the data are obtained on a wall operating at near ambient temperatures whereas the blade surface will be around $2000^{\circ}R$ in an actual turbine. The correlations are quite reasonable but their validity had not been tested at the conditions of an actual gas turbine.

The validations tests were conducted in a steady state experiment using a flat plate cooled by a double row of holes injecting air at an angle of 20° to the combustion gas stream. Test conditions were varied to provide gas temperatures from about $2200^{\circ}R$ to $3150^{\circ}R$. This corresponds to gas-to-wall temperature ratios of 3.6 to 5.2. An air preheater was used to heat the coolant air up to $800^{\circ}R$. This corresponds to coolant to gas ratios of 0.28 to 0.36 with blowing ratios of 0.1 to 2.1. Mach numbers over the plate were kept between 0.32 to 0.44. The heat source was a combustor burning JP4 with oxygen diluted with nitrogen to provide desired gas temperature. The combustor and the facility are normally used for MHD tests. The test flat plate formed one of the four walls of a constant area channel. The flat plate was 5" wide and 18" long. Upstream of the flat plate is an injection block with the two rows of holes having a diameter of 0.191". The pitch between holes of the same row is equal to two diameters. Four heat transfer gauges made of three thermocouples located at different

depths are located along the longitudinal axis of symmetry of the flat plate. The gauges are located at distances of 3.28", 5.53", 8.53" and 11.53" downstream of the second line of holes, corresponding to $y/p = 17.2$, 28.9, 44.7 and 60.4. Figure 17 gives a schematic of the film cooling test. It indicates the location of pressure sensors and thermocouples. Figure 18 gives the variation of isothermal effectiveness as a function of the blowing ratio at the different axial locations. Figure 19 gives the variation of measured isothermal effectiveness with the correlation parameter A_2. The data appear to be as well correlated as they were for shock tunnel data. Further, the comparison (Figure 20) of all shock tunnel data with the hot long duration data indicates that the hot data fall within the correlation hand of all shock tunnel data. This good agreement validates the simpler, lower cost shock tunnel and other short duration low temperature techniques.

4. <u>Analytical Study of the Thermal and Fluid Mechanical Evolution of a</u>

   <u>Cooling Film Injected from a Single Line of Inclined Round Holes</u>

4.1 Introduction

The use of a film of cooling air is a promising method of reducing the heat load and metal temperature of hot gas turbine components exposed to very high temperature combustion gases.

The rate of mixing of coolant with the hot main stream determines the effectiveness of the film as a thermal barrier. The film of coolant air can be obtained by blowing air through a porous surface, a slot, or an array of holes.

Transpiration cooling uses relatively small cooling flows. The momentum of blown air is negligible compared to the momentum of the main flow and boundary layer theory can be used to determine the thermal effectiveness of the film. However, the technological implementation of transpiration cooling has met severe difficulties and in practice the film is obtained by injection slots and more often through arrays of holes.

In a few instances, the film can be injected through slots parallel to the surface. In these cases, the mixed layer is dominated by wall shear stress and the evolution of the film can be described analytically [15] [16].

This analysis considers a more general type of film injection using a line of round holes inclined at a certain angle to the surface. (The projection of the hole axis on the surface is oriented in the streamwise direction). In this case, boundary layer theories cannot be applied, since the momentum normal to the wall is not negligible compared to tne main stream momentum. Further, the jets separate from the wall at the point of

injection and a pair of contra-rotating vortices is created within each jet by the velocity field interaction. The strength of the vortices can be determined from this interaction. The achievement of good film cooling effectiveness requires the reattachment of the individual jets to the wall at a distance which is short compared to the length of surface which has to be effectively cooled. The latter consideration puts a limit on the normal momentum of the jets. The decay of these contrarotating vortices is found to be negligible over the length of wall to be effectively cooled. Since the holes are fairly closely spaced, there is a mutual interaction between vortices issued from neighboring holes. The mixing of the two streams is due to both turbulent diffusion and vortical entrainment.

Experimental work has shown the importance of the separated region downstream of the separation point and of the contrarotating vortices in the mixing process[17]. A semi-empirical analysis of mixing by turbulent diffusion and vortical entrainment was developed for the case of inclined slot injection[18]. The concept of turbulent and vortical mixing for films injected from a line of inclined round holes was first used in an analysis[19] which determined the trajectory of a single jet and limited the effect of vortical entrainment to a short distance (15 hole diameters) compared to length of effectively cooled surface.

The present analysis[20] applies this mixing process and vortex inter-action to the initial trajectory of the jets up to the formation of a continuous layer and to the growth of the mixed layer.

The analysis is divided into two parts. The first describes the trajectory and mixing of the jets and their reattachment, whereas the second determines the growth of the mixed layer and the change of crosswise average film cooling effectiveness with distance from the injection point.

19

A comparison of the present theory is made with available data of film effectiveness measured for films injected from a single line of inclined holes.

4.2 Analysis of the Jet Trajectory and Mixing

Jets issue from a row of round holes (spacing s and diameter D_0) with an average velocity u_{j0} and a density ρ_{j0} at an angle β_0 (Fig. 21) and penetrate into a main-flow of velocity u_∞ and density ρ outside the boundary layer. The flow field is steady.

The boundary layer of the main flow is assumed to be turbulent with a thickness δ:

$$u = (\frac{z}{\delta})^{1/7} u_\infty \quad \text{if} \quad z < \delta$$

$$u = u_\infty \qquad\quad \text{if} \quad z \geq \delta \tag{1}$$

Contrarotative vortices appear inside the jets and are the characteristic feature of the flow field. A qualitative description of these vortices was given in Reference 21 and the first quantitative description of them is in Reference 22.

4.2.1. Equations of Motion

The equations are written in curvilinear coordinates (Fig. 24). Each cross section of the jet has an area A_j, an average velocity u_j, an average density ρ_j and an average temperature T_j; β is the angle of the jet with the horizontal (Fig. 22); E is the entrainment of the main flow per unit length of the jet. u_T and u_N are the tangential and normal component of the velocity of the main-flow relative to the jet in the vicinity of the

jet (main-flow velocity induced by the vortices), R is the local radius of curvature of the jet, c_D is the drag coefficient of the jet, and D is the large diameter of the jet.

The equations of motion are:[17]

Equation of Continuity $\qquad \dfrac{d}{d\Delta} (\rho_j U_j A_j) = E$ $\qquad\qquad$ (2)

Momentum Equation $\qquad \dfrac{d}{d\Delta} (\rho_j U_j A_j^2) = EU_T$ $\qquad\qquad$ (3)

Force Equation (normal to the jet)

$$\rho A_j \frac{U_j^2}{R} = EU_N + \frac{1}{2} \rho C_D U_N^2 D \qquad\qquad (4)$$

(The centrifugal force balances the normal components of the drag acting on the jet and of the variation of momentum due to the entrainment.)

The force equation can also be written:

$$-\rho_j A_j U_j^2 \frac{d\beta}{d\Delta} = EU_N + \frac{1}{2} \rho C_D U_N^2 D \qquad\qquad (5)$$

A dilution parameter in the jet, μ_j, is defined as the ratio of main flow which has been entrained inside the jet to the initial mass flow of the jet. Therefore:

$$\frac{d\mu_j}{d\Delta} = \frac{E}{\rho_{jo} U_{jo} A_{jo}} \qquad\qquad (6)$$

The average temperature in the jet is given by the equation of energy:

$$T_j = \frac{T_{jo} + \mu_s T}{1 + \mu_j} \qquad\qquad (7)$$

If the flow is assumed incompressible,

21

$$\frac{1}{p_j} = \frac{1/p_{jo} + \mu_j/p}{1 + \mu_j}$$

and

$$p_j = \frac{(1 + \mu_j)\, pp_{jo}}{\rho + \mu_j p_{jo}} \tag{8}$$

Equations (2), (3), (5), (6) and (8) are solved in a step-by-step calculation.

4.2.2 Entrainment

The entrainment of the main-flow is due partly to the contrarotative vortices generated inside the jets and partly to turbulent diffusion.

According to Ref. 19 the entrainment due to the vortices is equivalent to a sink singularity concentrated just behind the jet.

The complex potential of a flow due to a sink of strength E located at $z = a$ and with a velocity u_N at infinity is:

$$f_i(z) = U_N z - \frac{E}{2\pi\rho} L \tag{9}$$

with

$$z = x + iy$$

If the cross section of the jet remains almost circular, the flow has to be such that the circle $|z| = a$ is a streamline (Fig. 23). Hence the complex potential of the flow in presence of a circular cylinder of radius a is (Ref. 24, p. 422: Image effect of the sink relative to the circle):

$$f(z) = U\left(z + \frac{a^2}{z}\right) - \frac{E}{2\pi\rho} \log\left[\frac{(z-a)^2}{z}\right] + \text{const.} \tag{10}$$

The force acting on a unit length of the jet is given by Blasius formula[5]:

$$\frac{dF'}{ds} = \frac{i\rho}{2} \oint \left(\frac{df}{dz}\right)^2 dz = EU_N \qquad (11)$$

This force can also be expressed in terms of a drag coefficient c_D:

$$\frac{dF}{ds} = \frac{\rho U_N^{\,2}}{2} \, C_D D \qquad (12)$$

From Eqs. (11) and (12):

$$E = \frac{CD}{2} \, U_N D$$

$$E = \rho E_1 U_N D \qquad \text{with} \quad E_1 = \frac{CD}{2} \qquad (13)$$

This relation between the coefficient of entrainment E_1 and the drag

coefficient c_D is assumed to be valid even when the cross section of the

jet does not remain circular. In fact the cross section of the jet is .

changed from the circle to a characteristic kidney shape[21]: the sides of

the jet are shifted downwards faster than the core of the jet because of a

larger mixing with the main flow (Fig. 24). In the calculation it is

assumed that the cross section has an elliptic shape. The drag coefficient

of an elliptic cylinder is about 1.8[23]. Hence $E_1 = c_D/2 \simeq 0.9$.

The entrainment due to turbulent diffusion is proportional to the

difference of tangential velocities and to the circumference of the jet C:

$$E = \rho E_2 |u_T - u_j| C \qquad (14)$$

According to Ref. 25, $E_2 = 0.08$. Similar measurements[26] lead to

$E_2 = 0.116$. It is assumed that $E_2 = 0.08$.

Therefore the entrainment of the main-flow is

$$E = \rho E_1 u_N D + \rho E_2 |u_T - u_j| C \qquad (15)$$

with $E_1 = 0.9$ and $E_2 = 0.08$

4.2.3 First Section of the Jets

When the jets exhaust from the holes, the lower surface of the jets is touching the wall (Fig. 25). In this section the main velocity is assumed to be unchanged, therefore:

$$u_T = u \cos \beta$$

$$u_N = u \sin \beta \tag{16}$$

In fact, there is a contraction of the main flow due to the jets, and the main velocity is increased slightly. This contraction was neglected in the calculation. In section 1 the jet is turned from β_0 to β_1 and is squeezed between the main flow and the wall so that the shape of the cross section becomes elliptical. The calculation of the shape of the cross section is carried out[20].

4.2.4 Creation and Strength of the Contrarotative Vortices

In Section 4.2.2 of the jet (Fig. 25), the jet is unattached. The component of the main-flow velocity normal to the jet in cross section AB of Fig. 25 is $u_N = u \sin \beta_1$. Two contrarotative vortices appear inside the jet to balance this normal velocity so that the boundary of the jet is a streamline (Fig. 26). B and D are the small and large diameter of the elliptical cross section of the jet. The stream function in the first free jet cross section is such that

$$V = \frac{\partial \Psi}{\partial z} , \quad W = - \frac{\partial \Psi}{\partial y} \quad \text{and} \quad U_o = - \frac{\partial \Psi}{\partial r}$$

Therefore

$$\Psi = U \, y = \frac{r}{2\pi} \, \text{Log} \, \frac{r_1 r_3 r_5 \dots r_{2n-1}}{r_2 r_4 r_6 \dots r_{2n}} \tag{17}$$

24

where it is assumed that the velocity induced by a curved vortex line is the same as the one induced by an infinite rectilinear vortex line tangent to the curved vortex line (i.e. the flow starts rotating inside the holes). By symmetry, $\Psi_A = 0$

The boundary of the jet is a streamline, thus $\Psi_C = 0$:

$$U\frac{D}{2} + \frac{\Gamma}{2\pi} \text{Log} \left[\frac{D/2-Y_T}{D/2+Y_T} \times \frac{s-D/2+Y_T}{S-D/2-Y_T} \times \frac{S+D/2-Y_T}{S+d/2+Y_T} \times \ldots\right.$$

$$\left.\ldots \frac{ns-D/2+Y_T}{ns-D/2-Y_T} \times \frac{ns+D/2-Y_T}{ns+D/2+Y_T}\right] = 0 \qquad (18)$$

Point A at the top of the jet is a stagnation point, which implies $v_A = 0$:

$$U_N - \frac{\Gamma}{\pi}\left[\frac{Y_T}{Y_T^2+\frac{B^2}{4}} - \frac{s-Y_T}{(s-Y_T)^2+\frac{B^2}{4}} + \frac{S+Y_T}{(s+Y_T)^2+\frac{B^2}{4}} \ldots\right.$$

$$\left.- \frac{ns-Y_T}{(ns-Y_T)^2+\frac{B^2}{4}} + \frac{nS+Y_T}{(ns+Y_T)^2+\frac{B^2}{4}}\right] = 0 \qquad (19)$$

Eliminating Γ between (18) and (19):

$$\text{Log}\left[\frac{D/2+Y_T}{D/2-Y_T} \frac{s^2-(D/2+Y_T)^2}{s^2-(D/2-Y_T)^2} \cdots \frac{(ns)^2-(D/2+Y_T)^2}{(ns)^2-(D/2-Y_T)^2}\right]$$

$$= D\left[\frac{Y_T}{Y_T^2+\frac{B^2}{4}} - \frac{s-Y_T}{(s-Y_T)^2+\frac{B^2}{4}} + \frac{S+Y_T}{(s+Y_T)^2+\frac{B^2}{4}} \cdots\right.$$

$$\left.- \frac{ns-Y_T}{(ns-Y_T)^2+\frac{B^2}{4}} + \frac{ns+Y_T}{(ns+Y_T)^2+\frac{B^2}{4}}\right] \qquad (20)$$

Eq. (20) is solved to obtain Y_T.

25

From Eq. (19):

$$\Gamma = \pi U_N / [\frac{Y_T}{Y_T^2 + \frac{B^2}{4}} - \frac{s - Y_T}{(s-Y_T)^2 + \frac{B^2}{4}} + \frac{S + Y_T}{(s+Y_T)^2 + \frac{B^2}{4}} \cdots$$

$$- \frac{ns - Y_T}{(ns-Y_T)^2 + \frac{B^2}{4}} + \frac{ns + Y_T}{(ns+Y_T)^2 + \frac{B^2}{4}} \qquad (21)$$

The values of Γ obtained from this calculation are close to the ones obtained from the empirical relation given in Reference 22:

$$\Gamma = 1.4 \, u_{jo} \, \sin \beta_0 \, D_0 \qquad (22)$$

where it is assumed that only the normal component $u_{jo} \sin \beta_0$ of the jet velocity induces some vorticity.

In the configuration studied in Ref. 27, the calculation leads to an a dimensional strength of the vortices:

$$\frac{Q}{u_\infty D_0} = .490$$

while the application of Ref. 22 empirical relation gives:

$$\frac{Q}{u_\infty D_0} = .474$$

The difference is only 3%.

4.2.5 Induced Normal Velocity

Reference 20 shows that the damping of the vortices due to viscosity is felt from a distance of about 400 hole diameters. Therefore, in the range usually considered in film cooling (up to 100 hole diameters) the damping can be neglected; the fluid is assumed inviscid except for the entrainment of main-flow.

According to Kelvin's circulation theorem, the circulation around any closed material curve is invariant in an inviscid fluid. This can be applied to curve ζ in Fig. 27 which encircles half of the jet cross section.

By Stoke's theorem, the vorticity included inside the curve ζ is invariant; the strength of the contrarotative vortices is invariant.

Point A at the top of the jet cross section is a stagnation point in the cross section (Fig. 28). With the notations of Fig. 28:

$$U_A = -U_N + \frac{\Gamma}{\pi} \left[\frac{Y_T}{Y_T^2 + (\frac{B^2}{2} - z_T)} - \frac{s - Y_T}{(s-Y_T) + (\frac{B^2}{2} - z_T)^2} + \frac{s + Y_T}{(s+Y_T^2)\frac{B}{2} - Z_T)^2} \right.$$

$$\cdots \left. - \frac{ns - Y_T}{(ns-Y_T)^2 + (\frac{B}{2} - Z_T)^2} + \frac{ns + Y_T}{(ns+Y_T^2) + (\frac{B}{2} - Z_T)^2} \right] = 0$$

Therefore, the normal velocity of the main flow induced by the vortices in the vicinity of the jets is:

$$U_N = \frac{\Gamma}{\pi} \left[\frac{Y_T}{Y_T^2 + (\frac{B}{2} - z_T)^2} + \sum_m \left(\frac{ns + Y_T}{(s-Y_T) + (\frac{B}{2} - z_T)^2} - \frac{ns - Y_T}{(s+Y_T)^2 (\frac{B}{2} - Z_T)^2} \right) \right] \quad (23)$$

From the conservation of mass flow, the horizontal velocity of the main flow is unchanged, neglecting the increase of the jet cross section area. Consequently, the velocity of the main flow is deflected downwards from u to u' such that the normal compont is u_N (Fig. 29). The tangential velocity is

$$U_T = \frac{U}{\cos \beta} - U_N \tan\beta \quad (24)$$

27

4.2.6 Trajectory and Growth of the Jets

The jet centerline is obtained from the equations of motion (§ 1) with
the entrainment given in (§ 2) and the normal and tangential components of
the main velocity given in (§ 5). Due to the normal velocity induced by
the vortices, the jets are deflected downwards below the horizontal. The
jets reattach to the wall along line R (Fig. 30). The shape of the jets
remains the same as long as they are free jets. If the jets reattach to
the wall before touching one another, it is assumed that they continue to
grow only in the lateral direction (Fig. 31a). If the jets are in contact
with one another before reattaching, it is assumed that they continue to
grow only in the vertical direction (Fig. 31b).

4.2.7 Trajectory of the Vortices

In a cross section of the jet (Fig. 32) the vertical velocity of a
vortex located at (Y_T, Z_T) relative to the jet centerline in curvilinear
coordinates (Fig. 24) is:

$$V_z = -U_n + \frac{\lambda}{2\pi} \left[\frac{1}{2Y} - \frac{1}{S-2Y_T} + \frac{1}{S+2Y_T} \cdots - \frac{1}{nS-2Y_T} + \frac{1}{nS+2Y_T} \right] \tag{25}$$

For a step Δs along the jet centerline, the step in time is $\Delta t = \Delta s/u_j$ and

$$\Delta Z = Y \Delta T = \frac{V_z}{U_j} \Delta S \tag{26}$$

From the position of the vortices at a given step, Eq. (23) gives the value
of u_N and Eqs. (25) and (26) lead to the position of the vortices at the
next step. Since the location of the vortices in the first free jet cross
section is known [$Z_T = 0$ and Y_T computed from Eq. (20)], the path of the
vortices is deduced from the trajectory of the jet centerline.

28

4.2.8 Cooling Effectiveness for Reattached Jets

When the jets are touching the wall, it is assumed that the laterally averaged wall temperature is the same as the average temperature of a layer with a thickness equal to the small diameter of the jets. When the jets are in contact with one another and are touching the wall, they form a layer over the plate (Fig. 33).

The dilution parameter at the beginning of the layer is

$$\mu_{jF} = \mu_j + \frac{A-A_j}{A_j} (1 + \mu_j) \qquad (27)$$

The adiabatic effectiveness of the cooling is defined as

$$\eta = \frac{T-T_w}{T-T_{jo}} \qquad (28)$$

with

$$T_w = T_{Lo} = \frac{T_{jo} + \mu_{jf} T}{1 + \mu_{jF}}$$

therefore

$$\eta = \frac{1}{1+\mu_{jF}} = \frac{A_j}{A} \frac{1}{1+\mu_j} \qquad (29)$$

4.3 Analysis of the Mixed Layer

When the jets are in contact with the wall and with one another, the cool flow constitutes a layer over the plate. For the calculation it is assumed that the initial thickness of the layer is equal to the small diameter of the last cross section of the jets.

4.3.1 Equations of the Layer

An additional dilution of the main flow in the cool flow occurs in the layer. A dilution parameter in the layer μ_L is defined as the ratio of main flow which has been entrained inside the layer to the initial mass flow of the layer.

Equation of continuity:

$$\rho_L u_L h = (1 + \mu_L) \rho_{Lo} u_{Lo} h_o \tag{30}$$

Conservation of momentum:

$$(1 + \mu_L) U_L = U_{Lo} + \mu_L u_\infty \quad \text{or} \quad U_L = \frac{u_{Lo} + \mu_L U_\infty}{1 + \mu_L} \tag{31}$$

Equation of energy:

$$(1 + \mu_L) T_L = T_{Lo} + \mu_L T \tag{32}$$

$$\text{or} \quad T = \frac{T_{Lo} + \mu_L T}{1 + \mu_L}$$

If the flow is assumed incompressible, the equation of energy can be written:

$$(1 + \mu_L) \frac{1}{\rho_L} = \frac{1}{\rho_{Lo}} + \frac{\mu_L}{\rho} \tag{33}$$

or

$$\rho_L = (1 + \mu_L) \frac{\rho_{Lo} \rho}{\rho + \mu_L \rho_{Lo}}$$

Substituting Eqs. (31) and (33) into the equation of continuity (30) leads to:

$$h = (1 + \mu_L) \frac{1 + m_L \dfrac{\rho_{Lo}}{\rho}}{1 + \mu_L \dfrac{U_\infty}{U_{Lo}}} h_o \tag{34}$$

30

4.3.2 Dilution Due to the Vortices

The flow is considered inviscid. The velocity at the wall has to be tangent to the wall. Therefore, the velocity field is the same as the one induced by the vortices and their images symmetrical to the wall (Fig. 34).

The mass flow of main fluid entering the layer per unit area due to the vortices only is the same as the mass flow which would leave the layer in the velocity field induced by the vortices and their wall images:

$$\phi = 2 \frac{\rho}{s} \int_o^a v_z(M) \, dy \tag{35}$$

where a is the point of horizontal velocity at the boundary of the layer. With the notations of Fig. 14, and assuming $a \simeq Y_T$[20]

$$\phi = \frac{o\Gamma}{\pi s} \left[\log \frac{h+z_r}{h-z_r} + \sum_{n=0}^N \log \left[\frac{((n+1)s)^2 + (h+z_r)^2}{((n+1)s)^2 + (h-z_r)^2} \right. \right. \times$$

$$\left. \left. \frac{[(ns+2Y_T)^2 + (h-z_T)]^2 [((n+1)s-2Y_T)^2 + (h-z_r)^2]}{[(ns+2Y_T)^2 + (h+z_T)^2] [((n+1)s-2Y_T)^2 + (h+z_T)^2]} \right]^{1/2} \right. \tag{36}$$

4.3.3 Dilution Due to Turbulence

Acording to Fick's law, the mass flux entrained into the layer by turbulence is:

$$d\dot{m}_{e,t} = - \rho D_t \text{ grad } c \, dx \tag{37}$$

where c is the concentration of main fluid, grad $c = -\partial c/\partial z$ and D_t is the turbulent diffusion coefficient.

$$d\dot{m}_{e,r} = \rho \frac{h}{h_I} U_\infty \frac{1}{1+\mu} K(n) \, dx \tag{38}$$

31

where h_I is the distance between the wall and the inflection point of the concentration profile, μ is the overall dilution parameter defined as the ratio of fluid originating from the main flow to the fluid originating from the holes:

$$\mu = \mu_{jF} + \mu_L (1. + \mu_{jF}) = \mu j_F + \mu_L + m_{jF} \mu_L \qquad (39)$$

and

$$K(n) = 0.052353 - 0.032051n + 0.006582n^2 - 0.000433n^3 \qquad (40)$$

Overall Dilution

In a step Δx the mass flow of main fluid entering the layer by vortical and turbulent mixing is

$$\Delta \dot{m}_e = (\phi + \frac{\Delta \dot{m}_{e,r}}{\Delta x})\Delta x \qquad (41)$$

where ϕ is given by Eq. (36) and

$$\frac{\Delta \dot{m}_{e,r}}{\Delta x} \simeq \frac{d \dot{m}_{e,r}}{dx}$$

by Eqs. (38) and (40).

The variation of the layer dilution parameter μ_L is such that

$$\Delta \mu_L = \frac{\Delta \dot{m}_e}{\rho_{Lo} U_{Lo} h_o} \qquad (42)$$

4.3.5 Velocity Profile

The average velocity in the layer u_L is given by the conservation of momentum (31) neglecting the wall friction. The effect of the wall friction is to induce a velocity profile which is assumed to be of the form

$$U = U_\infty (\frac{z}{h})^{1/n} \qquad (43)$$

32

When the mixed layer is a boundary layer of thickness h, the velocity profile is assumed to be a turbulent one:

$$U = U_\infty \left(\frac{z}{h}\right)^{1/7} \tag{44}$$

It is assumed that the ratio of average velocities deduced from Eqs. (43) and (44) is equal to u_L/u_∞:

$$\frac{U_L}{U_\infty} \approx \frac{\int_0^h \left(\frac{z}{h}\right)^{\frac{1}{n}} dz}{\int_0^h \left(\frac{z}{h}\right)^{\frac{1}{7}} dz} = \frac{\int_0^1 r^{\frac{1}{n}} dt}{\int_0^1 r^{\frac{1}{7}} dt} = \frac{8}{7(1 + \frac{1}{n})} \tag{45}$$

Therefore

$$n = \frac{U_L/U_\infty}{8/7 - U_L/U_\infty}$$

Substituting the expression (31) of u_L into (45):

$$n = \frac{7 \frac{U_{Lo}}{U_\infty} + \mu_L}{\mu_L + 8 - 7 \frac{U_{Lo}}{U_\infty}} \tag{46}$$

If $u_{LO} < u_\infty$, n is increasing

$$\text{from } n_0 = \frac{7 \frac{U_{Lo}}{U_\infty}}{8 - 7 \frac{U_{Lo}}{U_\infty}} \qquad \text{to 7}$$

when μ_L is very large (Fig. 36), and if $u_{LO} > u_\infty$ n is decreasing from n_0 to 7.

4.3.6 Trajectory of the Vortices

The fluid inside the layer cannot leave the layer. Hence, the vertical velocity of a fluid particle inside the layer near the upper

33

surface of the layer cannot be larger than the growth rate of the layer which is very small. Therefore the velocity of this fluid particle in the cross section is almost horizontal.

In order to have an horizontal velocity at the surface, the velocity field inside the layer is the same as the one induced by the vortices and their symmetric images relative to the wall and relative to the upper line of the layer, and also by the symmetric images of those. The velocity field is induced by an infinity of double rows of vortices at a distance 2h from one another (Fig. 37). The velocity of a vortex located at (Y_T, Z_T) due to the other vortices is derived.

Knowing the induced velocity, the vortex trajectory can be computed as shown in Fig. 38. Since the layer is growing, the vortex is on an ascending spiral inside the layer (Fig. 39).

4.3.7 Film Cooling Effectiveness

The adiabatic film cooling effectiveness of the layer is defined as

$$\eta = \frac{T - T_w}{T - T_{jo}} = \frac{T - T_w}{T - T_{Lo}} \frac{T - T_{Lo}}{T - T_{jo}}$$

$$\eta = \eta_o \frac{T - T_w}{T - T_{Lo}} \tag{47}$$

where η_0 is the effectiveness at the beginning of the layer. Because of the presence of the wall, the diffusion of fluid particles is not symmetrical and there is a reflection . the wall (Fig. 40). Therefore, the concentration and temperature profiles have an inflection point at a distance h_I from the wall which is moving upwards.

When h is very large $h_I \approx h/2$. At the beginning of the layer it is assumed that $h_I \approx 0.7 \, h_0$. Therefore,

$$h_I \approx 0.2 \, h_0 + 0.5 \, h \qquad (48)$$

The temperature profiles are shown in Fig. 41. The average temperature in the layer is approximated by

$$T_L = \frac{h_I}{h} T_w + (1 - \frac{h_I}{h})T$$

$$T_w = \frac{h}{h_I} T_L + (\frac{h}{h_I} - 1)T \qquad (49)$$

and the adiabatic effectiveness is:

$$\eta = \frac{h}{h_I} \frac{T - T_L}{T - T_{Lo}} \eta_o$$

replacing T_L by its expression (32)

$$\eta = \frac{h}{h_I} \frac{1}{1 + \mu_L} \eta_o \qquad (50)$$

This analysis can be extended to multiple lines of equally spaced holes using the additive superposition proposed in Ref. 29. The validity and limitations of this treatment are determined in Refs. 30 and 31.

4.4 Comparison with Experimental Data

4.4.1 Jet Trajectory, Growth of the Layer and Path of the Vortices

The calculation has been made for the cases presented recently in Reference 27. It includes the results presented in Ref. 32. The spacing between the holes is 3 hole diameters, the angle of injection is 35 degrees and the density velocity ratio defined as

$$m = \frac{\rho_{jo} \, U_{jo}}{\rho \, U_\infty} \qquad (51)$$

is 0.5.

Since the density ratio ρ_{jO}/ρ is about 0.85, the velocity ratio u_{jO}/u_{∞} is about 0.59.

When the ratio of the boundary layer thickness to the hole diameter is 0.245, the jet trajectory and the path of the vortices inside the jets are presented in Fig. 42. The reattachment to the wall is found at a distance of 4.35 hole diameters from the holes. The growth of the layer and the path of the vortices inside the layer are presented in Fig. 43 for the same case. At the bottom of the figure the projection of the path of the vortices in the cross section of the layer shows that the vortices have an helicoidal motion inside the layer.

4.4.2 Film Cooling Effectiveness

The calculated film cooling effectiveness compared to the experimental results for the case described above is presented in Fig. 44. The calculated curve is above the experimental results of average film cooling effectiveness near the reattachment, but the agreement is good at a certain distance from the reattachment.

The calculation has also been done for some cases presented in Ref. 33. The geometric configuration is the same as for the case of Ref. 27 ($s = 3D_O$ and $\beta = 35^{\circ}$). Two curves are presented in Fig. 45, where the ratio of the boundary layer thickness to the hole diameter is 0.174: one for the density velocity ratio $m = 0.31$ ($\rho_{jO}/\rho = 0.742$ and $u_{jO}/u_{\infty} = 0.418$) and the other for $m = 0.70$ ($\rho_{jO}/\rho = 0.769$ and $u_{jO}/u_{\infty} = 0.910$). In these cases the agreement between the calculation and the experimental results is good except very near the injection (up to 5 hole diameters).

Two cases presented recently[34] for a single line of holes were also calculated. The spacing between the holes is 3 hole diameters, the

ejection angle is 45°, the ratio of the boundary layer thickness to the hole diameter is 0.104, and the density ratio is $\rho_{jO}/\rho = 0.94$. Two curves are shown in Fig. 46: one for a density velocity ratio, m = 0.27 ($u_{jO}/u_\infty = 0.29$), and the other for m = 0.54 ($u_{jO}/u_\infty = 0.57$). The agreement between the calculation and the experimental results is good except very near the injection point. The model is not very accurate near the injection because the velocity profile inside the tubes has been assumed constant. In fact, the low momentum fluid is deflected much more rapidly than the core fluid by the main flow and increases the cooling effectiveness near the injection point.

4.4.3 Distance of Reattachment

The calculated distances x_R between the holes and the reattachment point in the different cases presented above are as follow:

Ref. 27

$$\frac{S}{D_O} = 3. \qquad\qquad \beta_O = 35 \qquad\qquad m = 0.5$$

$$\frac{\delta}{D_O} = 0.175 \qquad\qquad \frac{x_R}{D_O} = 4.13$$

$$\frac{\delta}{D_O} = 0.245 \qquad\qquad \frac{x_R}{D_O} = 4.35$$

Ref. 33

$$\frac{S}{D_O} = 3. \qquad\qquad \beta_O = 35^\circ \qquad\qquad \frac{S}{D_O} = 0.174$$

$$m = 0.31 \qquad\qquad\qquad\qquad\qquad \frac{x_R}{D_O} = 2.75$$

$$m = 0.70 \qquad \qquad \frac{x_R}{D_o} = 12.70$$

Ref. 34

$$\frac{S}{D_o} = 3. \qquad \beta_o = 45^o \qquad \frac{S}{D_o} = 0.104$$

$$m = 0.27 \qquad \frac{x_R}{D_o} = 2.20$$

$$m = 0.54 \qquad \frac{x_R}{D_o} = 3.86$$

These results show that the distance between the holes and the reattachment point increases when m increases (more penetration of the jets) and also when δ/D_o increases (less deflection of the jets).

This study provides a comprehensive analysis of the fluid mechanical and thermal evolution of the film formed by the coolant injected through a line of closely spaced round holes inclined to the surface.

The first part of the analysis describes the growth of the jets from the injection to the formation of a continuous mixed layer. The strength of the vortices, the mutual interaction of vortices induced in neighboring jets, and the mixing due to both turbulent diffusion and vortex entrainment are used to determine the trajectory and growth of the jets. The second part of the analysis describes the growth of the mixed layer as influenced by both turbulent diffusion and vortex entrainment since the decay of the vortex strength is found to be negligible over the length of wall effectively cooled.

The results of the analysis compare very satisfactorily with available experimental data of average film cooling effectiveness obtained for a single line of holes.

38

The analysis can be extended to the film produced by injection of coolant through multiple lines of holes using the principle of super-position[29] within the limitations determined in References 30 and 31.

4.5 Nomenclature

T_L Temperature in the layer (average)

T_w Wall temperature (adiabatic)

E Entrainment of the main flow

E_1, E_2 Entrainment coefficients

c_D Drag coefficient

f Complex potential

ψ Stream function

μ_j Dilution parameter in the jet

μ_{jF} Dilution parameter at the beginning of the layer

μ_L Dilution parameter in the layer

μ Overall dilution parameter

η Adiabatic film cooling efficiency

Γ Strength of the vortices

ϕ Mass flow entrained by the vortices

$\dot{m}_{e,t}$ Mass flow entrained by turbulent

D_t Turbulent diffusion coefficient

c Concentration

μ_t Turbulent viscosity

ℓ_m Velocity mixing length

$\ell_{m,c}$ Concentration mixing length

σ_t Turbulent Schmidt number

Q Heat transfer

$\tilde{h}$ Heat transfer coefficient

m Density velocity ratio $m = \dfrac{\rho_{j0} u_{j0}}{\rho u_\infty}$

Nomenclature (Cont'd)

Subscripts:

        j   in the jets

        j0   at the beginning of the jets

        L   in the layer

        L0   at the beginning of the layer

        w   at the wall

        T   relative to the vortices

        iso isothermal

        a   adiabatic

        c   coolant

        R   reattachment

Superscript: —   average

5. <u>Aerodynamic Performance and Heat Transfer Characteristics of Film-Cooled Airfoils in a Subsonic Cascade Flow</u>

5.1 Introduction

The use of a film of air coolant is an effective technique for the reduction of heat transfer to hot components of gas turbines. Therefore, the interaction and mixing of the coolant with the high temperature mainstream over the blade surface influences not only the thermal effectiveness of the film, but also the aerodynamic profile losses of film cooled blades.

The film of coolant can be obtained by blowing air through a porous surface, arrays of holes, and slots. (The last technique is seldom used in blade cooling because of mechanical difficulties.) The first technique, transpiration cooling, uses cooling flows of low momentum which can be described by boundary layer theory. The aerodynamic and heat transfer performance of transpiration cooled blades has been investigated[35,36,37]. The difficulties of technological implementation of transpiration cooling and the significant aerodynamic penalty have impeded the application of this mode of cooling.

In present practice, the film is obtained by the injection of a film through an array of holes inclined to the wall. The cool jets issued from these holes were found to have a momentum normal to the wall which was not negligible compared to the momentum of the mainstream, and boundary layer could not be applied to the development of the film. Further, the jets separated at the point of injection and a pair of contrarotating vortices was created within each jet by the velocity field interaction. When the jets reattached to the wall and formed a mixing layer, the vortices

remained imbedded in the layer. The evolution of the coolant film was, therefore, determined by entrainment of the main flow due to two mechanisms: turbulent diffusion and the velocity field induced by the vortices. The concept of turbulent and vortical mixing for cooling films has only recently been formulated for the evolution of films over flat plates[38,39].

Although considerable information exists on the thermal effectiveness of films issued from arrays of holes over flat surfaces, very limited information exists on the effects of flow curvature, pressure gradients and turbulence levels on the behavior of a coolant film along a turbine blade. The thermal performance of a blade cooled through a discrete number of lines of round holes has been investigated[40] and, more recently, the aerodynamic and heat transfer performance of a full coverage film cooled blade has been reported[41].

This study presents a comprehensive set of aerodynamic and heat transfer studies obtained on film cooled blades with straight suction back in a linear cascade. The influence of location[42] of the coolant injection on performance is investigated.

5.2 Experimental Conditions and Apparatus

The aerodynamic and heat transfer measurements reported in this paper were made on the M.I.T. hot turbine blowdown facility (Figure 47). This facility uses a pebble bed heater to deliver hot flow to a stationary linear cascade at a selected pressure and temperature. In the experiments, test times were 0.8s with steady flow achieved after 0.2s.

The injection of the coolant was synchronized with the hot flow. Thus, aerodynamic and heat transfer data were taken under steady flow

conditions for 0.6s. The short duration of the test means that the blade surface was nearly isothermal during the test. The isothermal condition approximates actual blade operating conditions and meets the design objective of avoiding significant temperature gradients within the blade. The isothermal wall conditions allow a logical application of local heat transfer results to the design of film cooled blades.

Pressure, temperature and blade length modeling[42] were used in order to scale actual gas turbine conditions corresponding to a turbine inlet temperature of 1800 K (2750°F) to a cascade inlet temperature of 450 K (320°F). The temperatures of the blade surface and of the coolant at injection corresponded to two-thirds and one-half of the inlet absolute temperature, respectively. The Reynolds number based on blade chord was 5×10^5. The turbulence level of the main inlet flow was 10%. The details of the blowdown facility and the flow modeling are given in Ref. 42.

The cascade was instrumented with total pressure and temperature probes located at a distance of three axial blade chords upstream of the nine blade cascade (Figure 48). A traversing mechanism carried a total pressure directional probe at mid-span with a speed of 2.2 cm per second. During the steady flow part of the test time, the probe covered a distance larger than the blade wake at a distance from the trailing edge of one-third of an axial chord.

All tests were performed at closely identical thermodynamic conditions for the hot flow and with blade surface close to 300 K and a coolant temperature of 225 K.

The blade under study had a thick trailing edge and straight suction side (Figure 49) and was previously investigated in the M.I.T. blowdown

44

facility by Demuren[43] and Hajjar, et. al.[44] for both off- and design
conditions. The thick blade provided space for the cooling plenums while
leaving an adequate structure for a thick skin. The locations of the line
of film cooling holes (Figure 49) were selected to match the hot spot
regions on the blade surface. Therefore, five single rows of holes were
drilled at the leading edge. At the transition point on the suction side,
at the mid-chord on the pressure side, and upstream of the trailing edge on
both sides, the coolant was injected through a double line of holes. The
angles of injection with respect to the blade surface were of 20°, based on
flat plate maximum effectiveness except at the leading edge and on the
suction side where, because of manufacturing constraints, these angles were
90° and 43°, respectively. The diameter of the holes was 1mm and the hole
interspace was equal to two hole diameters. The double line of holes
located at the transition point corresponded to the joint of minimum
pressure. The double line of holes upstream of the trailing edge was
located using the results of Amana's study[45] on trailing edge heat
transfer.

Among the nine aluminum blades in the cascade, the three at the center
were film cooled and only the middle one was instrumented (Figure 3).
Fourteen surface static pressure taps and eighteen heat transfer gauges
allowed the determination of aerodynamic and heat transfer characteristics.

The pressure taps, located along the center line of the blade, were
connected by using holes drilled spanwise in the blade skin, to pressure
transducers.

The heat flux into the blade surface at a given location was measured
with a calorimetric gauge mounted flush with the surface. The heat
transfer gauge consists of a cylindrical copper slug, 0.24 cm diameter and

0.05 cm in thickness, insulated from the blade and having a thermocouple

attached to its backside to measure the slug temperature. If the heat flow

into the blade is modeled as one-dimensional, and the insulation is assumed

to be

perfect, then a heat balance for the gauge is given by:

$$q = h(T_\infty - T_g) = d/dt \ (mC_p/A \ T_g) \tag{52}$$

or

$$h = mC_p/A \ (T_\infty - T_g) \ dTg/dt \tag{53}$$

By measuring the local slope of the gauge and main flow stagnation

temperature under steady flow conditions, the heat transfer coefficient can

be obtaintained since mC_p/A is a constant.

The heat losses from the gauge are also minimized by designing the

insulation thickness to have a longer diffusion time than the test time.

The Nusselt number is calculated as:

$$Nu = hc/k \tag{54}$$

where k is based on the mainstream stagnation temperature and the blade

chord, c, of 6.5 cm.

The study of the wake profiles allowed us to investigate the effects

of the cooling on the blade profile loss. A stagnation pressure loss

coefficient, ξ_m, was obtained by taking the ratio of the stagnation

pressure drop over the ideal dynamic pressure present in the flow (in the

absence of any loss mechanism), averaged over a pitch length and weighted

by the mass flow as:

$$\xi_m = \frac{\int_0^{s_2} (P_{01} - P_{02})ds + \Sigma \frac{\dot{m}_c}{\dot{m}_\infty} \int_0^{s_2} (P_{0C} - P_{02})ds}{\int_0^{s_2} (P_{01} - P_2)ds + \Sigma \frac{\dot{m}_c}{\dot{m}_\infty} \int_0^{s_2} (P_{0C} - P_2)ds} \tag{55}$$

The effect of cooling on the heat transfer was analyzed with the isothermal effectiness η variations, defined in Ref. 42 as:

$$\eta = \frac{\dot{q}_o'' - \dot{q}_c''}{\dot{q}_o''} \tag{56}$$

where q_o'' = heat transfer rate to the blade without cooling

q_c'' = heat transfer rate to the blade with cooling.

For each of the seven following cooling configurations, six blowing ratios have been investigated ($m = (\rho U)_c / (\rho U)_\infty$ = 0; 0.3; 0.5; 0.7; 1; 1.2).

The injection configuations (Figure 49) are:

1) leading edge injection, plenum A

2) suction side injection, plenum B

3) pressure side injection, plenum C

4) trailing edge injection, plenum D

5) leading edge and suction side injection, plenums (A + B)

6) leading edge and pressure side injection, plenums (A + C)

7) full injection, plenums (A + B + C + D)

Nitrogen refrigerated at the desired temperature of 225 K was used as a coolant. Nitrogen was cooled by passing it through a coil immersed in liquid nitrogen and fed into one of the four tanks. Each plenum (A, B, C, or D) had its independent cooling system fed from one of the four tanks. The flow was metered into each individual plenum. The coolant was

47

introduced from top and bottom in each plenum in order to maintain low flow velocities and attain uniform injection. Each plenum was also instrumented with its own thermocouple and pressure gauge so that the flow properties of the coolant were exactly known at injection.

5.3 Experimental Results

5.3.1 Pressure Distribution

The static pressure distribution around the blade was found to vary slightly with the coolant mass flow injected[47]. Figure 50 gives the pressure distribution for different values of the injection parameter (m) when coolant was injected through all the plenums.

The blade passage cross section can be reduced either by the local jet penetration or by the existence of a thick boundary layer fed by the coolant. Consequently, the pressure in the blade passage will rise, for a constant pressure drop across the cascade, as the mass flow decreases in the film cooled blade passages. The pressure distribution on the pressure side near the leading edge was also found to vary because of a change in incidence associated with changes of the effective shape of the leading edge.

5.3.2 Effects of the Leading Edge Injection

On the pressure side, the injection of the coolant causes the transition to a turbulent boundary layer to occur earlier than for the uncooled blade (around $s/L = 0.2$ instead of $s/L = 0.3$). The roughness of the mid-chord coolant orifices trips (Figure 51) the boundary layer and a high heat transfer is locally recorded. For the highest coolant mass flow injected, good cooling is obtained as far as the trailing edge.

48

On the suction side (Figure 51) at low blowing value (m = 0.3) a poor cooling is obtained due to the rapid mixing of the small amount of injected coolant, while at the highest blowing rate a large heat transfer reduction (up to 50%) is measured along the blade.

The wake profiles display, for all m, a shape similar to the uncooled blade wake. Changes in the location of the transition point due to coolant injection have a negligible effect on the wake and losses (Figures 62, 63).

5.3.4 Effects of the Suction Side Injection

The injection of coolant on the suction side occurs near the maximum suction point and the coolant is therefore introduced in an adverse pressure gradient.

The measurements of the wake width (Figure 52) indicate that even for the small values of the blowing factor (m = 0.3), the boundary layer thickness is greatly increased. This thick boundary layer with the cooler gas near the wall leads to high values of the film cooling effectiveness as far as the trailing edge located at a distance equivalent to eighty hole diameters (Figure 53).

The depth of the wakes also indicate that the stagnation pressure loss is substantially increased (Figures 62, 63).

As the blowing factor increases, the wake is found to become wider and deeper up to a value of m = 1.2, where the wake width is shown to be reduced because the boundary layer energization (by the cooling jets) becomes more important.

5.3.5 Effects of the Presure Side Injection

On the pressure side (Figure 54), downstream of the injection region, a fairly good heat transfer reduction is obtained. At a low coolant mass flow, the Nusselt number rises sharply behind the injection location. As the coolant mass flow increases, better cooling is achieved but the rate of heat transfer reduction levels off beyond $m = 0.7$. The jet penetration is evidenced at $m = 1$ and 1.2 by the minimum of heat transfer rate observed at the second gauge indicating the zone of jets reattachment. Close to the injection holes an optimum blowing factor of $m = 1.0$ is observed, whereas beyond the second gauge the thermal effectiveness increases with coolant flow rate.

5.3.6 Effects of the Trailing Edge Injection

The instrumentation of this section of the blade shows a quite remarkable heat transfer reduction (Figure 55). The isothermal effectiveness reaches 98%.

At low values of the blowing ratio m, the wake profile deepens and widens a little. At $m = 1.2$, the wake width and depth are reduced because of a local energization of the boundary layer. Therefore, the total loss coefficient is found to have a maximum at a value of m close to 1.0.

5.3.7 Effects of the Combined Injections

The effect of combined leading edge and suction side injection around the blade nose is similar to the sole plenum A injection; while around the plenum B, the rate at which the heat transfer increases downstream of the injection is observed to be slightly less than for the injection through plenum B alone[46], (Figure 59). The wake profiles observed in this case

50

and in the sole plenum B injection are almost identical. However, higher loss coefficient follows (Figures 62, 63).

The combined injections of the leading edge and the pressure side provide a heat transfer reduction around the leading edge and at the blade mid-chord similar to those observed for plenums A and C tested individually. The wake profiles follow the same trend and the higher loss coefficient varies linearly with the coolant mass flow (Figures 62, 63).

5.3.8 Effects of the Full Injection

The reduction of the Nusselt number (Figure 56) is found to be dominated by the nearest upstream injection. Around the trailing edge very good cooling is observed on both sides and overcooling of the blade occurs at $m = 1.2$. The distribution of the reduction of heat transfer with the cooling indicates a fairly judicious selection of the location of the coolant injection. The wake profiles are found to be close to those observed for the other case of injection on the suction side. The total loss coefficient is found to be larger than in any other configuration (Figures 62, 63).

5.3.9 Variation of Isothermal Effectiveness with Blowing Ratio and Comparison with Flat Plate Correlations

The variation of the isothermal effectiveness η with the blowing parameter m is shown in Figures 57 to 60. Around the leading edge (plenum A) on both sides (Figure 57), η varies linearly with m. However, a higher effectiveness is achieved on the pressure side because of a larger number of coolant orifices.

51

On the suction side (plenum B) (Figure 58), the effectiveness reaches a maximum value which, close to the injection (s/D < 12), is obtained for m = 0.7 and for m = 1., further downstream.

On the pressure side (plenum C) (Figure 58), the rate of change of the effectiveness with m varies significantly from location to location. Around the coolant outlets, η reaches a maximum for m beyond 0.7. Further downstream (s/D > 10) η increases at a smaller rate and no maximum value is observed.

For combined and full injection (Figures 59, 60), the curves display a similar trend in the variation of η with m. As above, an upstream injection does not significantly influence the effects of downstream injection.

An attempt was made to compare the recent data with the correlation introduced in Ref. (42,43), for isothermal effectiveness measured dowstream of the line of holes and is shown in Figure 61. It displays the variation of the isothermal effectiveness versus A_0 as defined (Figure 61)

$$as\ A_0 = k_0^{-1.35}\ \theta^{-1.35}\ Re_c^{-0.25}\ (Cos^2\alpha)^{-1.35}\ s/D \tag{57}$$

The law for injection ⌣⌣ ⌣gh a double row of holes on flat plate without pressure gradient has ⌣ correlated as follows:

$$\eta = 1.46\ A_0^{\ exp(-.25)} \tag{58}$$

This is represented by a straight line on Figure 61. The data obtained on the suction side lies slightly above it. As commonly found by experimental researches, injection on a convex wall improves the cooling.

On the blade pressure side (plenum C) the lower effectiveness confirms that the coolant undergoes a larger mixing than when injected through a slot on a flat plate in the absence of a pressure gradient.

Similar discrepancies occur when the results of a different correlation which uses the concept of an equivalent width for injection through

holes[42] are compared with the data. These discrepancies are not un-
expected since individual jets issued from the holes penetrate deeper into
the hot flow on the suction than on the pressure side for the same value of
the blowing ratio (m) because the variation of pressure between the two
sides leads to a difference in momentum normal to the flow for the same
value of m.

A calculation[39] of the individual jet penetration indicates that the
jet center penetrates up to 1.2 hole diameters on the suction side as com-
pared to 0.76 hole diameters on the pressure side for the same value of the
blowing ratio m = 1.0.

The depth of penetration of the jet and the local dynamic pressure
influence the drag of the jets on the hot flow, which will therefore in-
crease with the depth of penetration or with the blowing ratio.

This mechanism appears to describe the quasi-linear dependence of the
profile losses on the blowing pressure observed when films are injected
either from the pressure or suction side. For injection upstream of the
trailing edge, a similar mechanism is likely to dominate for small values
of the blowing ratio. For larger values of m the film energizes the wake
and reduces the losses.

The depth of penetration of the individual jets influences the
thickness of the mixing layer formed when the jets are in contact with each
other and with the wall. The thickness of this layer is larger on the
suction side than on the pressure side where the layer is quickly
accelerated and subjected to rapid mixing under the influence of a strong
negative pressure gradient.

5.4 Conclusions

1) Static pressure distribution around the blades varies only slightly with the coolant mass flow injected.

2) The leading edge injection provides at high injection (m = 1.2) effective cooling along the blade wall with low stagnation pressure loss. The dependence of the profile losses is found to be non-linear with the mass flow rate of coolant, because they are influenced by mixing, motion of the transition point and changes in the location of the stagnation point.

3) Injection on the suction side leads to important heat transfer reduction, but also to the largest loss among the cases tested. The profile losses are found to be linear to the rate of coolant injected.

4) Injection on the pressure side provides good cooling close to the injection zone. Further downstream strong mixing dominates, while losses are linearly dependent upon the cooling mass flow rate.

5) Trailing edge cooling is achieved effectively on both sides. The profile losses are found to vary linearly with the coolant mass flow rate up to a value of m ≈ 1.0 when the profile losses are reduced due to the energization of the wake by the coolant.

6) When combined injection is used, the heat transfer reduction achieved downstream of each coolant outlet is mostly determined by the effect of the closest upstream injection. Full injection leads to important losses in stagnation pressure; e.g., for a value of the blowing parameter m ≈ 1.0, the overall profile losses are eighty percent larger than for the case with no cooling.

5.5 Nomenclature

A = heat transfer slug area open to the main stream

c = blade chord

C_p = specific heat

D = hole diameter

h = convective heat transfer coefficient

k = thermal conductivity

k_o = momentum ratio parameter = $(\rho U^2)_c / (\rho U^2)_m$ $^{1/2}$

L = total length along the blade from L.E to trailing edge

m = blowing ratio $m = (\rho U)_c / (\rho U)_\infty$

m_c = coolant mass flow

m_∞ = main stream mass flow

Nu = Nusselt number

P = static pressure

q_o = heat flux to the blade without cooling

q_c = heat flux to the blade with cooling

Re_c = Reynolds number based on coolant conditions and injection slot or hole dimension

s = curvilinear coordinate along the blade from the leading edge

T_∞ = main stream total temperature

T_c = coolant temperature

T_g = heat transfer slug temperature

U = velocity

Subscript

0 = stagnation condition

1 = position upstream of the cascade

2 = position downstream of the cascade

Greek

α = angle of injection

ξ_m = stagnation pressure loss coefficient

ρ = density

θ = T_c / T_∞

Other

A_0 = empirical correlation coefficient for isothermal effectiveness on a flat plate

REFERENCES

1. Louis, J.F., et al., "Short Duration Studies of Gas Turbine Heat Transfer and Film Cooling Effectiveness", ASME, 1974-GT-131, 1974.

2. Stollery, G.L., and El-Ehwany, A.A. International Journal Heat Transfer, Vol. 8, No. 1 1965.

3. Kutateladze, S.S., and Leontev, A.I., "Thermal Physics of High Temperatures", Vol. 1, No. 2, pp 281-290 (1963).

4. Papell and Trout, NASA, TW, ND-9, 1959.

5. Hartnett, Birkebak and Eckert, Journal of Heat Transfer, ASME, Series C, Vol. 82, No. 3, 1961.

6. Seban, Trans. ASME, Ser. C, Vol, 82, No. 4, 1960.

7. Kutateladze, S.S., and Leontev, A.I., Heat-Mass Transfer and Friction in a Turbulent Boundary Layer, Energiya Press, Moscow 1972.

8. Hruby, V., "Flow Visualization Studies in a Water Channel with Slot Injection Simulating Film Cooling", M.I.T., Gas Turbine Laboratory Internal Report, 1972.

9. Amana, O.M., et al., "Aerodynamics and Heat Transfer at the Trailing Edge of Transonic Blades", ASME, 76-GT-95, 1976.

10. Demirjian, A.M., "An Analytical and Experimental Investigation of Film Cooling Effectivness over a Flat Plate", Ph.D. thesis, Department of Aeronautics and Astronautics, M.I.T. September 1975.

11. Bakos, J.H., "Film Cooling by Cross Flow Hole Injection", S.M. thesis, Department of Aeronautics and Astronautics, M.I.T. September 1975.

12. Ortiz, M., "The Effect of Geometry on Film Cooling Effectiveness", S.M. thesis, Department of Aeronautics and Astronautics, M.I.T. February 1976.

13. Meroney, R.N.. "Measurements of Turbulent Boundary Layer Growth Over a Longitudinally Curved Surface," Project Thesis, Technical Report No. 25.

14. Tani, I., "Production of Longitudinally Vortices in a Boundary Layer Along A Concave Wall," Jour. Geophys.   Vol. 67, No. 8, 1962.

References (Cont'd)

15. Stollery, G. L. and El Ehwany, A. A., "International Journal of Heat Transfer", Vol. 8, No. 1, 1965.

16. Kutateladze, S. S. and Leontev, A. I., "Thermal Physics of High Temperatures", Vol. 1, No. 2, pp. 281-290 (1963).

17. Louis, J. F., "Systematic Studies of Heat Transfer and Film Cooling Effectiveness", Paper No. 28, AGARD Conf., P. 229, Ankara, September 1977.

18. Demirjian, A. M., "An Analytical and Experimental Investigation of Film Cooling Effectiveness over a.Flat Plate", Ph.D. Thesis, Department of Aeronautics and Astronautics, M.I.T., September 1975.

19. Le Grives, E., and Nicolas, J. J., "New Computation Method of Turbine Blade Film Cooling Efficiency, "AGARD Conf., Ankara, September 1977.

20. Ramette, P. H., "A Theoretical Study of Film Cooling", S.M. Thesis, Department of Aeronautics and Astronautics, M.I.T., September 1978.

21. Keffer, J. F. and Baines, W. D., "The Round Turbulent Jet in a Cross-Wind", J. Fluid Mech. 15, 4, pp. 481-497, 1963.

22. Fearn, R., and Weston, R. F., "Vorticity Associated with a Jet in a Cross-Flow", AIAA J. 12, 12, pp. 1666-1671, 1976.

23. Wooler, P. T., Burghart, G. H., and Gallagher, J. T., "Pressure Distribution on a Rectangular Wing with a Jet Exhausting Normally into an Airstream", J. Aircraft 4, 6, p. 537, 1967.

24. Batchelor, G. K., An Introduction to Fluid Dynamics, Cambridge University Press, 1970.

25. Ricou, F. P., and Spalding, D. B., "Measurements of Entrainment by Axisymmetric Turbulent Jets", J. Fluid Mech. 11, 1, pp. 25-32, 1961.

26. Morton, B. R., "On a Momentum-Mass Flux Diagram for Turbulent Jets, Plumes and Wakes", J. Fluid Mech. 10, 101, 1961.

27. Goldstein, R. J., and Kadotani, K., "Effect on Mainstream Variables on Jets Issuing from a Row of Inclined Round Holes", ASME Paper No. 78-GT-138, April 1978.

28. Launder, B. E. and Spaulding, D. B., Lectures in Mathematical Models of Turbulence, Academic Press, 1972.

29. Sellers, J. P. Jr., "Gaseous Film Cooling with Multiple Injection Stations", AIAA Journal, Vol. 1, No. 9, 1963, pp. 2154-2156.

References (Cont'd)

30. Muska, J. F., Fish, R. W. and Sud, M., "The Additive Nature of Film
    Cooling from Rows of Holes", ASME Journal of Engineering for Power,
    Vol. 98, pp. 457-464, October 1976.

31. Mayle, R. E., and Camarata, F. J., "Multihole Cooling Film
    Effectiveness and Heat Transfer", ASME Journal of Heat Transfer,
    Vol. 97, November 1975, pp. 534-538.

32. Eriksen, V. L., and Goldstein, R. J., "Heat Transfer and Film Cooling
    Folowing Injection Through Inclined Circular Tubes", J. Heat
    Transfer 96, 1, pp. 233-243, 1974.

33. Liess, C., "Film Cooling with Ejection from a Row of Inclined Circular
    Holes", TN 97, Von Karman Institute, Belgium, March 1973.

34. Sasaki, M., Takahara, K., Kumagai, T., and Hamano, M., "Film Cooling
    Effectiveness for Injection from Multirow Holes", ASME Paper
    No. 78-GT-32, April 1978.

35. Bailey, F. J., "Performance and Design of Transpiration Cooling on
    Turbine Blades", AGARD, C.P. 229, 1977.

36. Moffitt, T. P., Nasek, S. M. and R. J. Roelke, "Turbine Aerodynamic
    Considerations for Advanced Turbines", NASA, S.P. 259, 1971.

37. Morris, A. H. W., Bullard, J. E., and L. D. Wigg, "Experimental
    Evaluation of a Transpiration Cooled Nozzle Guide Vane", Paper 12,
    AGARD, C.P. 229, 1977.

38. LeGrives, E. and J. J. Nicolas, "New Computation Method of Turbine
    Blades Film Cooling Efficiency", Paper No. 36, AGARD, C.P. 229,
    1977.

39. Ramette, P. H. and J. F. Louis, "Analyticl Study of the Thermal and
    Fluid Mechanical Evolution of a Cooling Film Injected from a Single
    Line of Holes", submitted for publication July 1978.

40. Muska, J. F., Fish, R. W. and M. Suo, "The Additive Nature of Film
    Cooling from Rows of Holes", ASME Journal of Engineering for Power,
    Vol. 98, pp. 457-464, October 1976.

41. "Profile Loss Characteristics and Heat Transfer of Full Coverage
    Film-Coled Blading", ASME Paper 78-GT-98.

42. Louis, J. F., "Systematic Studies of Heat Transfer and Film Cooling
    Effectiveness", Paper No. 28, AGARD, C.P. 229.

43. Demuren, H. O., "Aerodynamic Performance and Heat Transfer
    Characteristics of High Pressure Ratio Transonic Turbines", Sc.D.
    Thesis, Department of Aeronautics and Astronautics, M.I.T., 1976.

References (Cont'd)

44. Hajjar, F. G., Amana, O. M., and J. F. Louis, "Aerodynamics and Heat
    Transfer of Transonic Turbine Blades at Off-Design Angles of
    Incidence", to be presented at the ASME Winter Annual Meeting,
    December 1978.

45. Amana, O. M., "Film Cooling Studies for High Performance Transonic
    Turbines with Particular Application to Trailing Edge Flow", Sc.D.
    Thesis, Department of Mechanical Engineering, M.I.T., January 1975.

46. Berenfeld, A., "Aerodynamic and Heat Transfer Characteristics of
    Film-Cooled Turbine Blades", S.M. Thesis, Department of Aeronautics
    and Astronautics, M.I.T., May 1978.

47. Louis, J. F., et. al., "Short Duration Studies of Turbine Heat Transfer
    and Film Cooling Effectiveness", ASME, Paper 74-GT-131, June 1974.
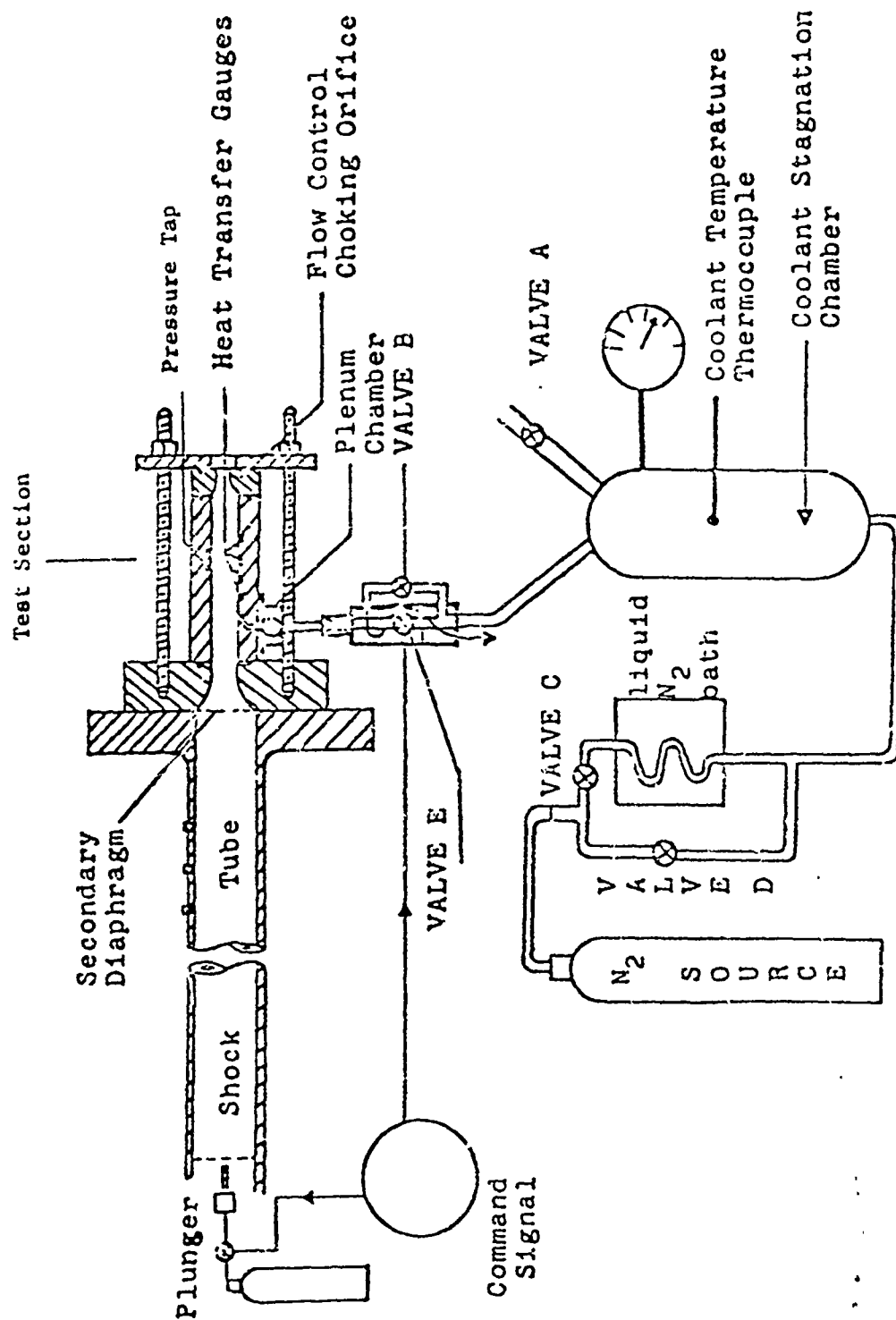
Figure 1. Shock tunnel apparatus
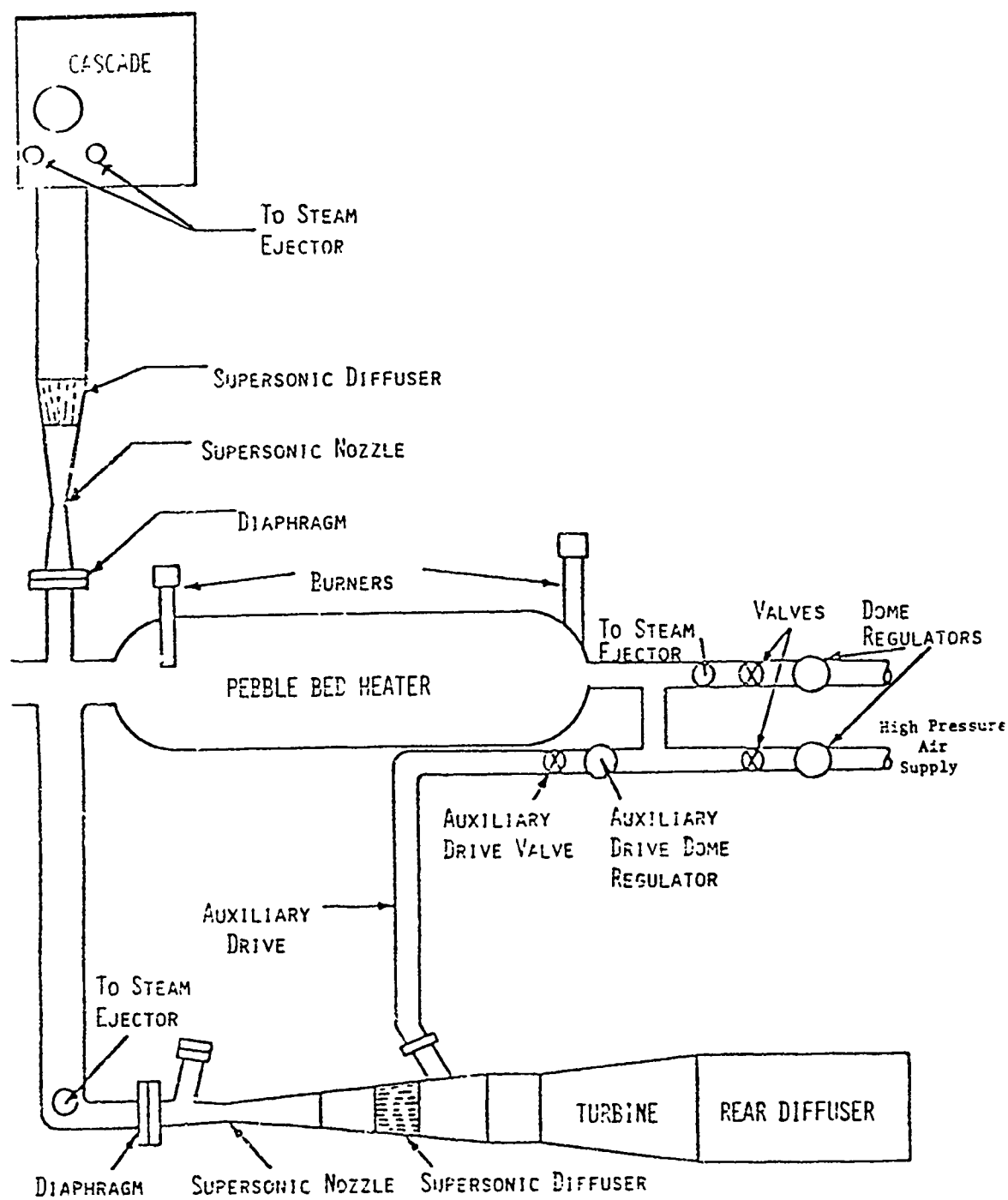
Figure 2. Cascade and turbine blowdown facilities
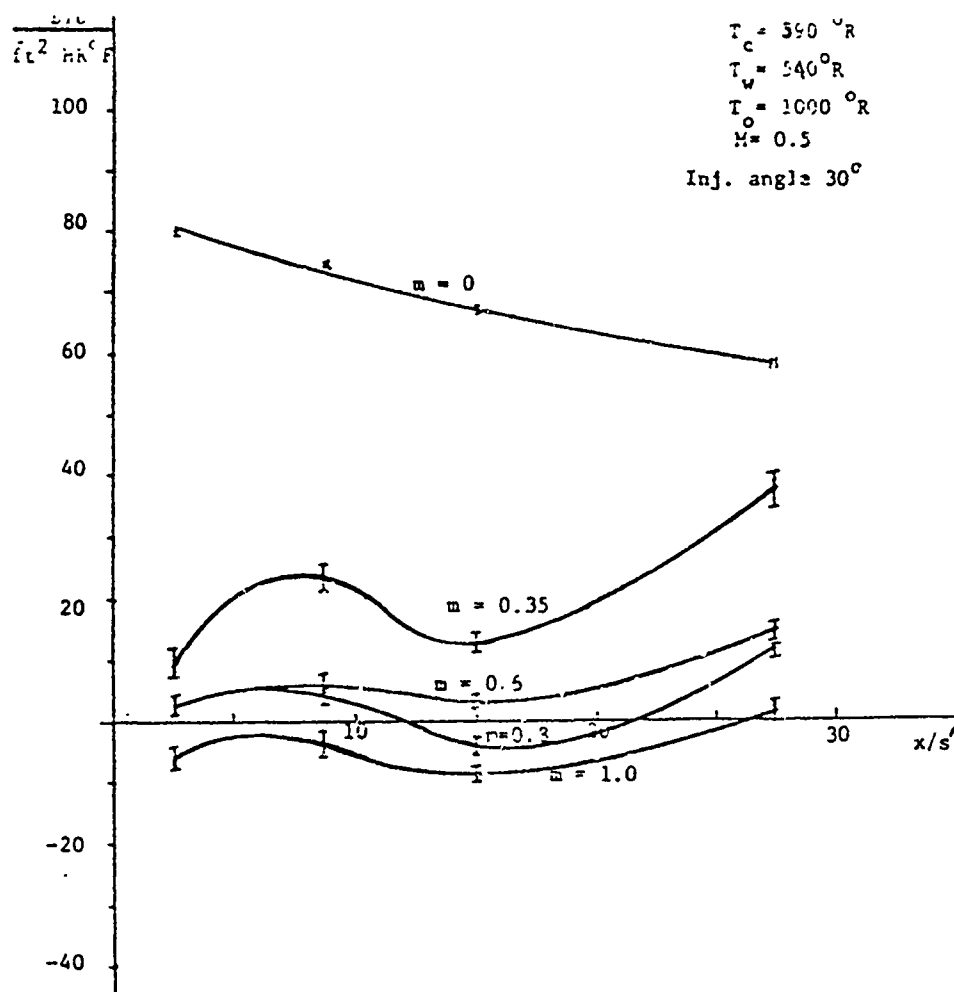
Figure 3. Heat transfer coefficients with film cooling
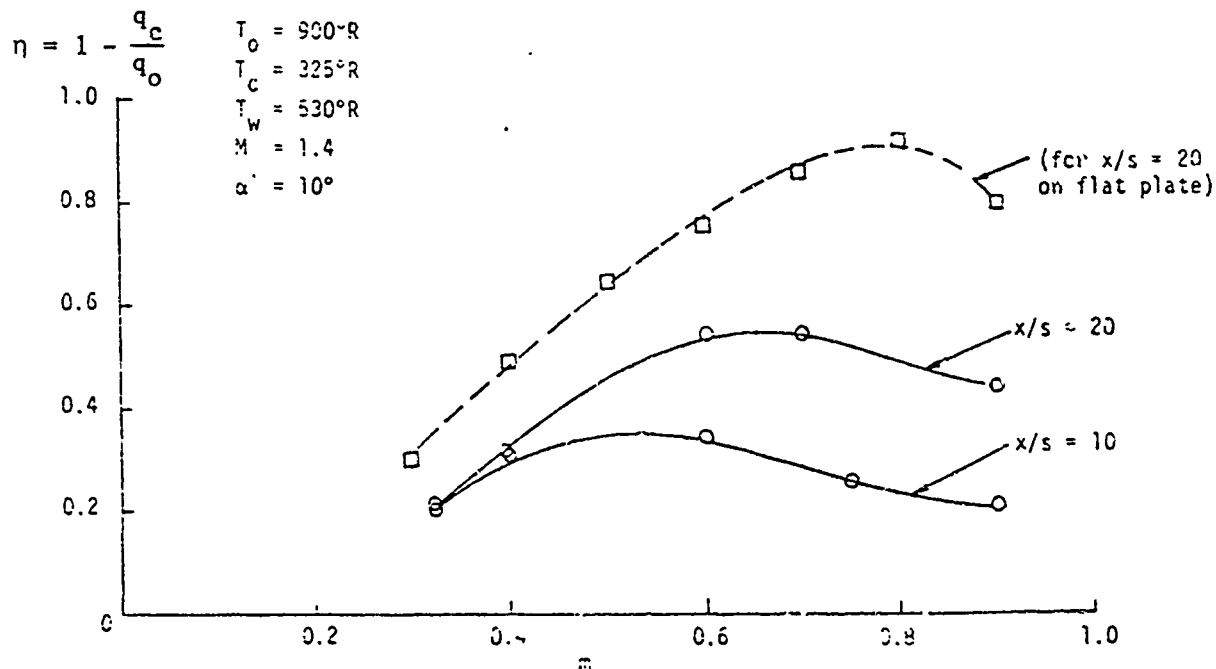
Figure 4. Variation of η with m for trailing edge. Injection from suction side only

Boundary Layer
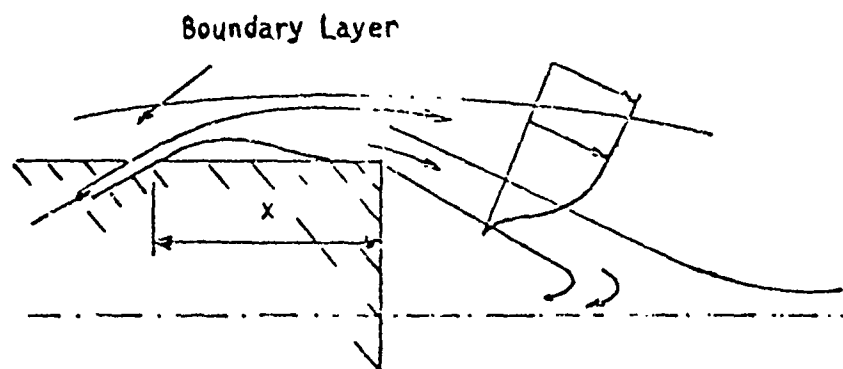
(a) Coolant Film Reattaches before Trailing Edge

Most of the coolant
flow stays in the upper
reaches of shear layer

$x < x_{re}$
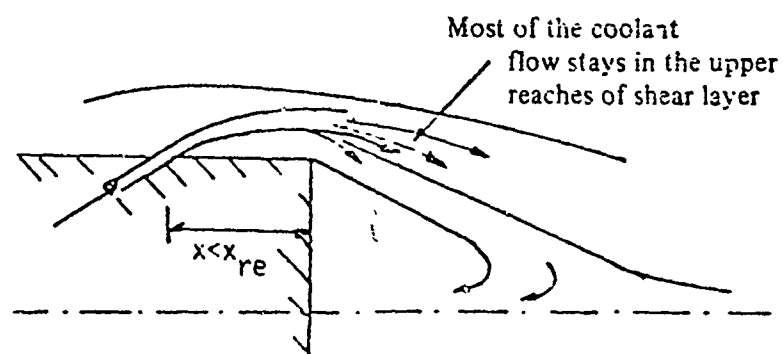
(b) Coolant Film Does Not Reattach before Trailing Edge

Figure 5. Effect of the distance x on the coolant film
entrainment into the recirculating region

63
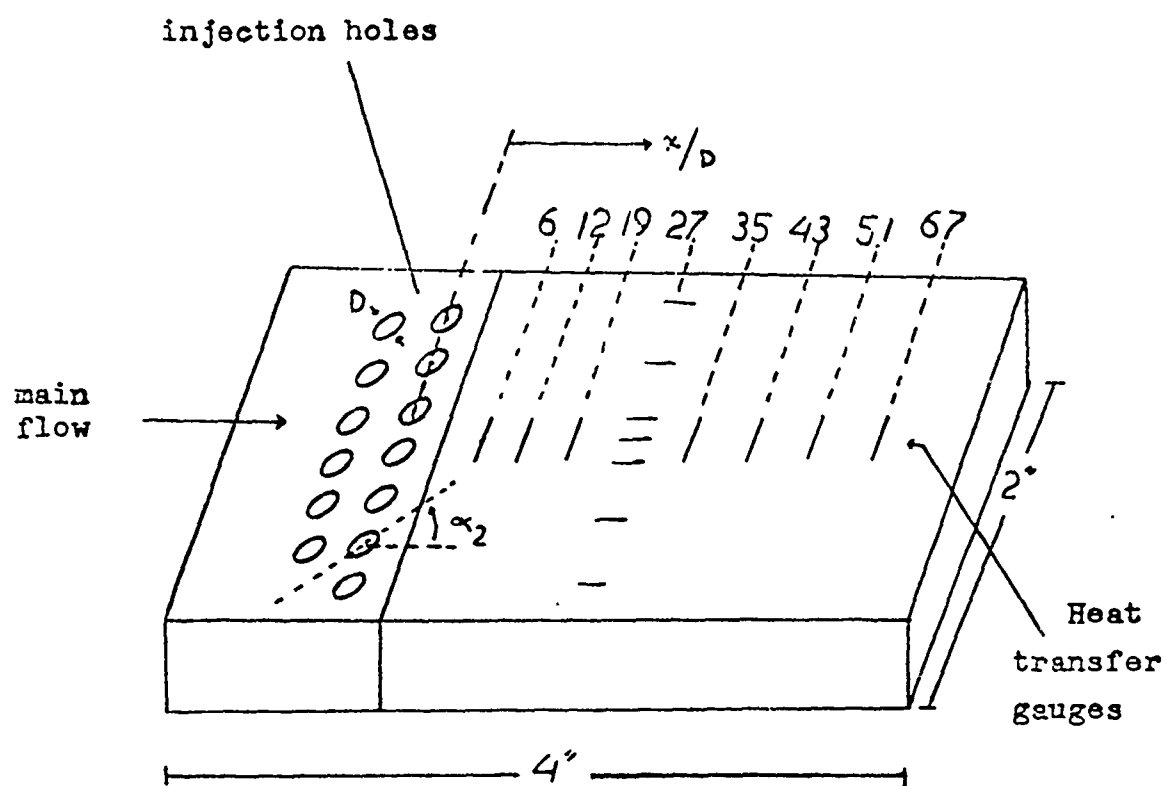
Figure 6(a). Layout of flat plate with double line of holes
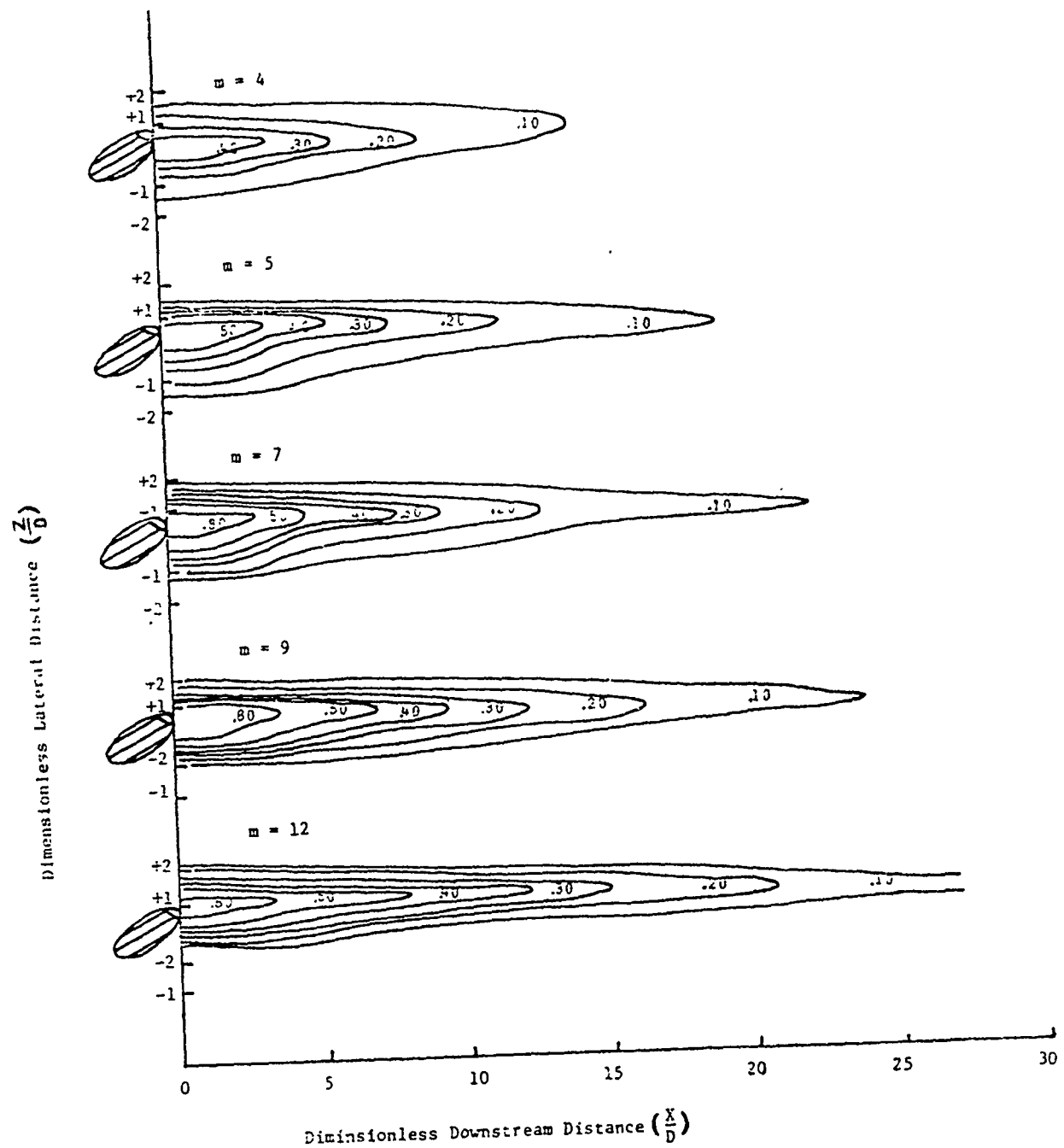
Figure 6(b). Effectiveness footprints obtained from the single hole experiments

65
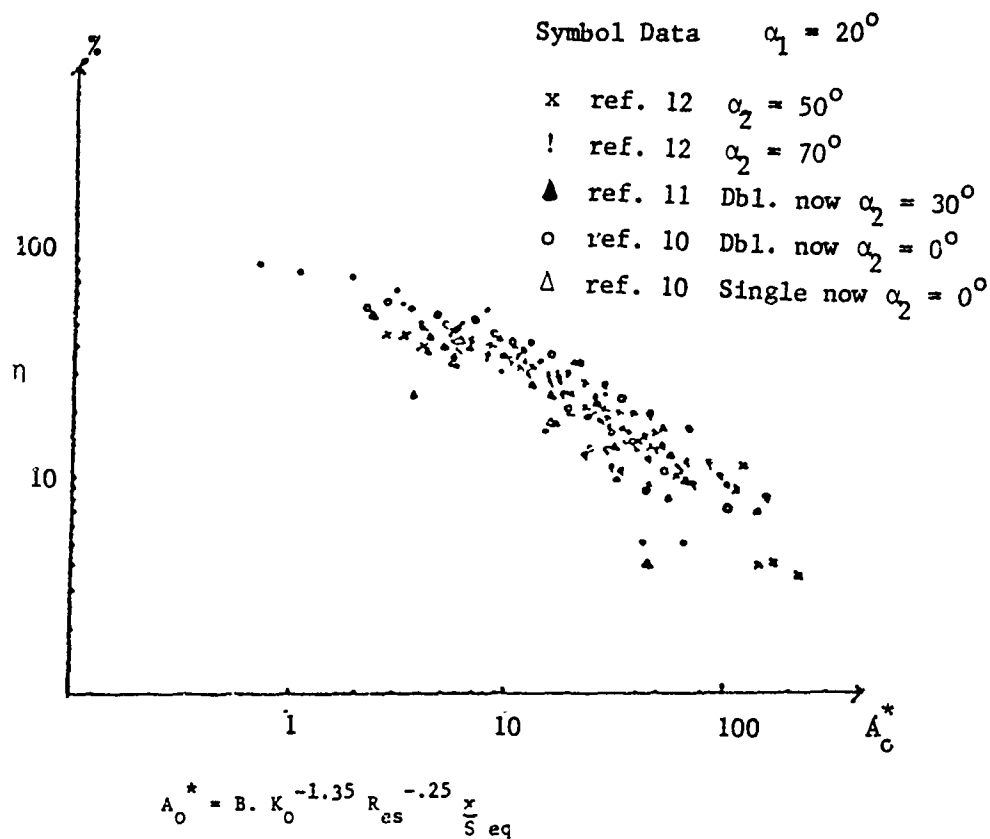
Figure 7. Hole data correlated by using the equivalent slot width

$$A_o^* = B \cdot K_o^{-1.35} R_{es}^{-.25} \frac{x}{S}\bigg|_{eq}$$
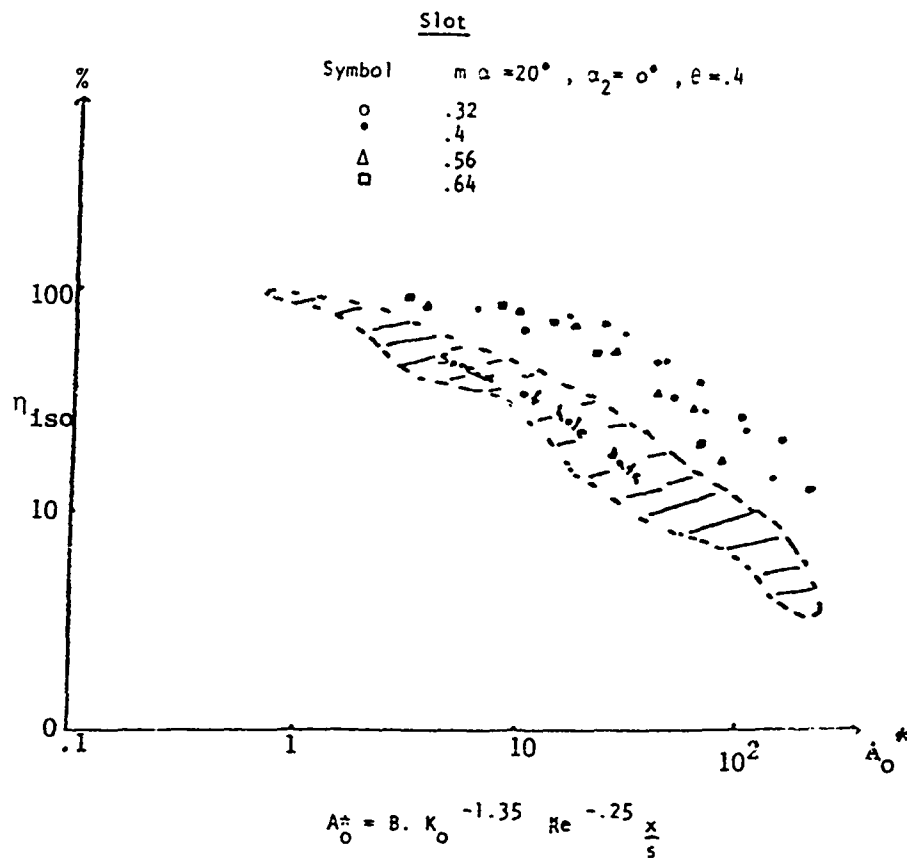
Figure 8. Slot data[10] compared to hole data from Figure 7

$$A_o^* = B \cdot K_o^{-1.35} Re^{-.25} \frac{x}{s}$$
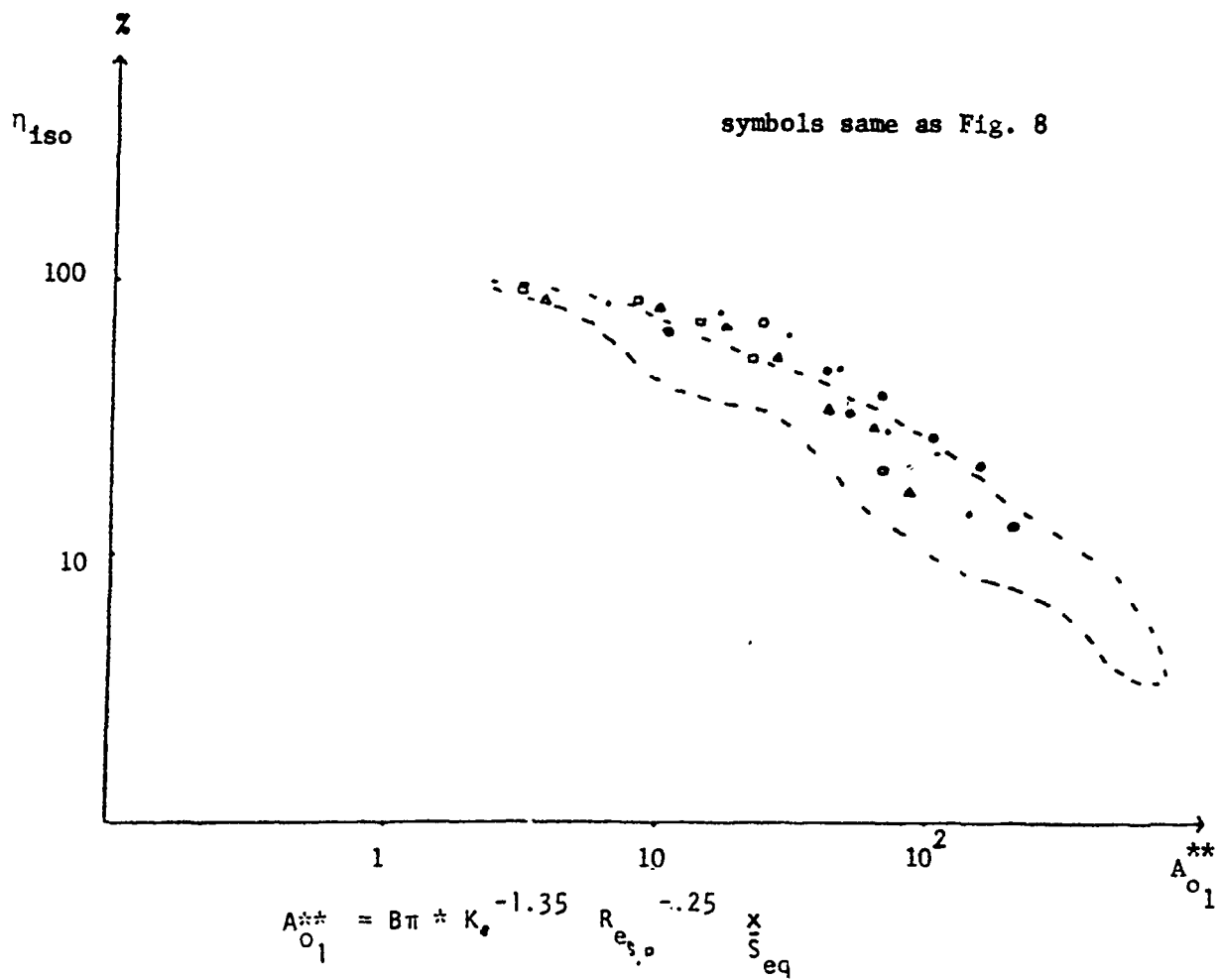
Figure 9.   The hole and slot data align using the π^* correction in the parameter A_o

			# of		
Holes:	Symbol	Ref.	rows	θ	α_2
	x	(11)	2	.4	30°
	Y	(11)	1	.4	30°
	•	(10)	2	.31	0°
	▲	(10)	1	.54	0°
	σ	(12)	2	.4	50°
	φ	(12)	2	.4	70°
Slots:					
	o	(10)	–	.4	0°
	▵	(10)	–	.22	0°

$\alpha_1 = 20^{\circ}$ in all cases

$$A2 = \pi^{1.41} \, k_o^{-1.35} \, \frac{X}{seq.}$$
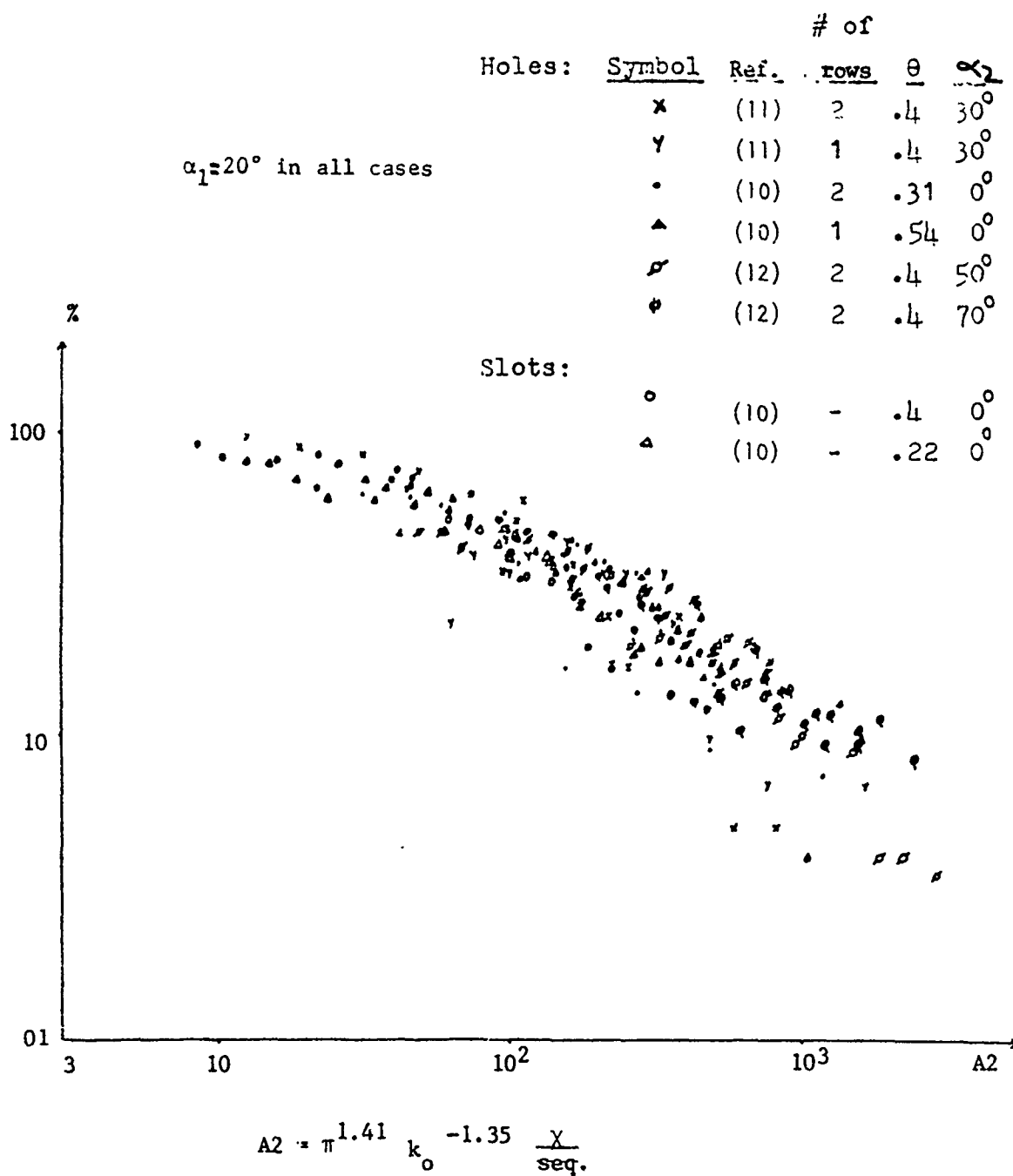
Figure 10. General correlation of film cooling data utilizing many different geometries
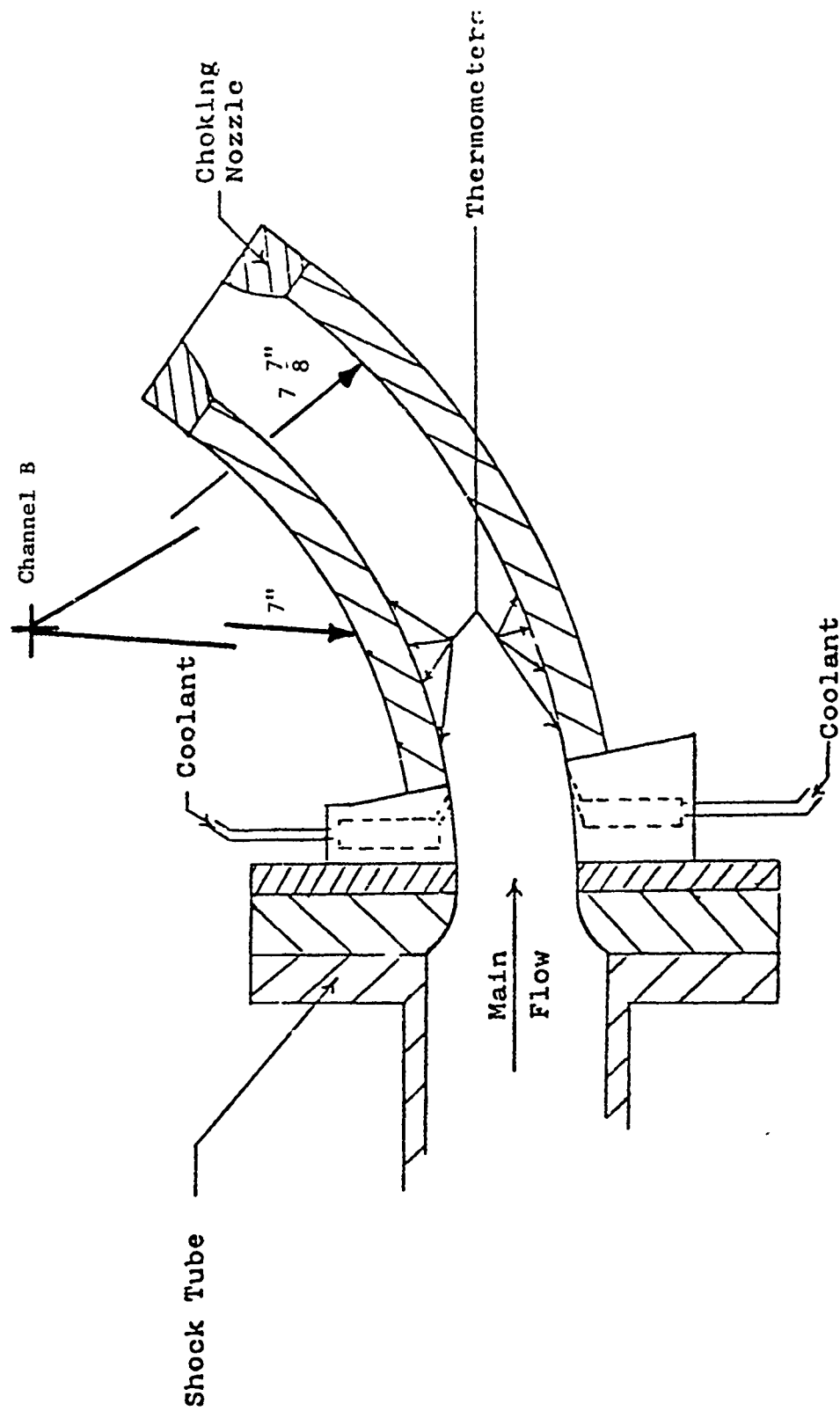
Figure 11. Schematic of test channel

69
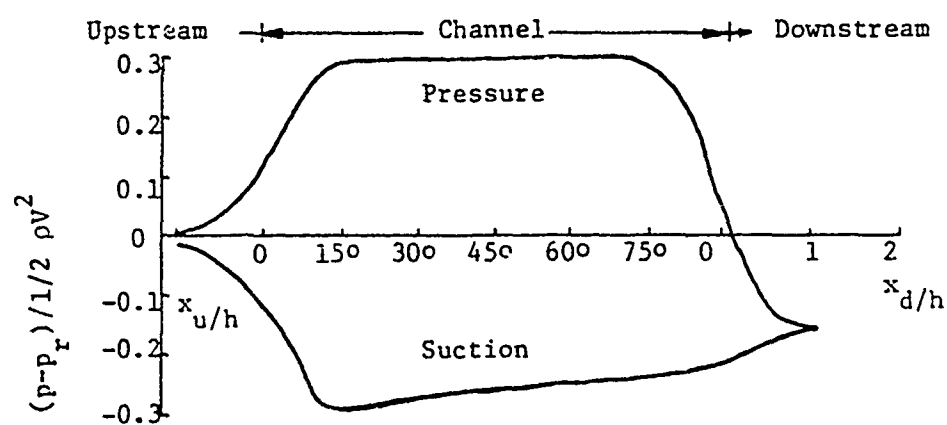
Figure 12. Static pressure distribution after Ward Smith[3]
R/h = 3.45 R_D = 10^5
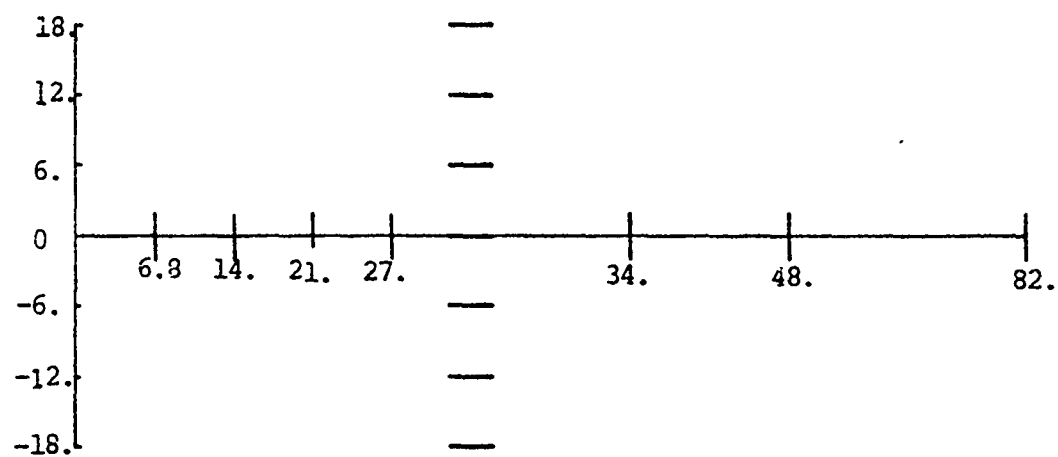
Figure 13. Thermometer placement
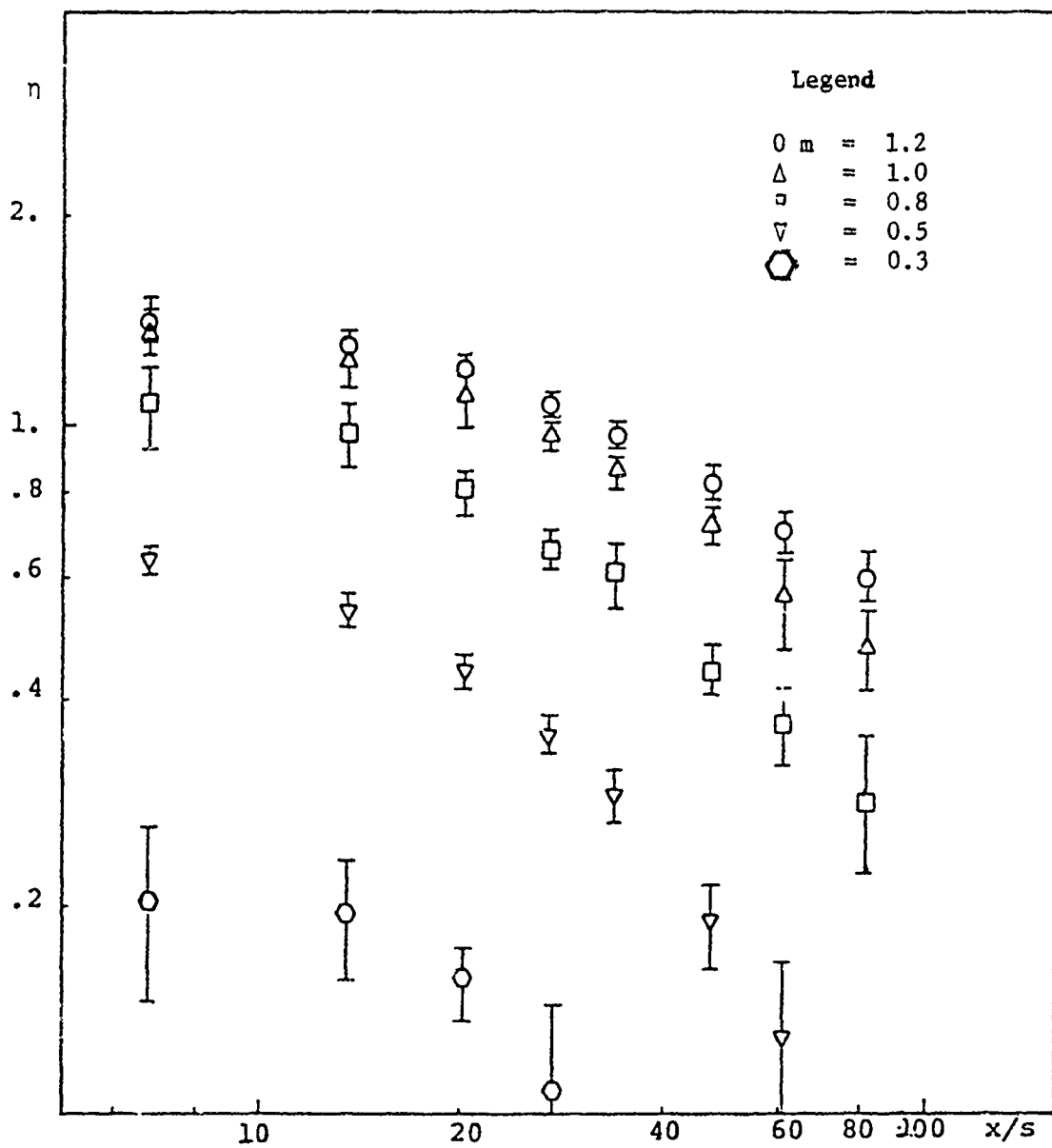
Figure 14.   Effectiveness profiles on 3 7/8" pressure surface
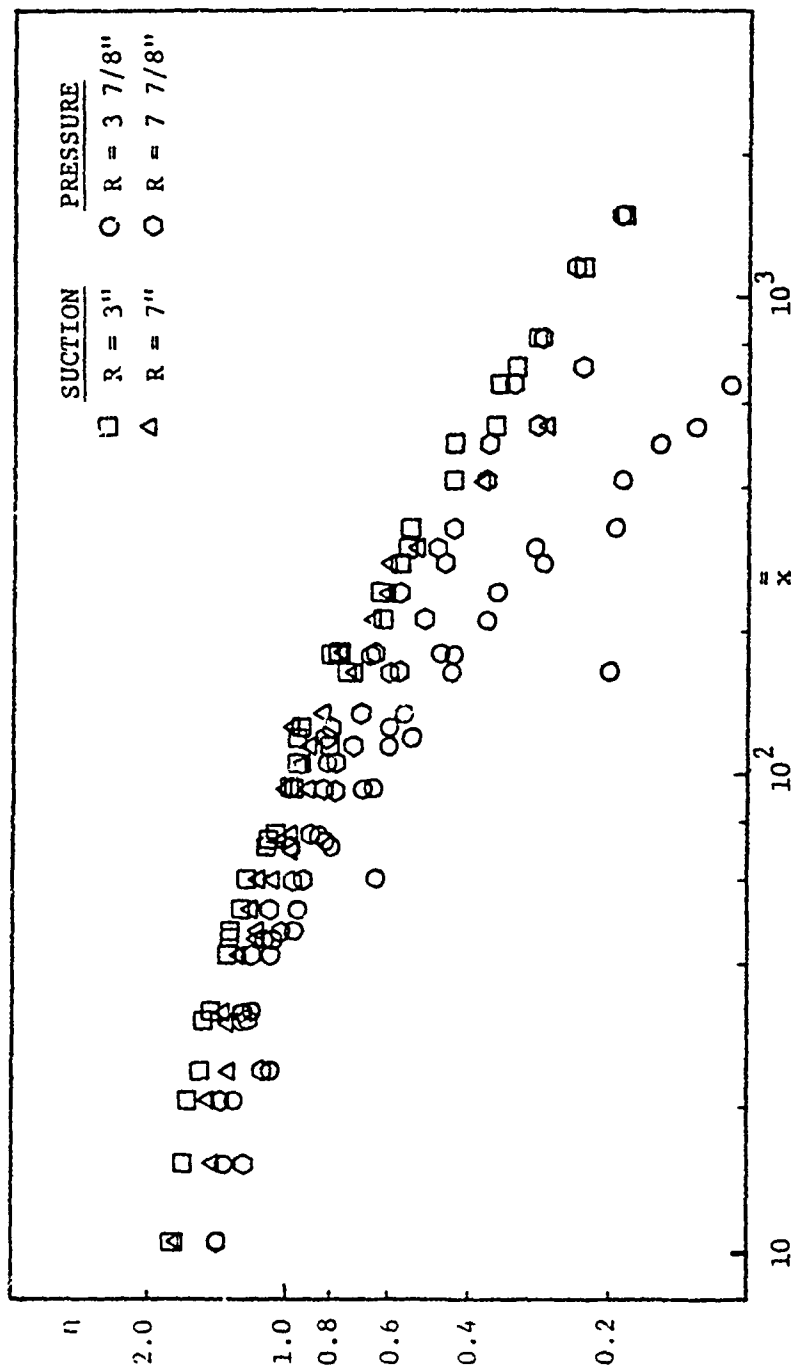
Figure 15. The $\bar{\bar{x}} = \dfrac{x}{sK_0^2}$ Correlation

73
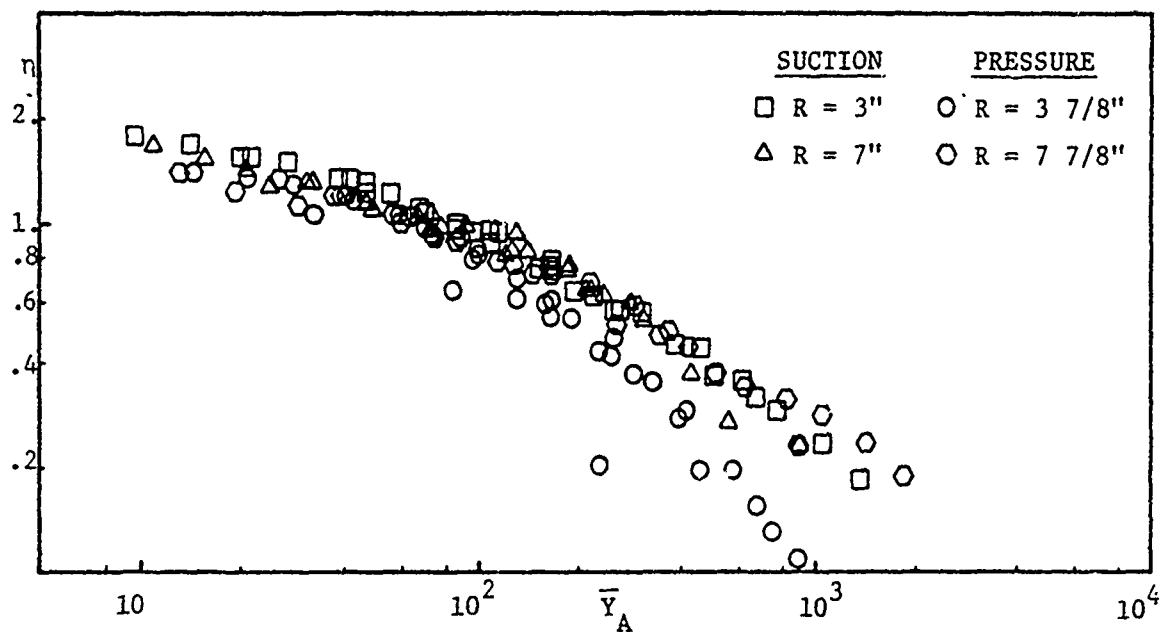
Figure 16.   The $\overline{Y}_A = K_0^{-2} \ [\cos^2\alpha \pm 92.0 \ \dfrac{D}{R}\dfrac{s}{R} \ \sin^2\alpha]^{-1} \ \dfrac{x}{s}$ Correlation
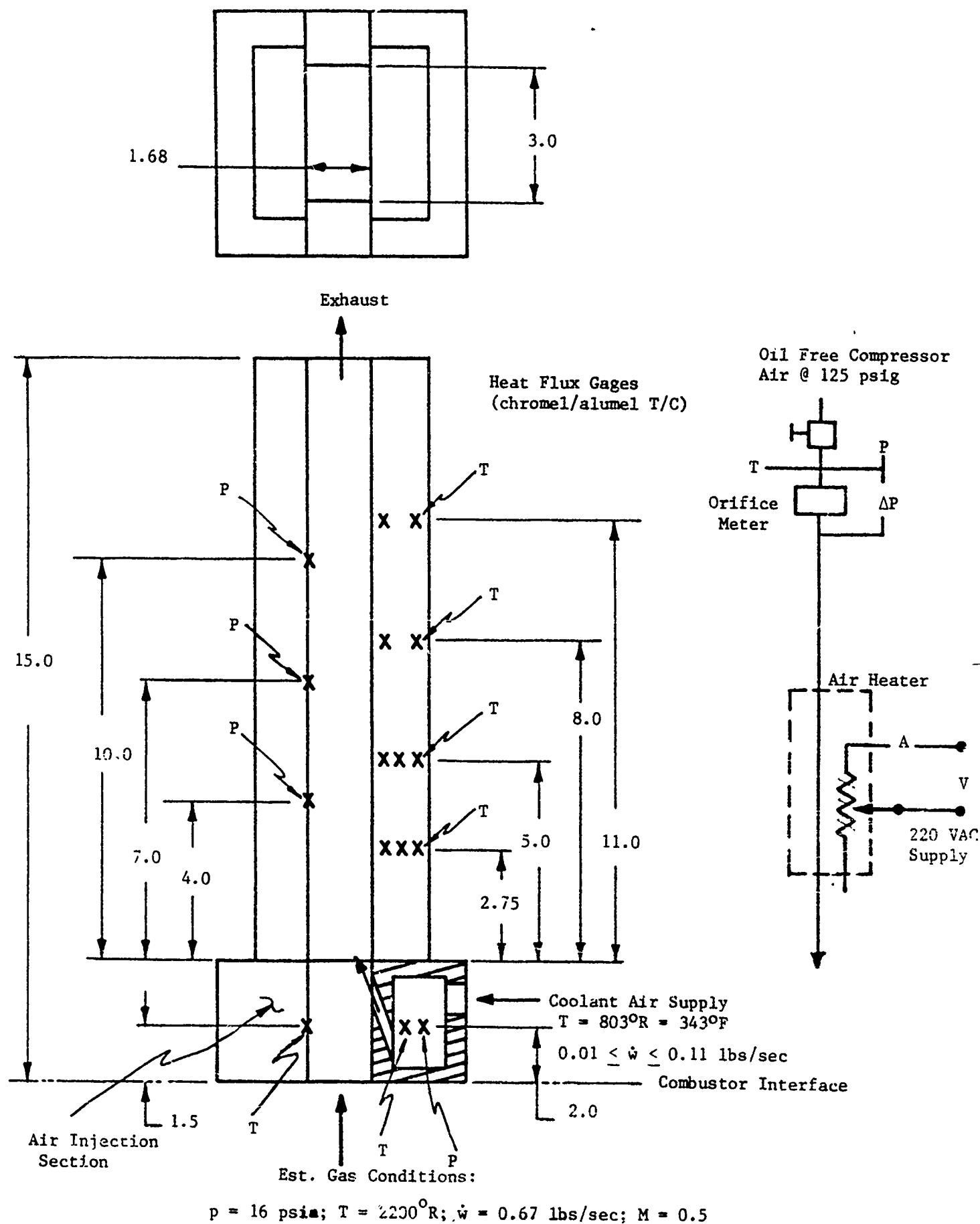
Figure 17. Film Cooling Test Schematic
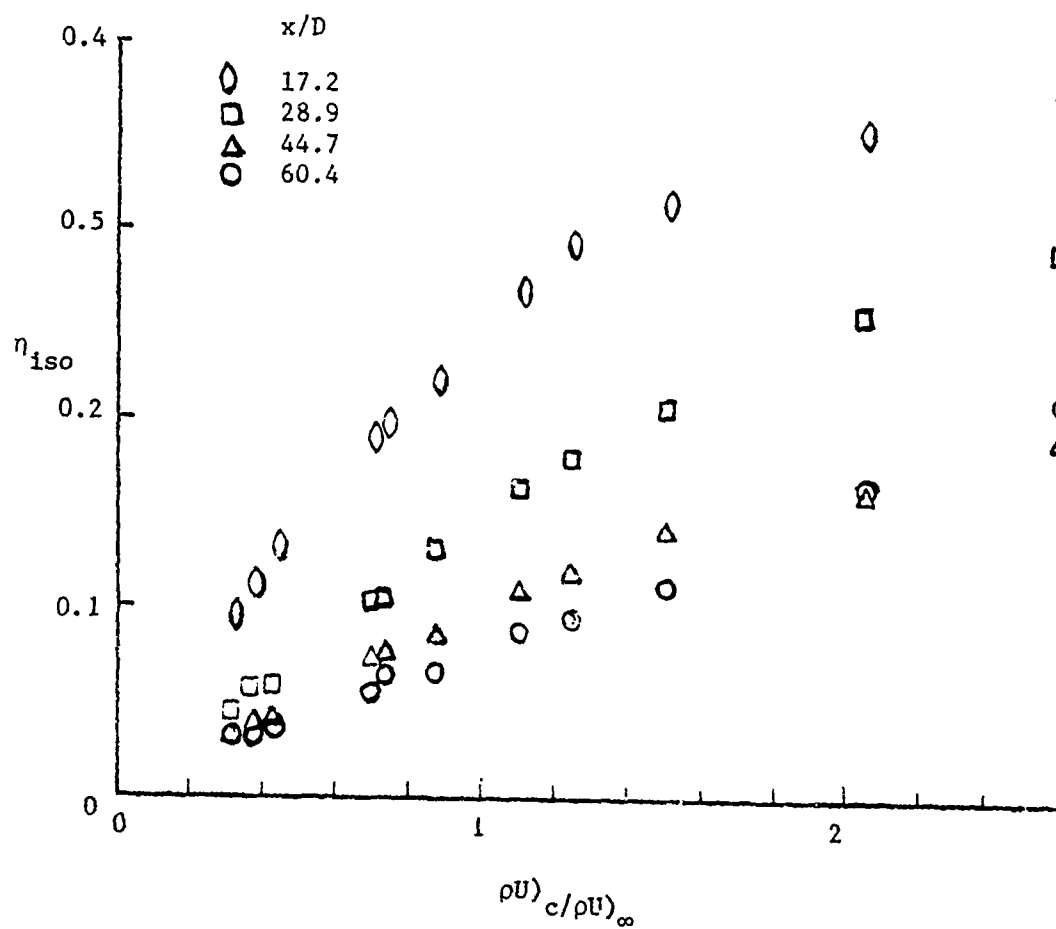
Figure 18. Isothermal Effectiveness Versus Blowing Rate (Hot Test)
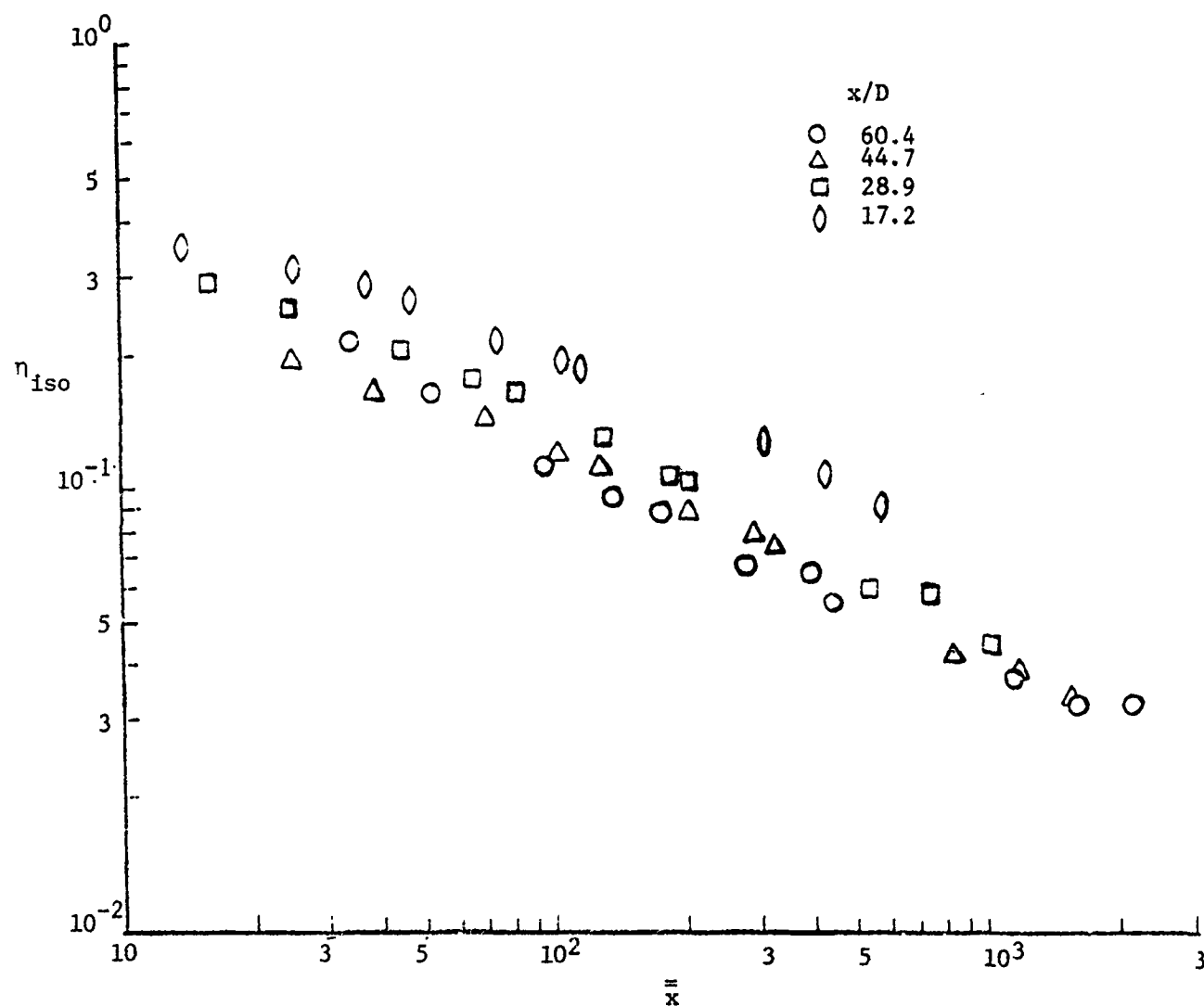
Figure 19. Correlation of Film Cooling Data From Hot Test
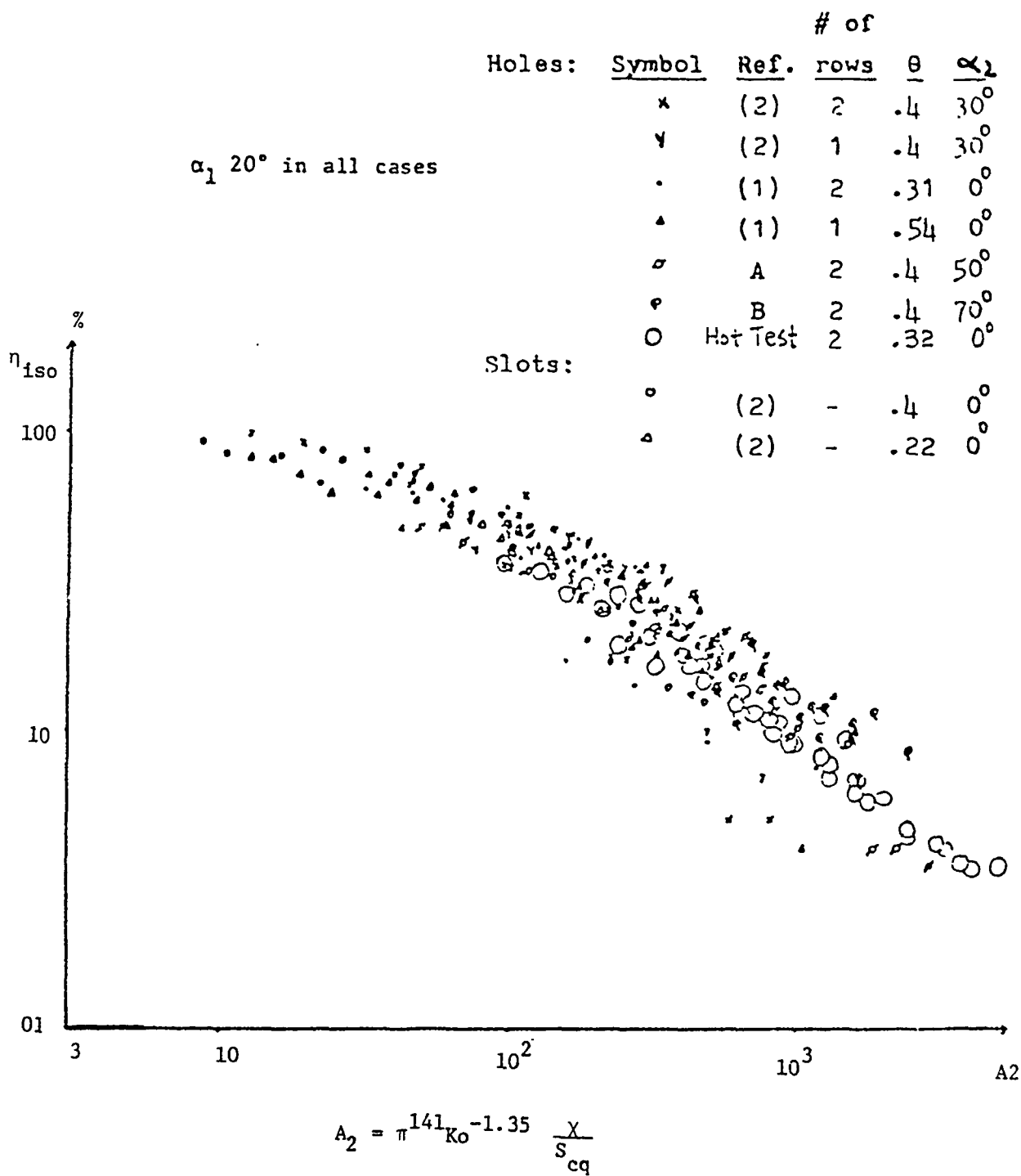
Figure 20. Comparison of Shock Tunnel and Hot Test Results
with Correlation η_{iso} Versus A_2
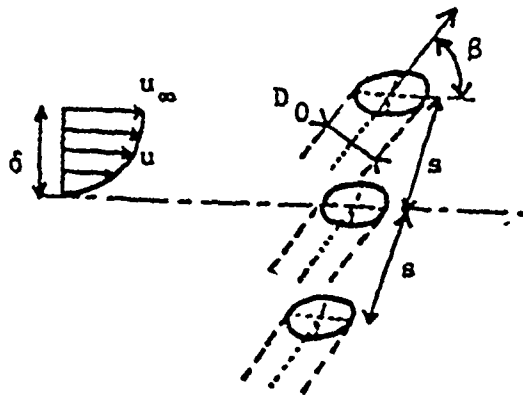
FIG. 21. EJECTION CONFIGURATION
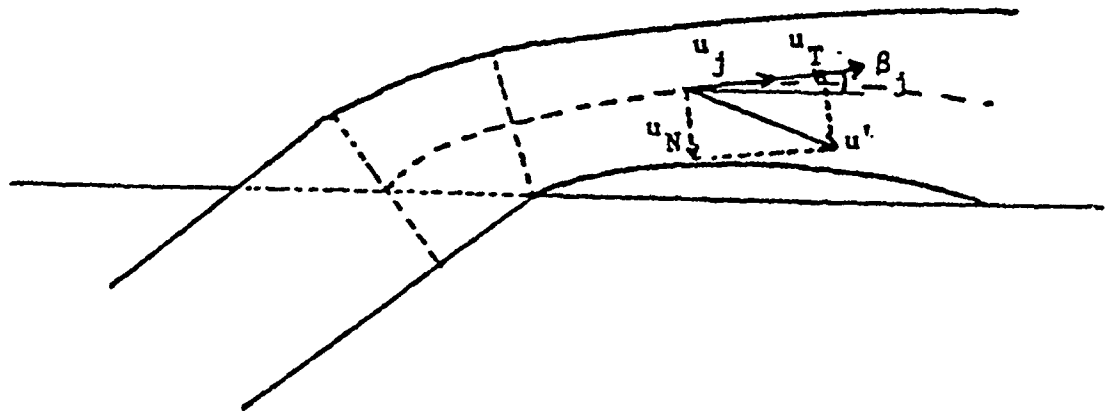
FIG 22. JET PARAMETERS
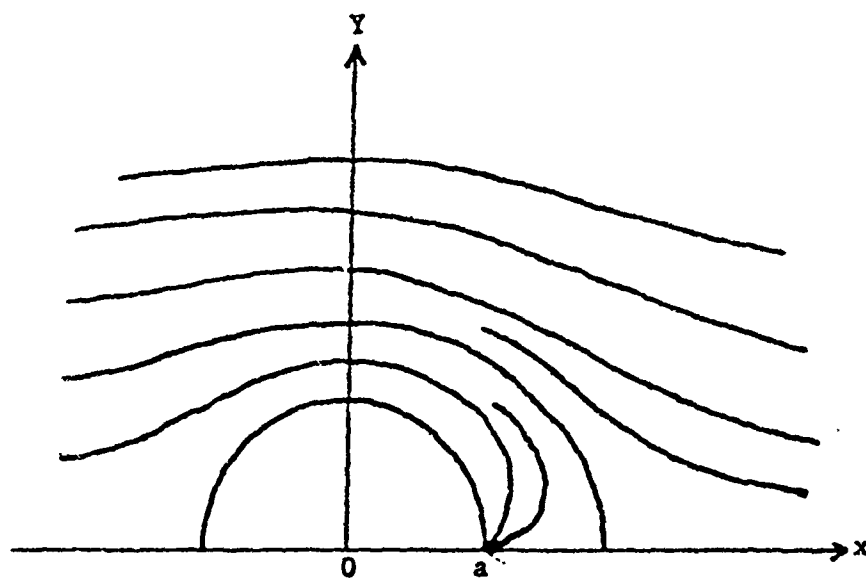
FIG 23. STREAMLINE DUE TO A SINK SINGULARITY BEHIND A CYLINDER
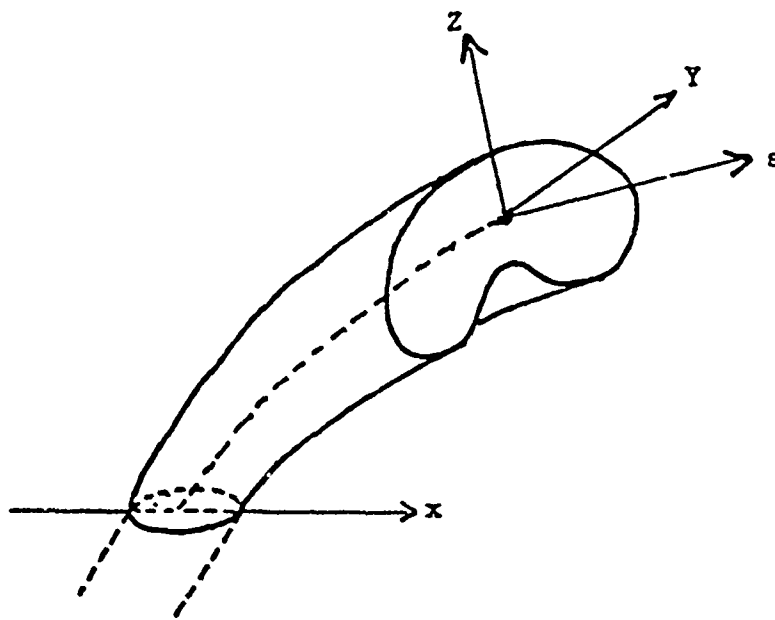
FIG. 24. JET CROSS SECTION AND CURVILINEAR COORDINATES
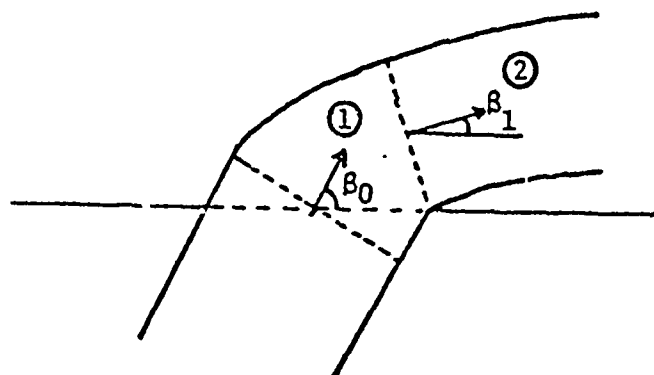
FIG. 25. SECTIONS OF THE JET
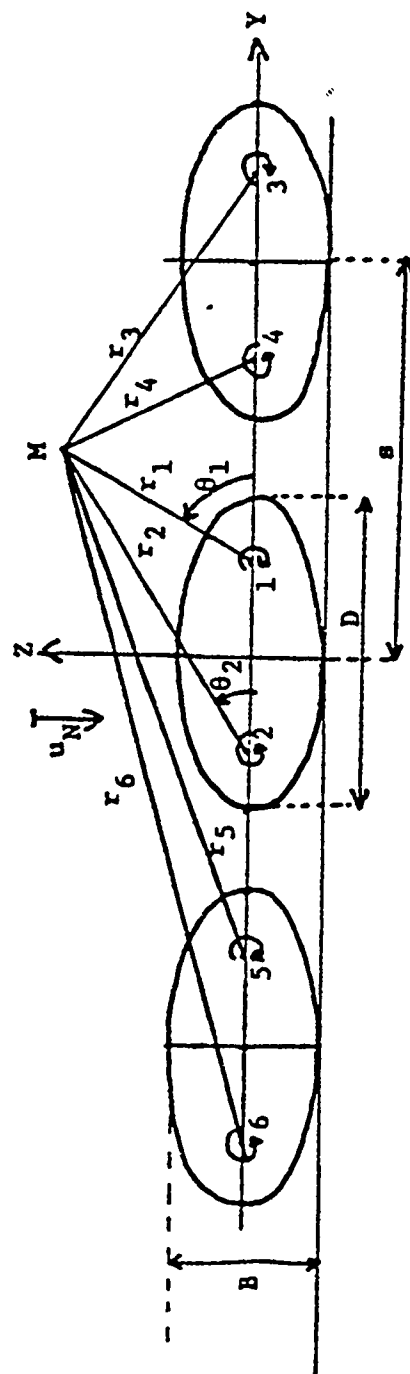
FIG. 26. CONTRAROTATING VORTICES IN THE FIRST SECTION
OF THE FREE JET
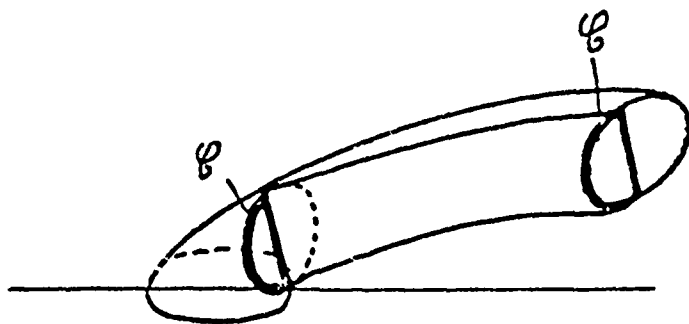
FIG. 27. CURVE $\mathscr{C}$ ALONG WHICH KELVIN'S CIRCULATION THEOREM IS APPLIED
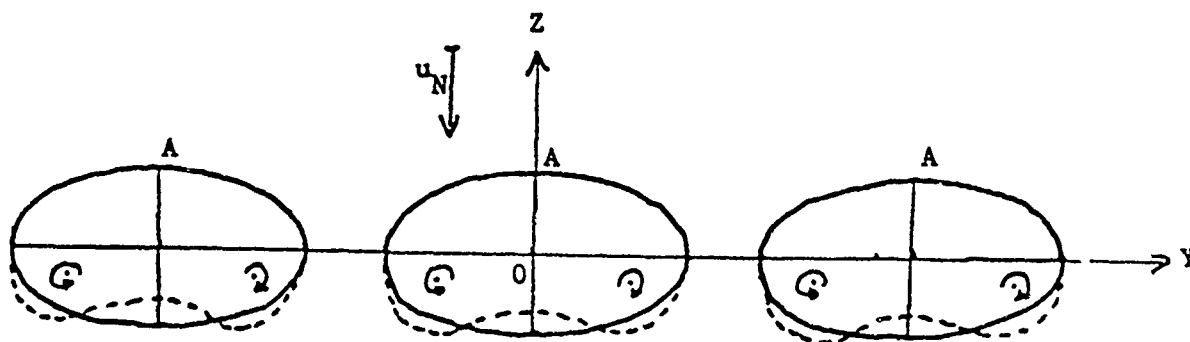
FIG 28. CONTRAROTATIVE VORTICES IN ANY CROSS SECTION OF THE FREE JET
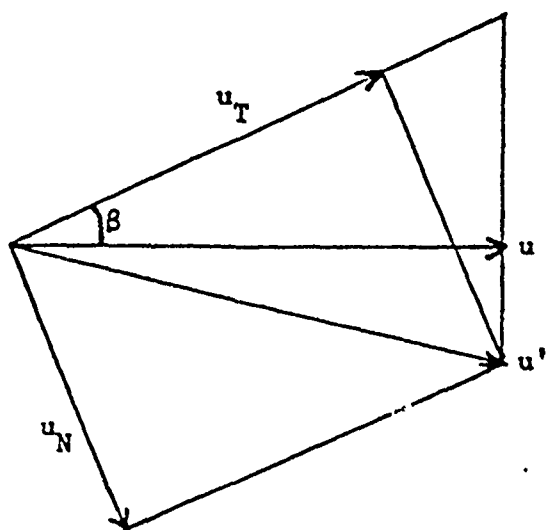
FIG. 29. TANGENTIAL AND NORMAL MAIN FLOW VELOCITY IN THE VICINITY OF THE JETS
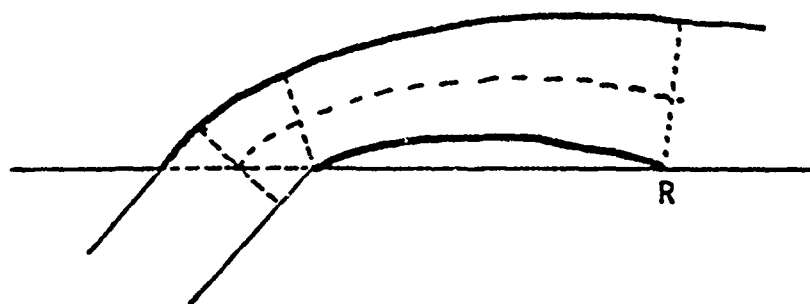
FIG. 30. REATTACHMENT OF THE JETS
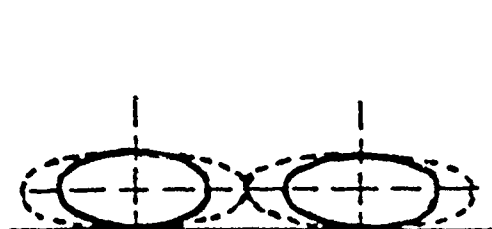
a) Jets reattach before
    touching one another
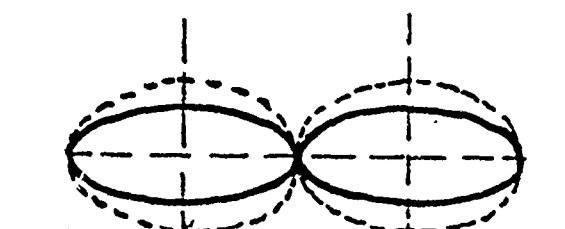
b) Jets are in contact with
    one another before reattaching

FIG. 31. GROWTH OF THE JETS
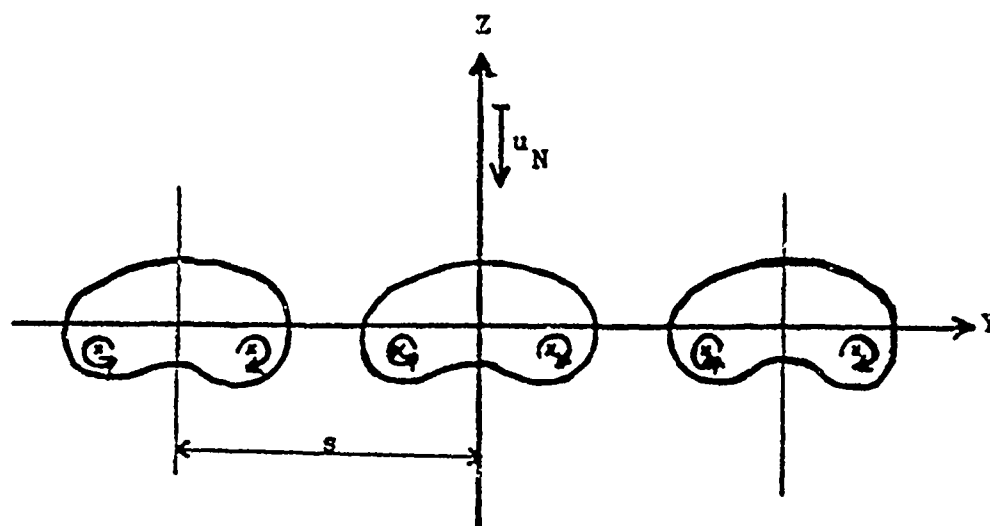
FIG. 32. VELOCITY INDUCED ON A VORTEX IN THE CROSS SECTION
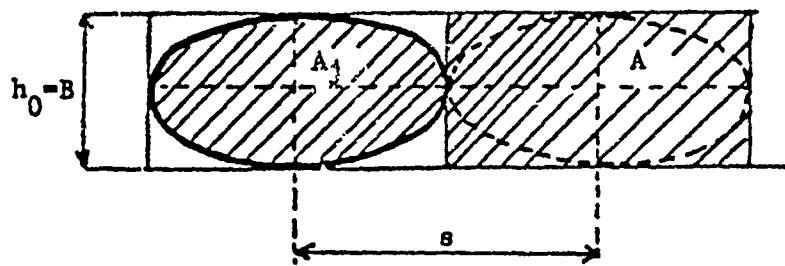
FIG. 33. TRANSFORMATION FROM THE JETS INTO A LAYER
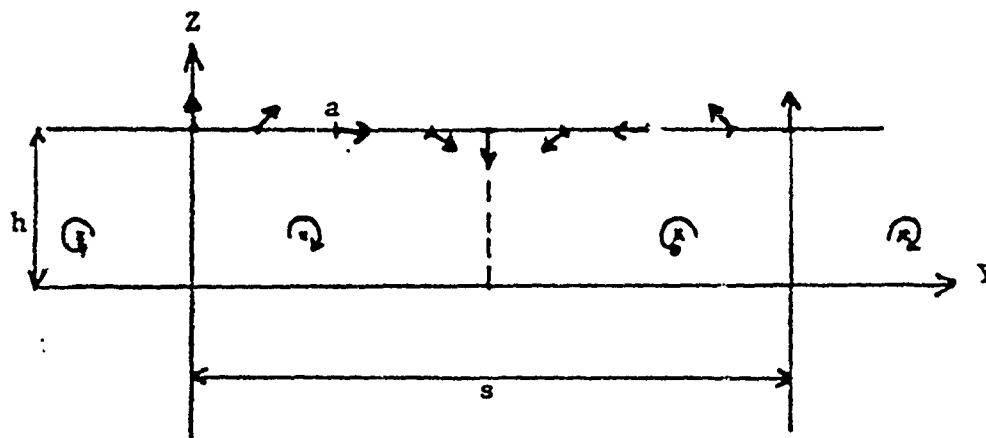
FIG. 34. FLOW ENTERING THE LAYER DUE TO THE VORTICES
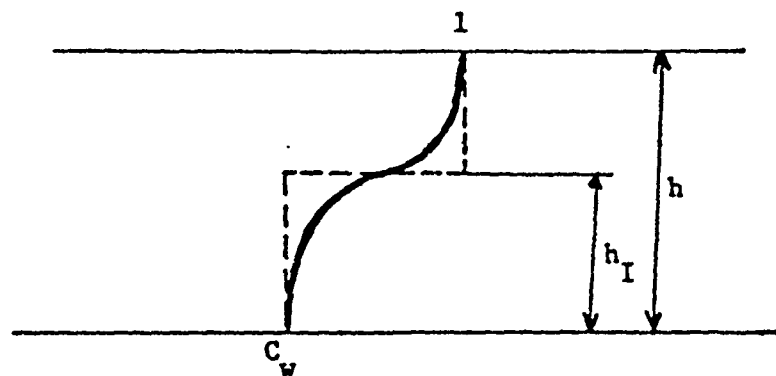
FIG. 35. CONCENTRATION PROFILE

84
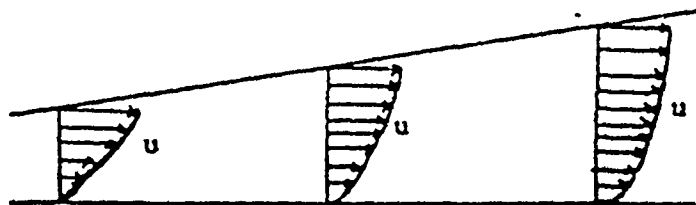
FIG. 36.   EVOLUTION OF THE VELOCITY PROFILE
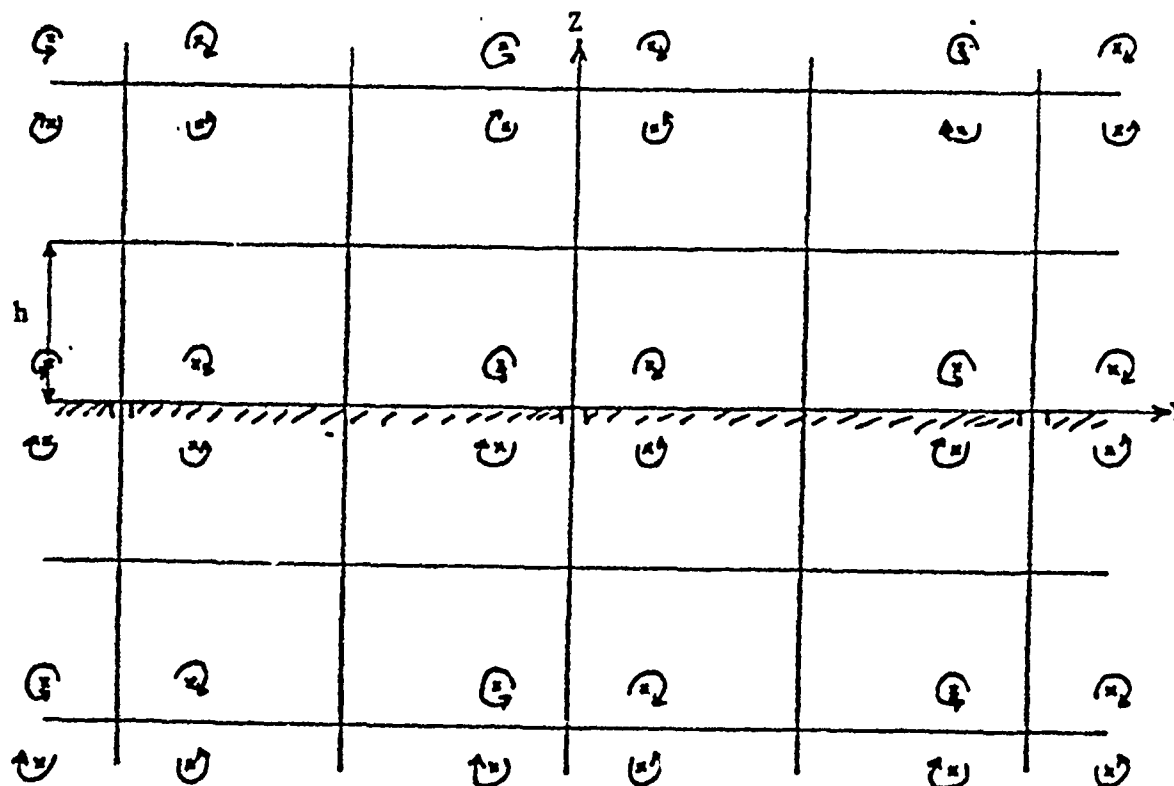
FIG. 37.   VELOCITY FIELD INSIDE THE LAYER
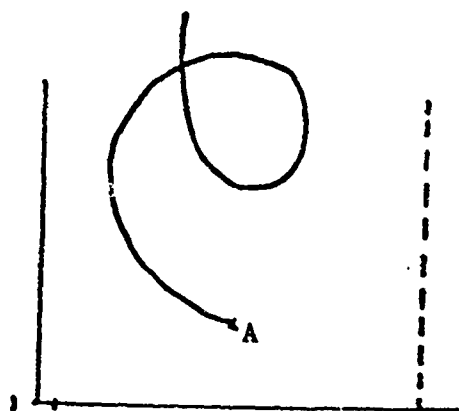
FIG. 38.   PROJECTION IN THE CROSS SECTION OF A VORTEX
TRAJECTORY

85
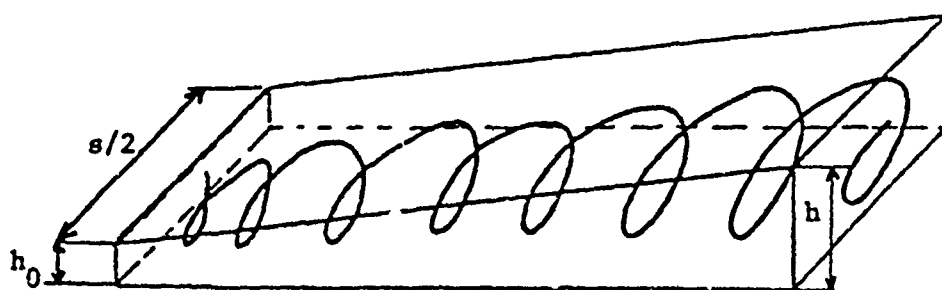
FIG. 39. TRAJECTORY OF A VORTEX IN THE LAYER

a) Without the wall

b) With the wall
(reflection on the wall)
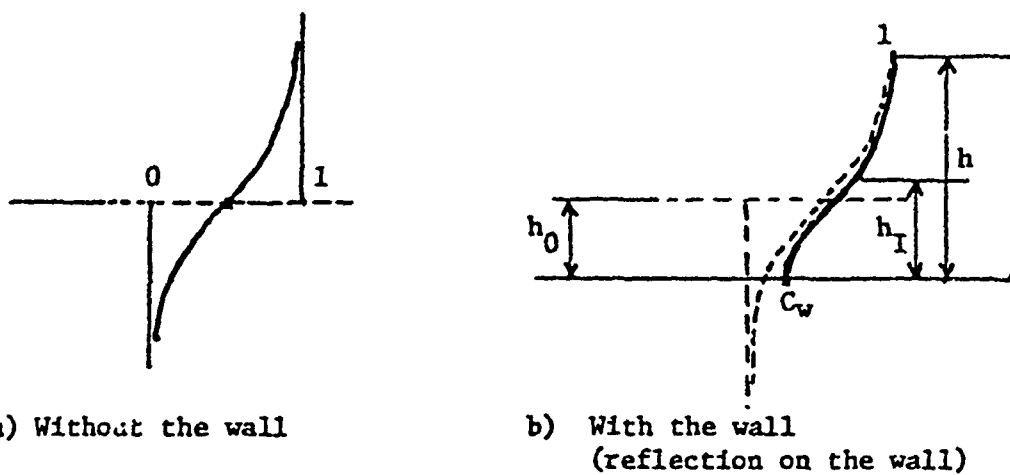
FIG. 40. CONCENTRATION PROFILE IN THE LAYER
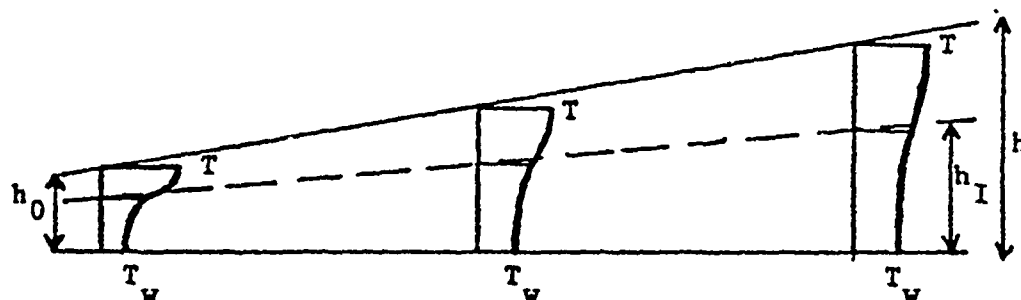
FIG. 41. TEMPERATURE PROFILES IN THE LAYER

86
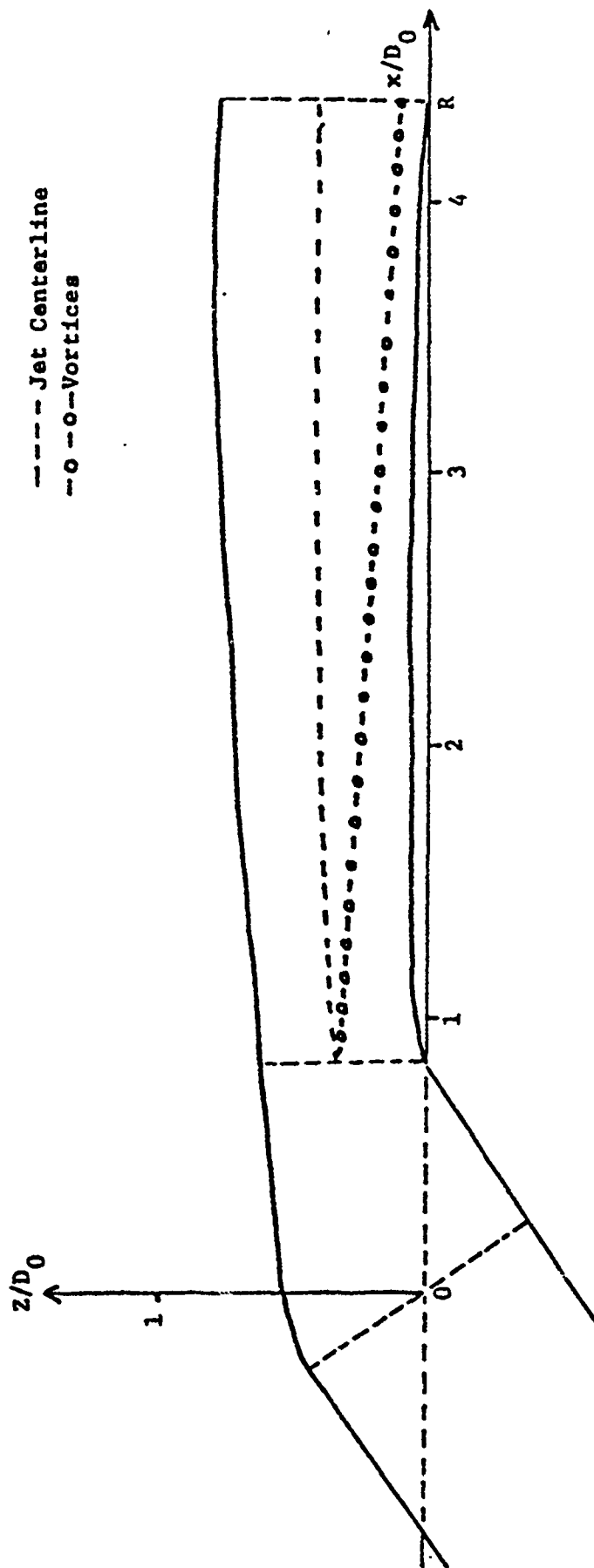
FIG. 42. JET TRAJECTORY AND PATH OF THE VORTICES IN THE JETS
(GOLDSTEIN CONDITIONS)
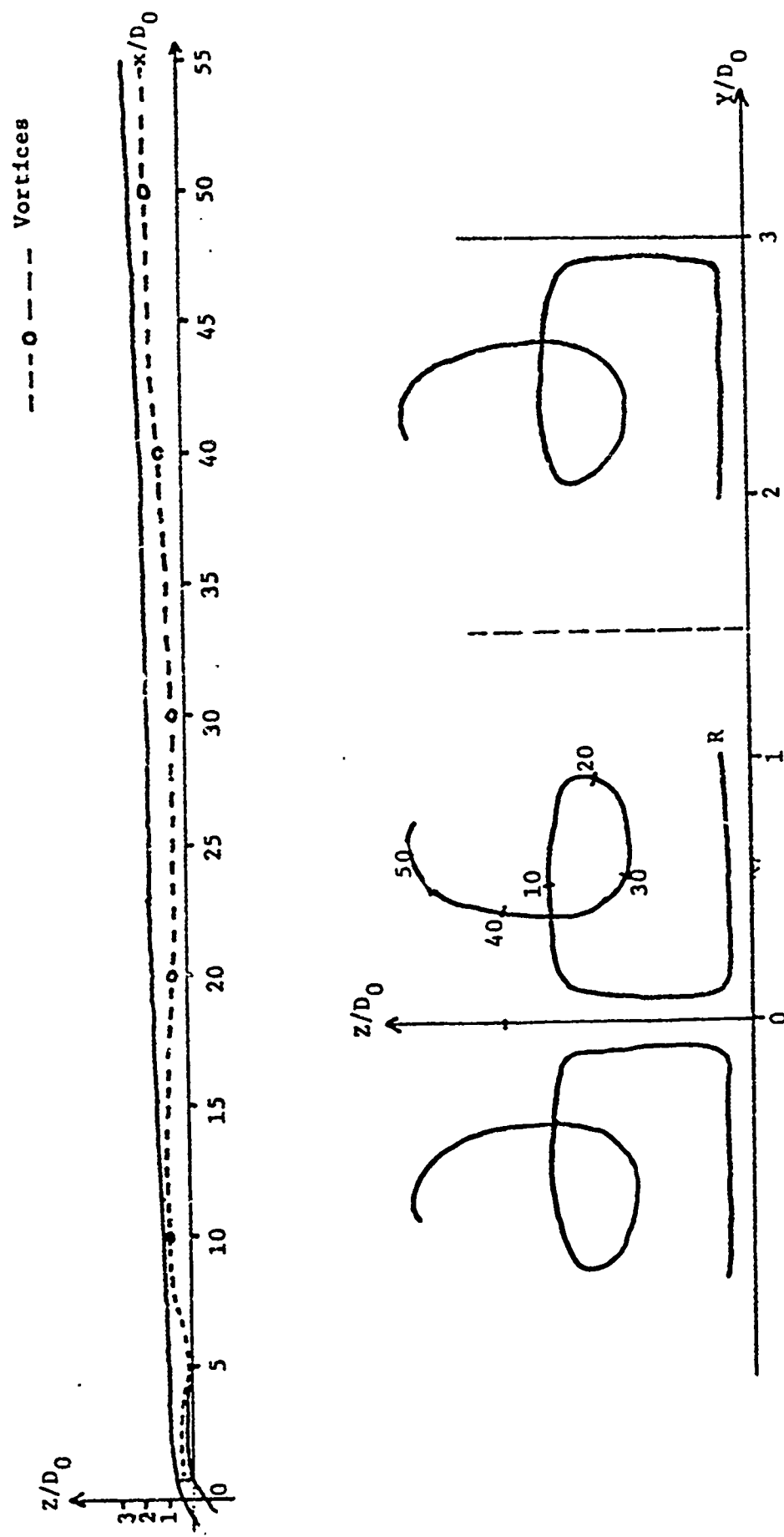
FIG. 43. GROWTH OF THE LAYER AND PATH OF THE VORTICES IN THE LAYER (GOLDSTEIN CONDITIONS)
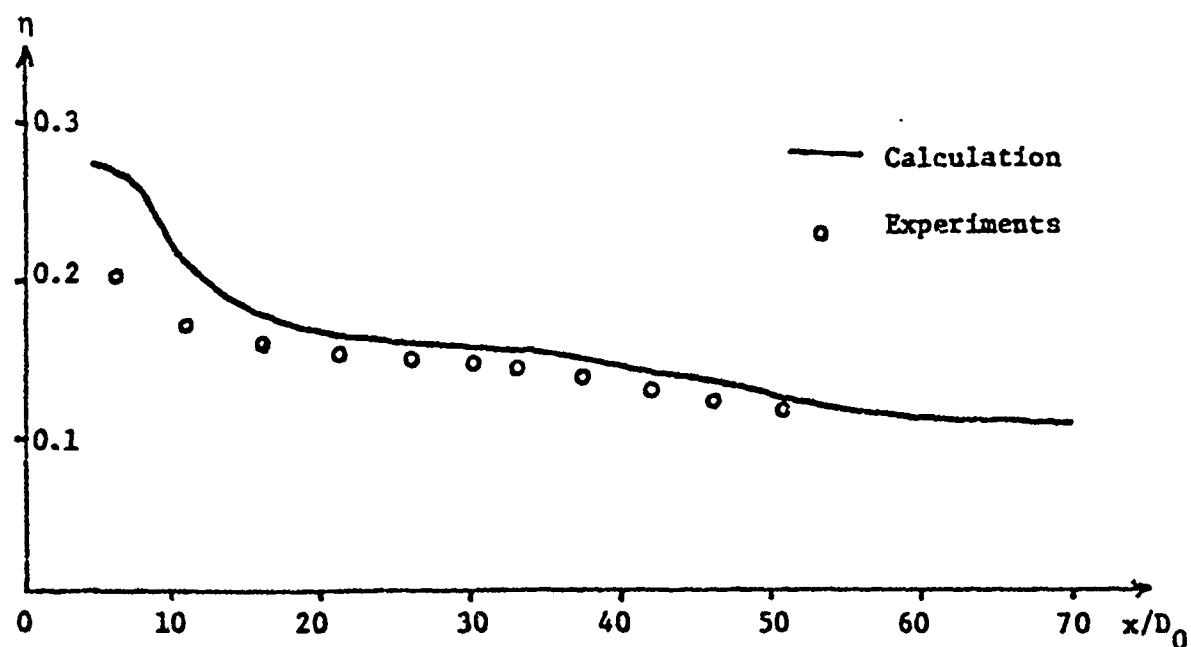
FIG. 44. FILM COOLING EFFECTIVENESS (GOLDSTEIN CONDITIONS)
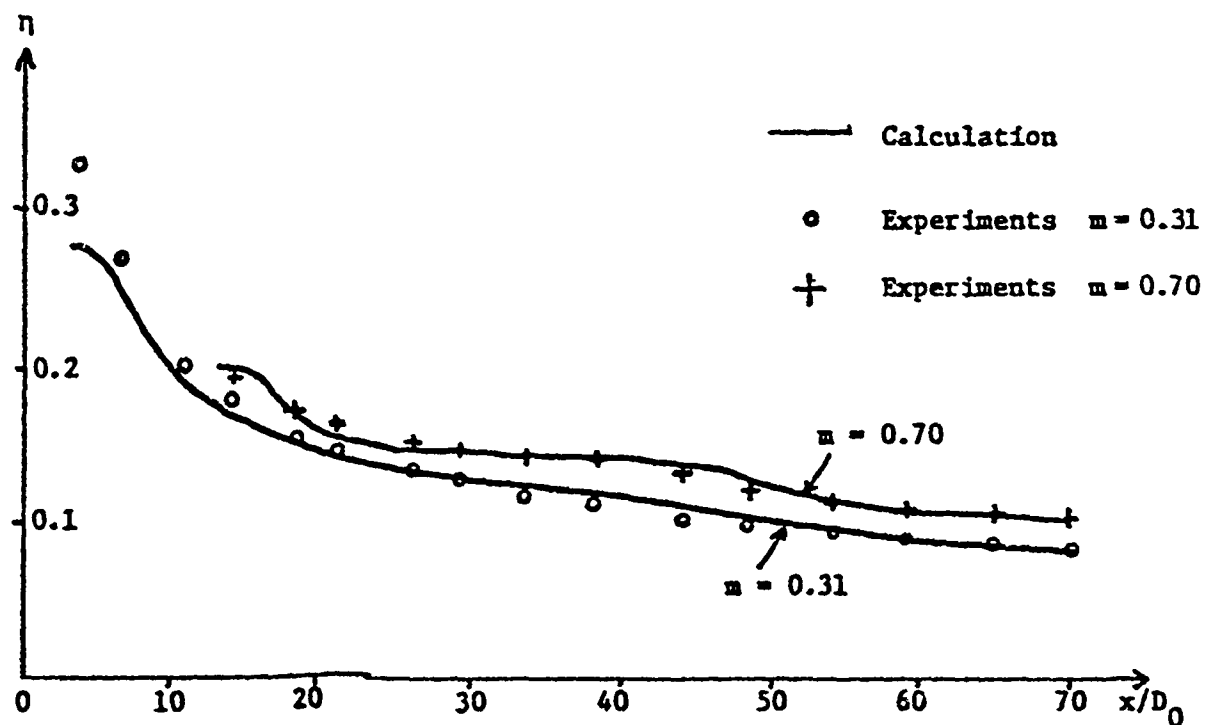
FIG. 45. FILM COOLING EFFECTIVENESS (LIESS CONDITIONS)
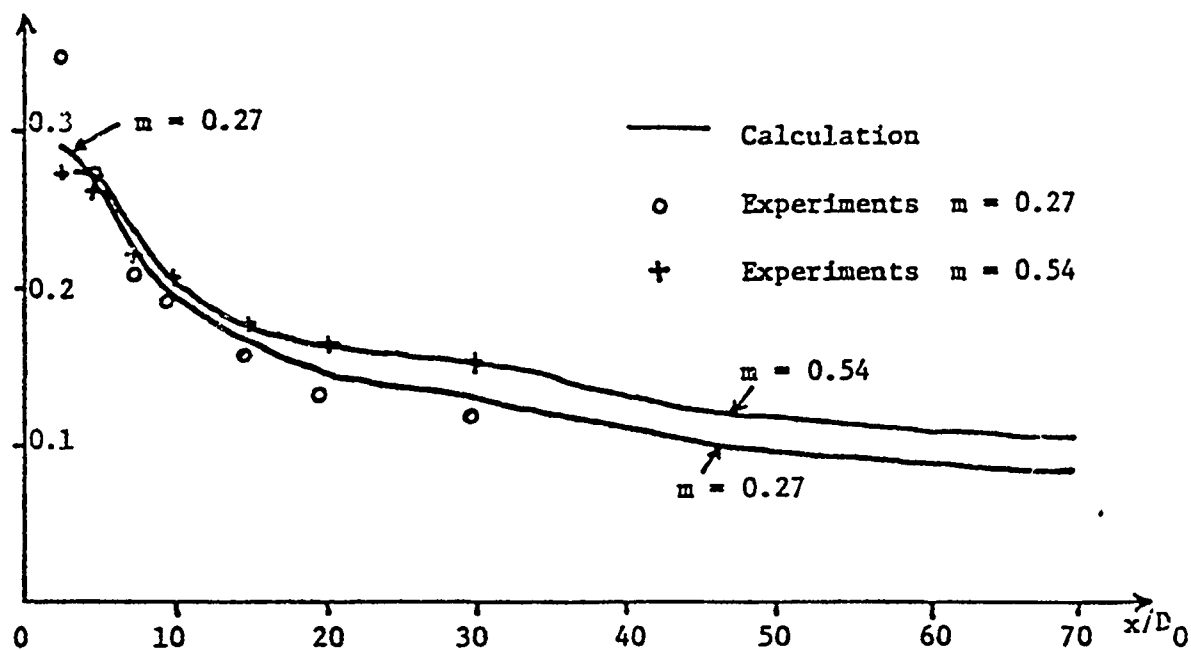
FIG. 46. FILM COOLING EFFECTIVENESS (SASAKI CONDITIONS)
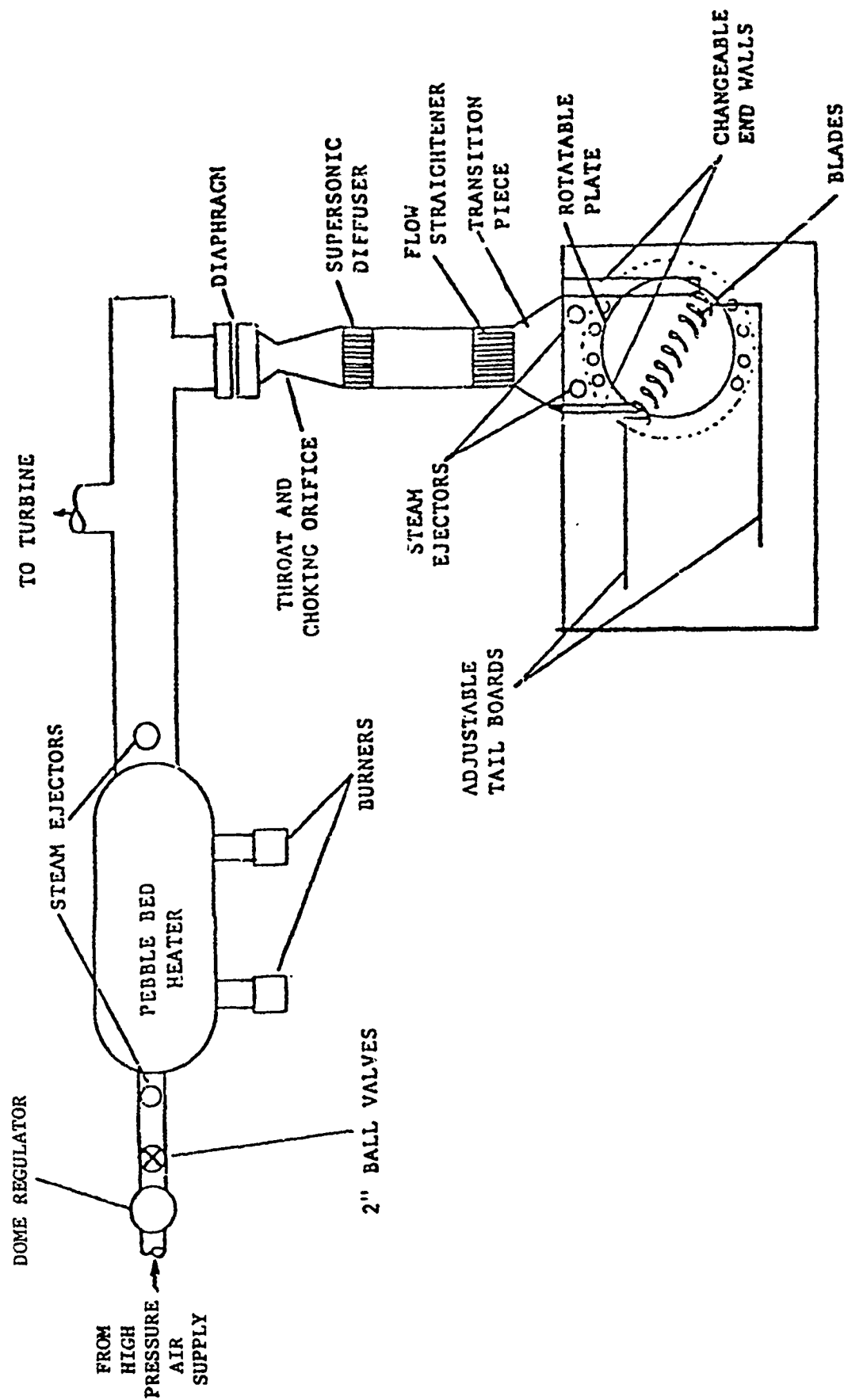
Figure 47. Hot Blowdown Facility, Cascade Side.
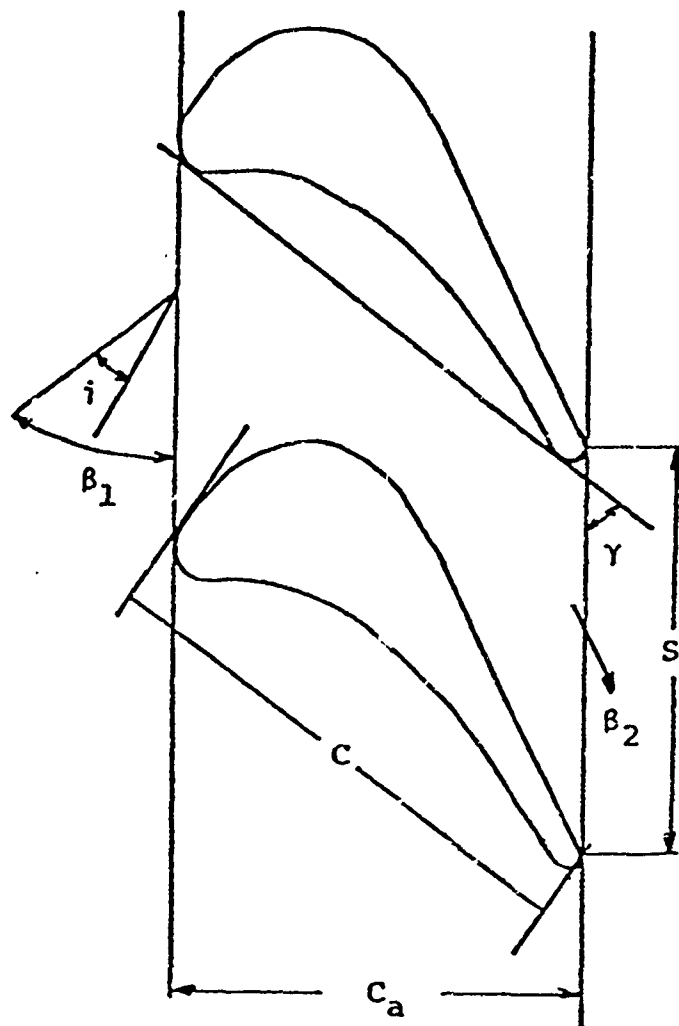
91

C   – Chord 2.6" β_1 – Inlet angle 60°

C_a – Axial Chord 2.0" γ – Stagger Angle 51°

S   – Blade Space 2.0" β_2 – Exit Angle   25°

                             i – Angle of Incidence

Figure 48. Blade Geometry.

View – <u>Section A-A</u>

View – <u>Section B-B</u>
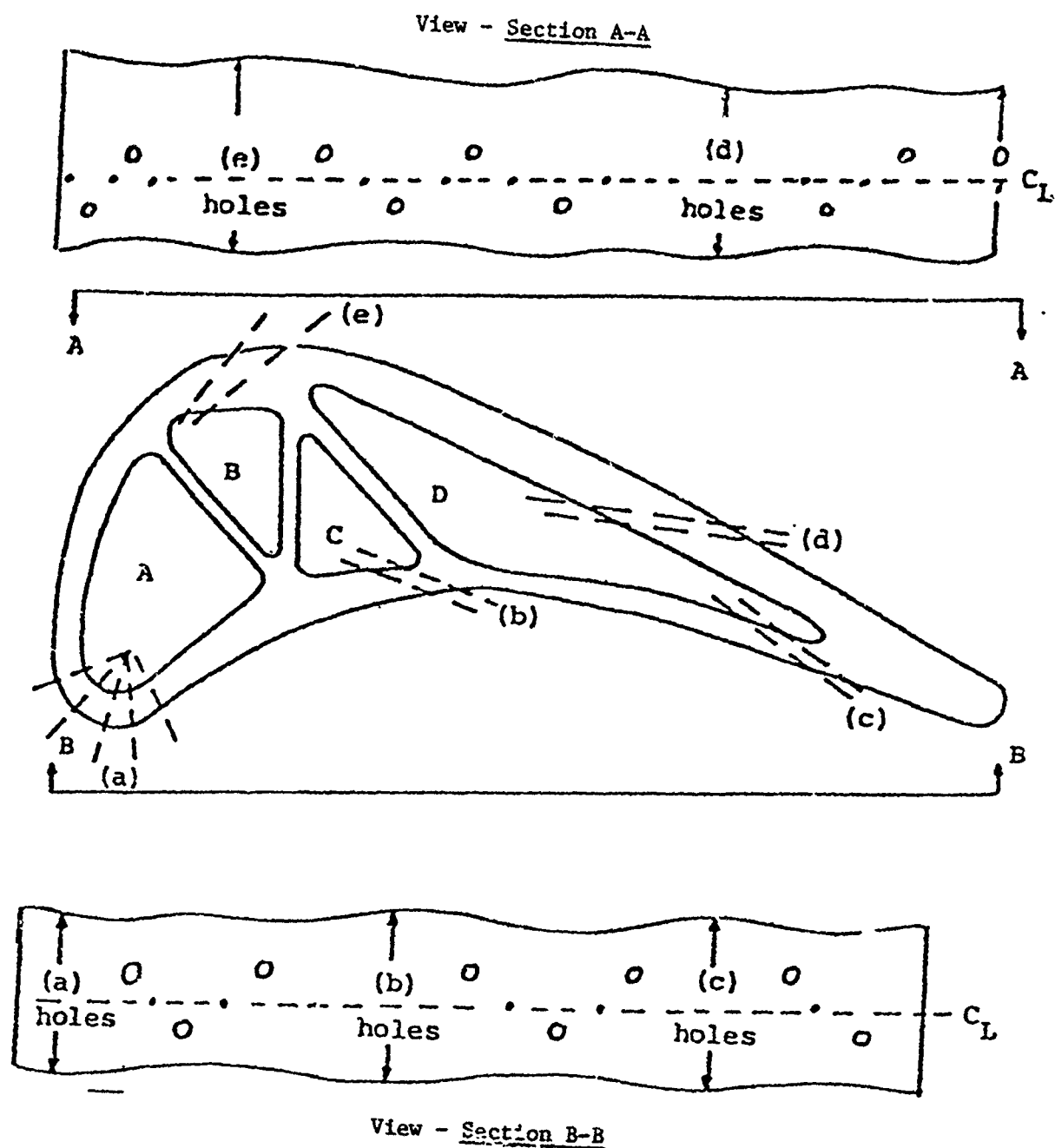
Figure 49. Dashed lines are hole center lines. All holes are
0.040" diameter. Angles of holes α, to surface tangent are:
(a) = 90°, (b) and (c) = 19°, (d) = 20°, (e) = 40°

o – represent heat transfer gauges
. – represent pressure taps

93
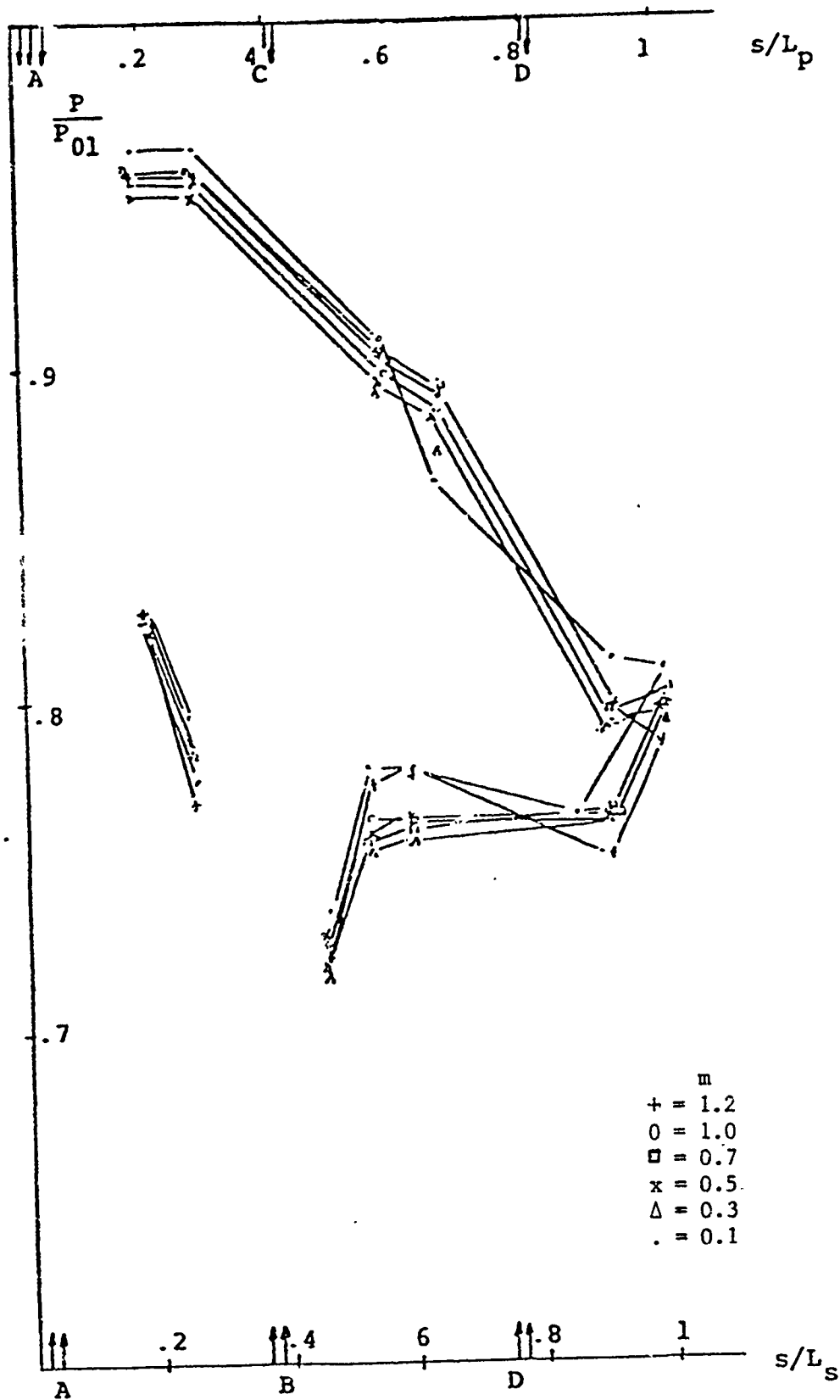
Figure 50. Full Injection – Pressure Distribution.
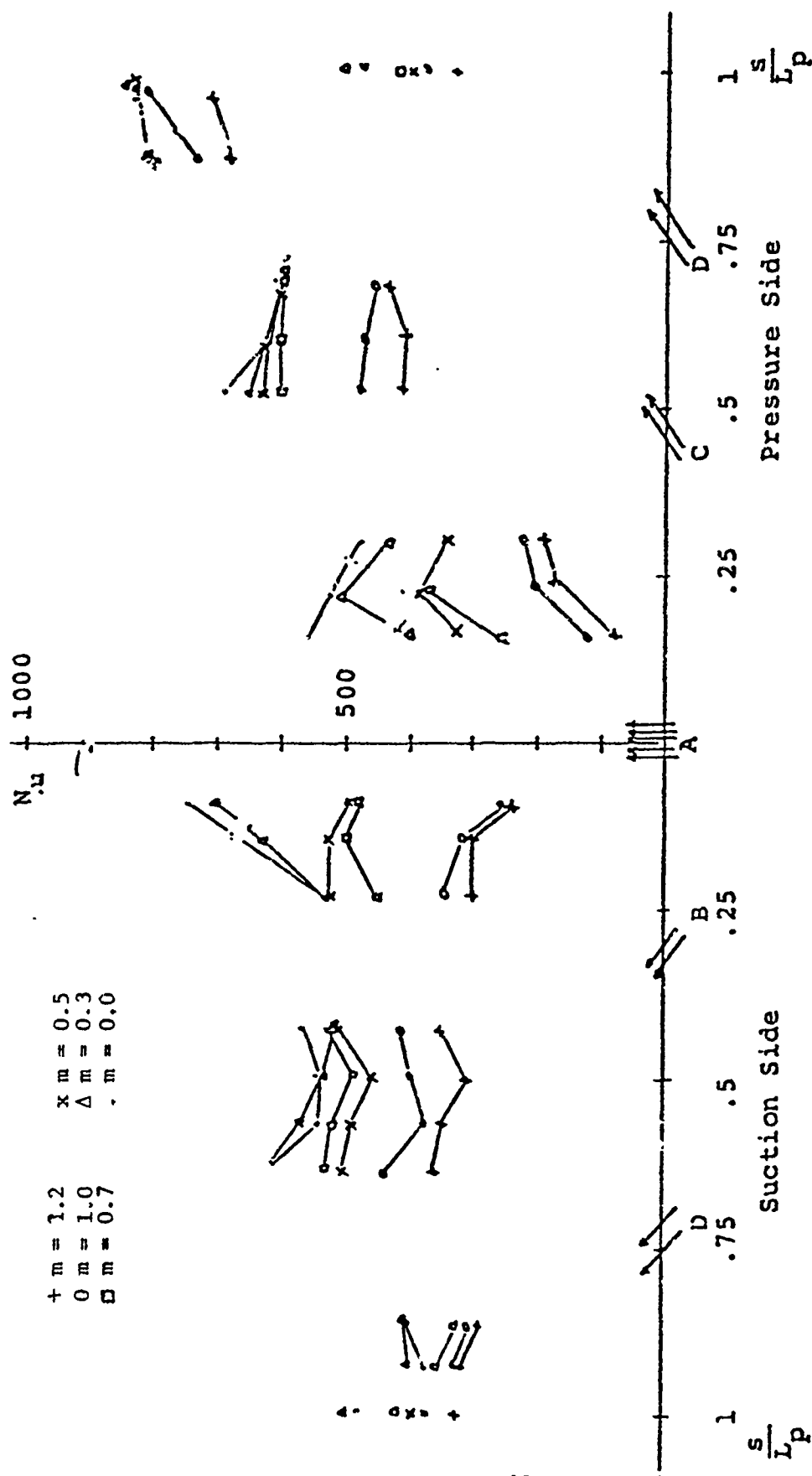
Figure 51. Leading Edge Injection - Heat Transfer.
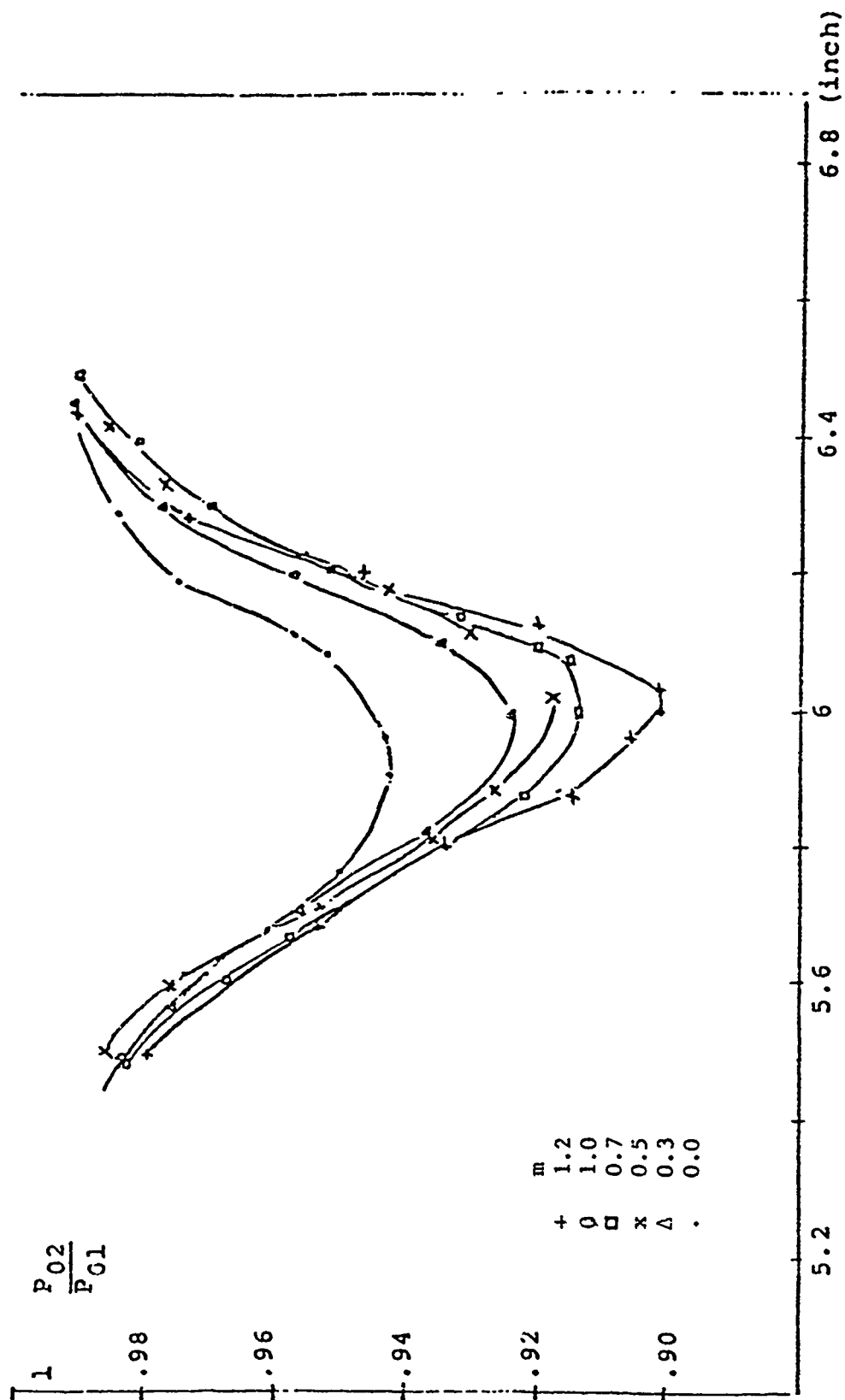
Figure 52. Suction Side Injection – Wake Profile.

96
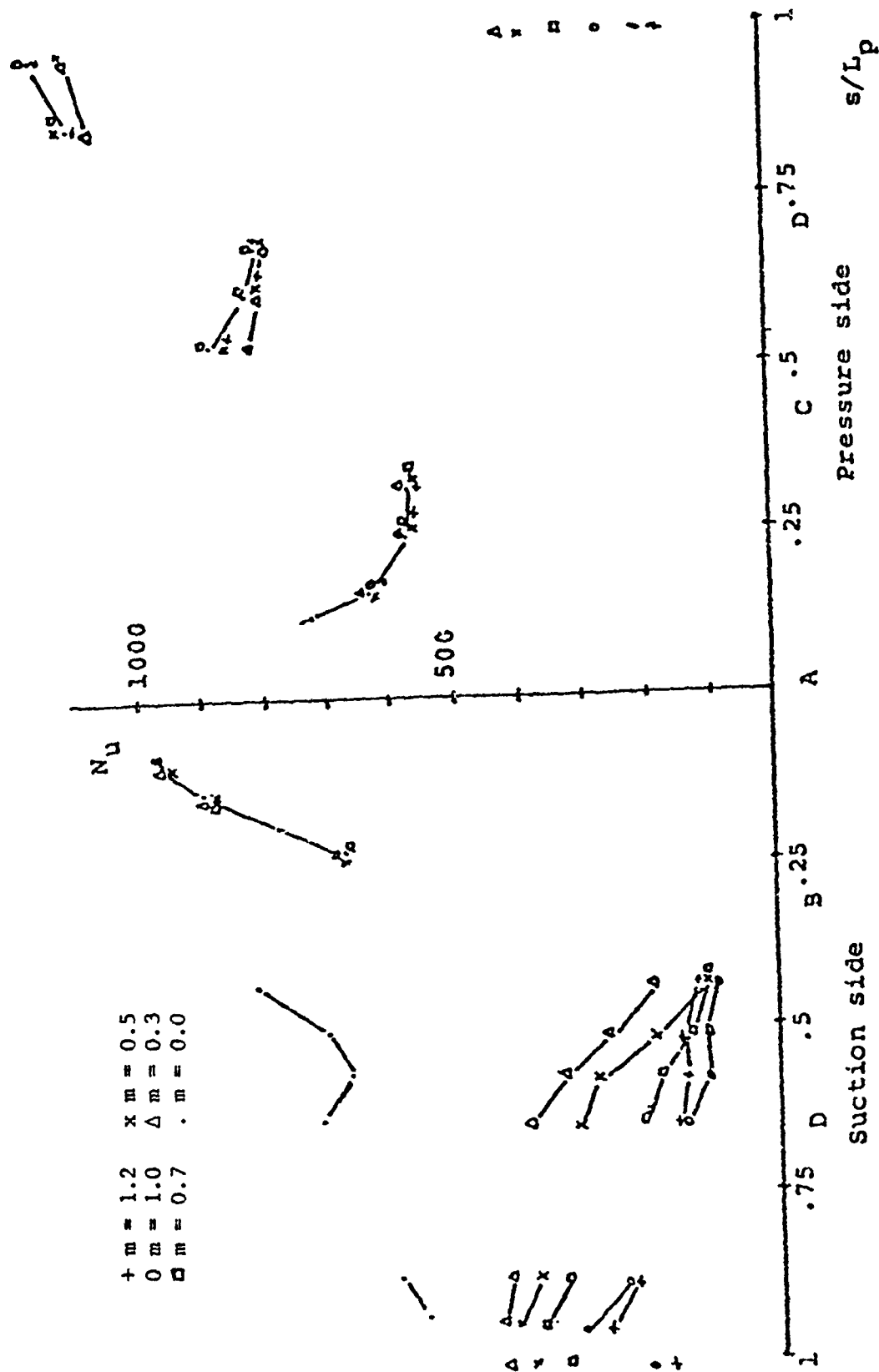
Figure 53. Suction Side Injection - Heat Transfer Distribution.

97
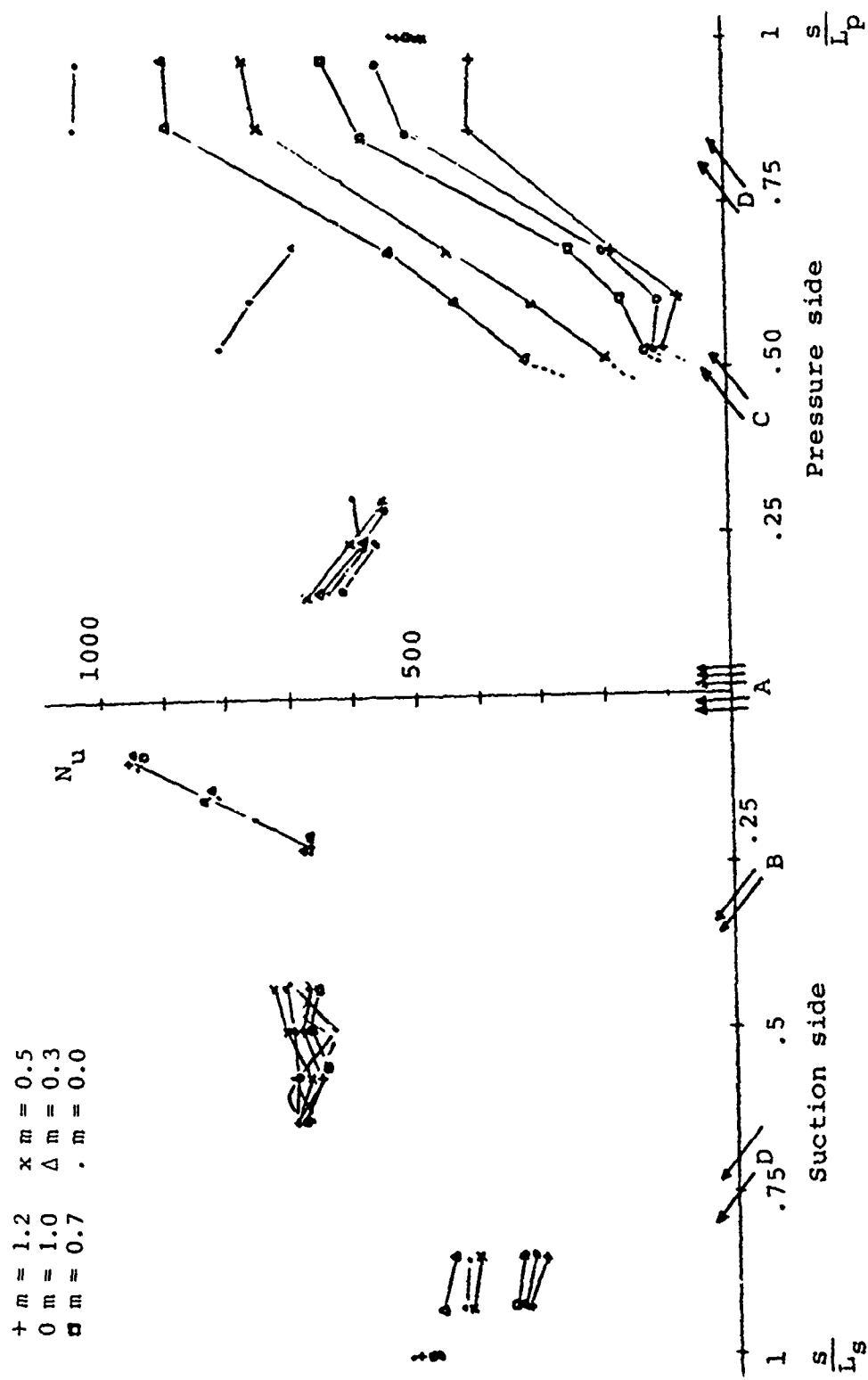
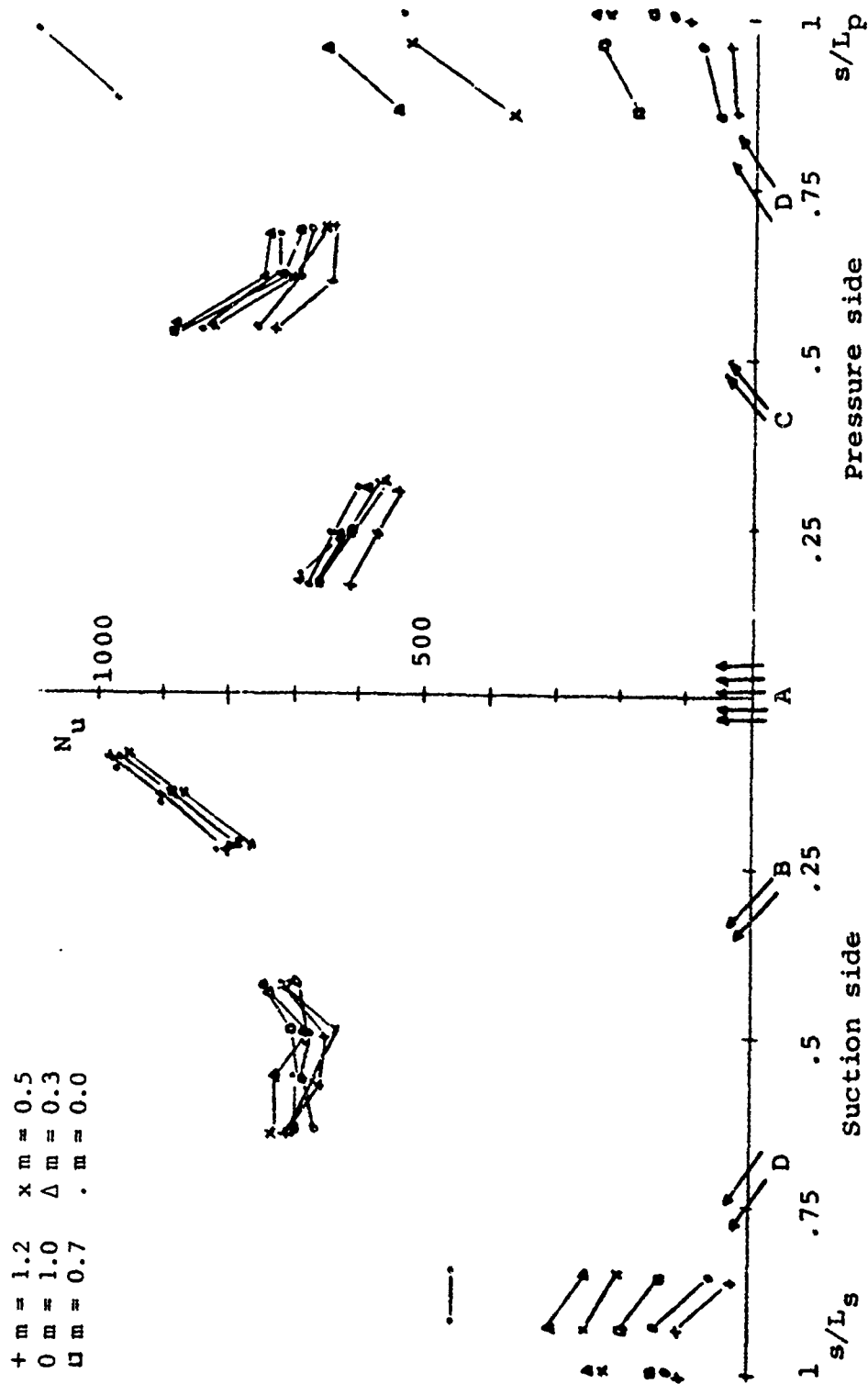Figure 54. Injection on Pressure Side - Heat Transfer Distribution.

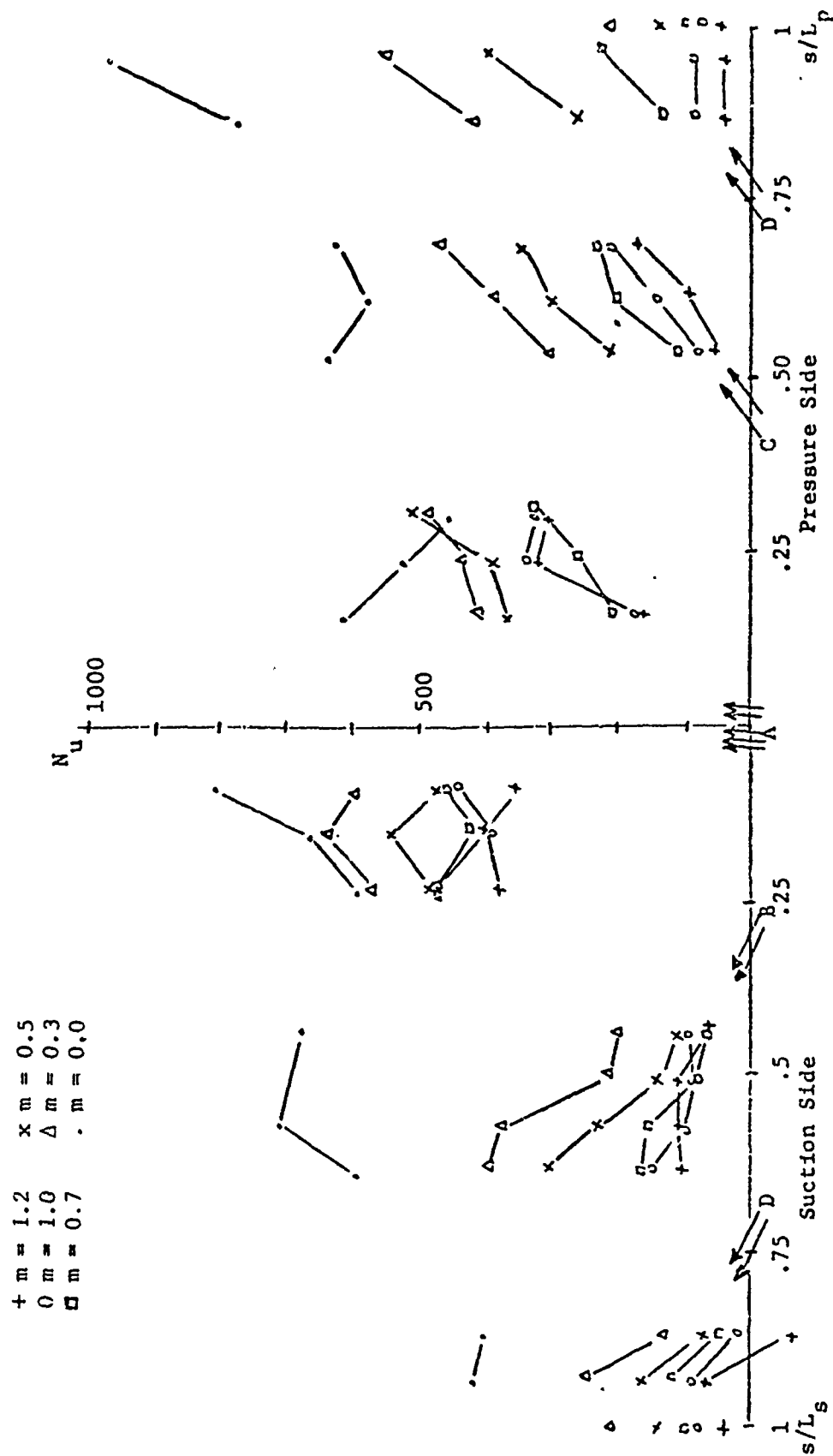Figure 55. Trailing Edge Injection - Heat Transfer Distribution.

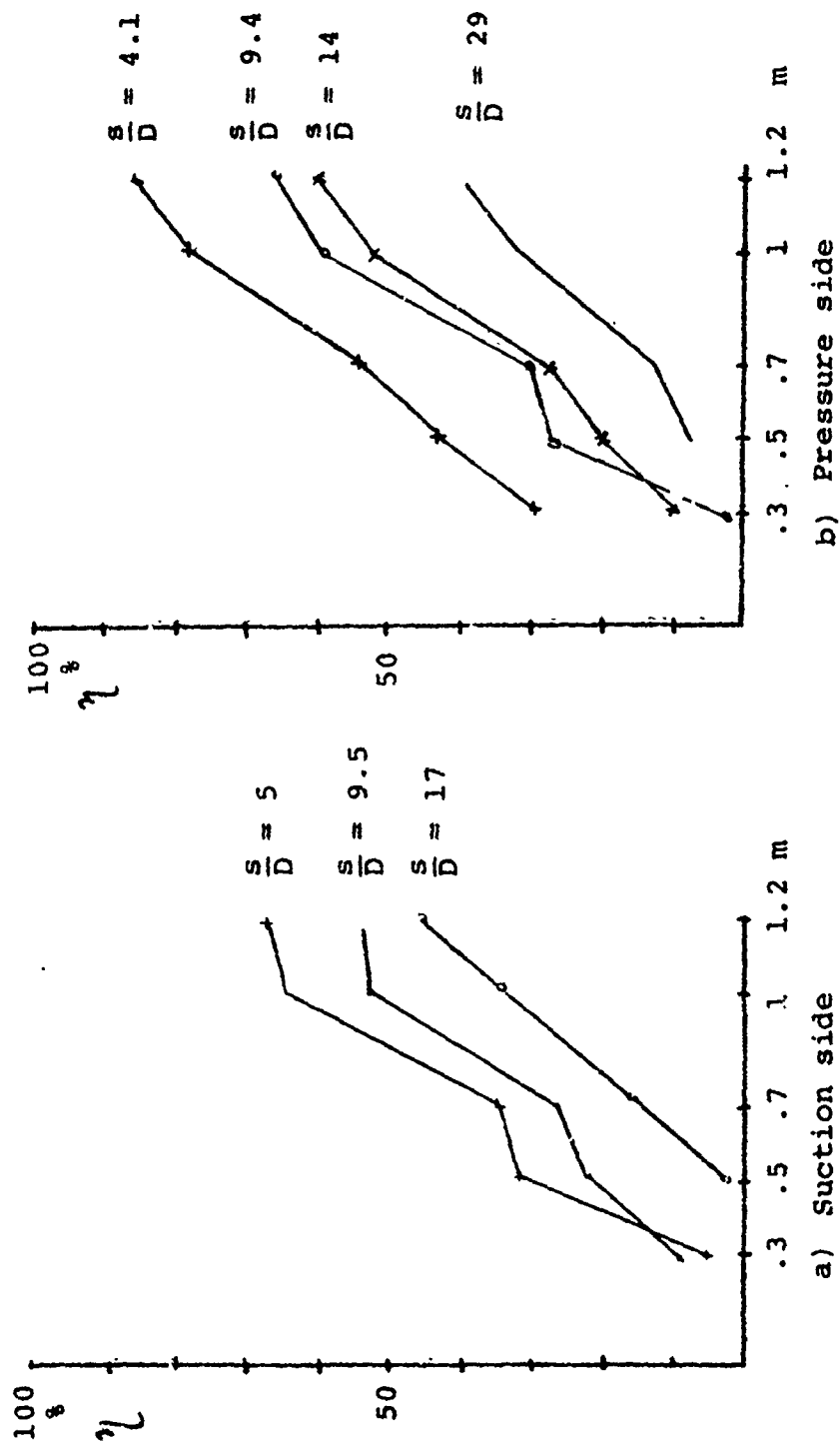Figure 56. Full Injection – Heat Transfer Distribution.

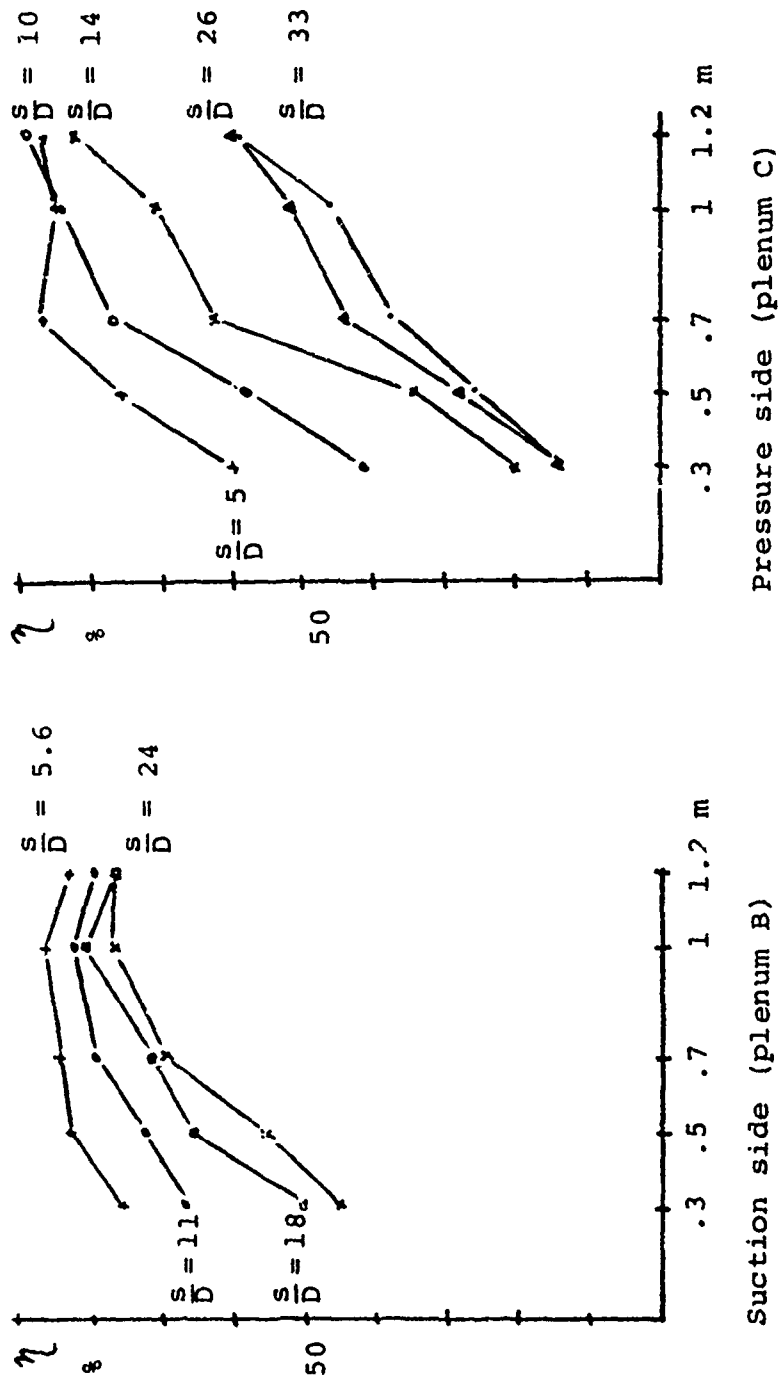Figure 57. Variation of η Versus m at Leading Edge.

101

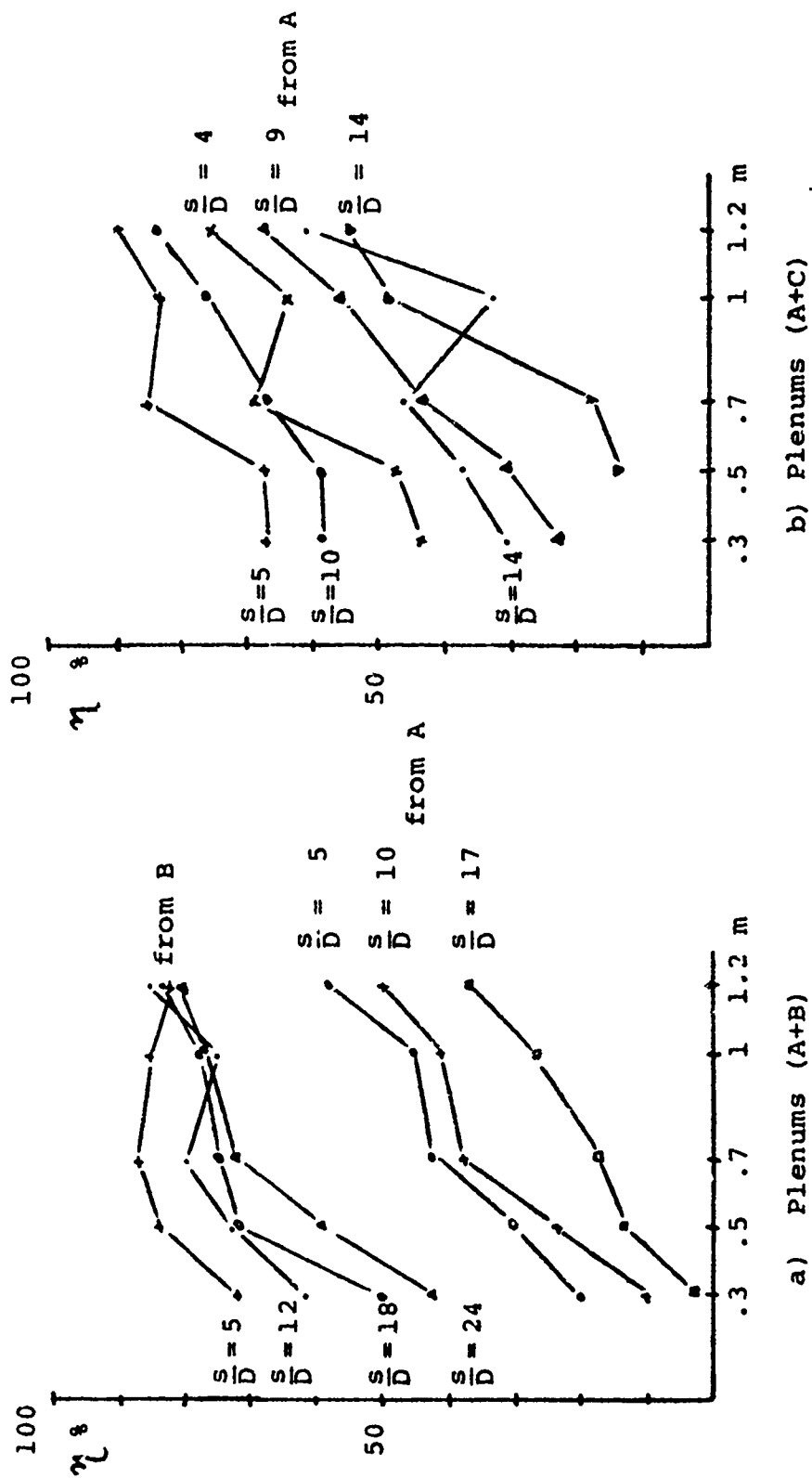Figure 58. Variation of η Versus m for Combined Injection.

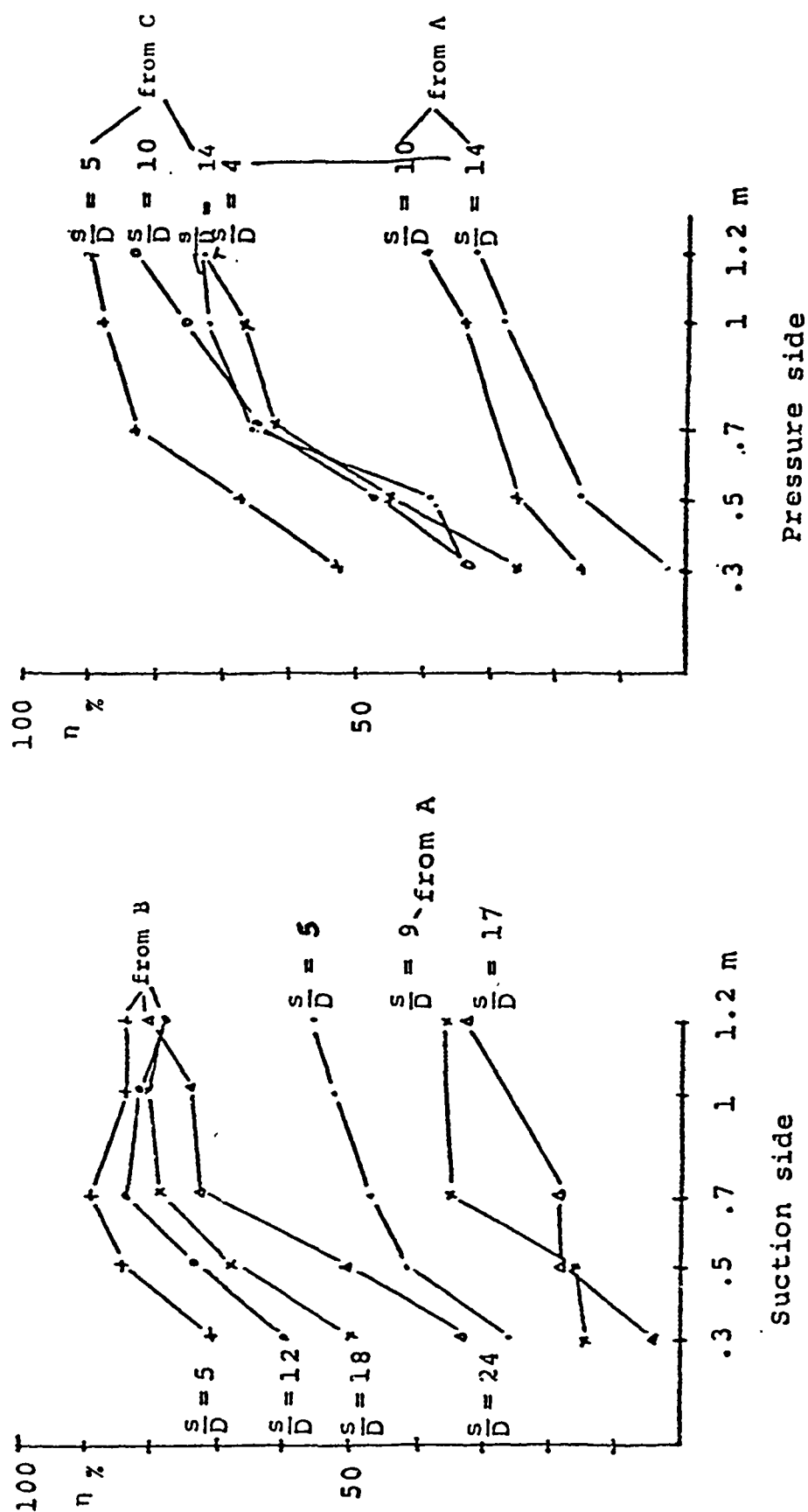Figure 59. Variation of η Versus m for Combined Injection.

103

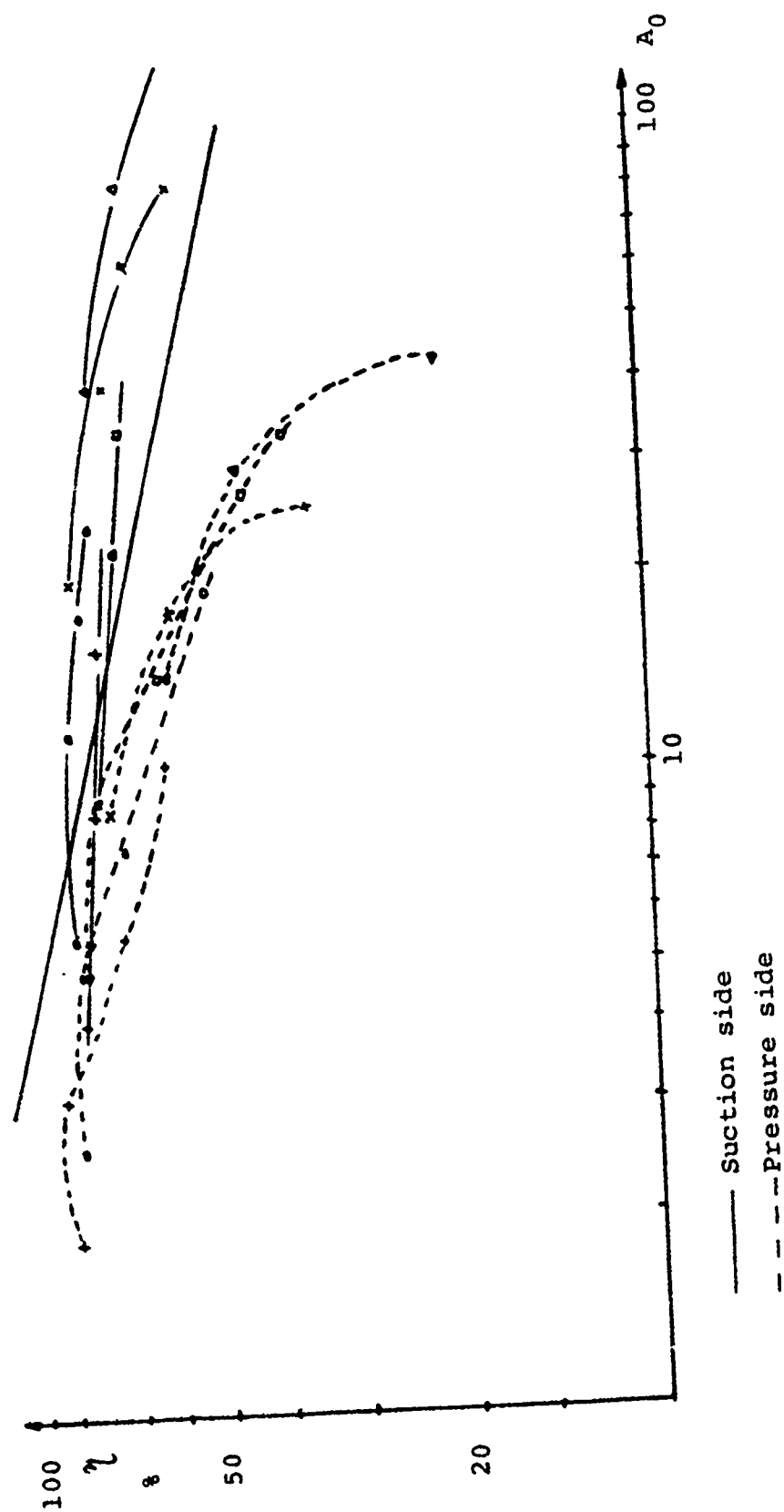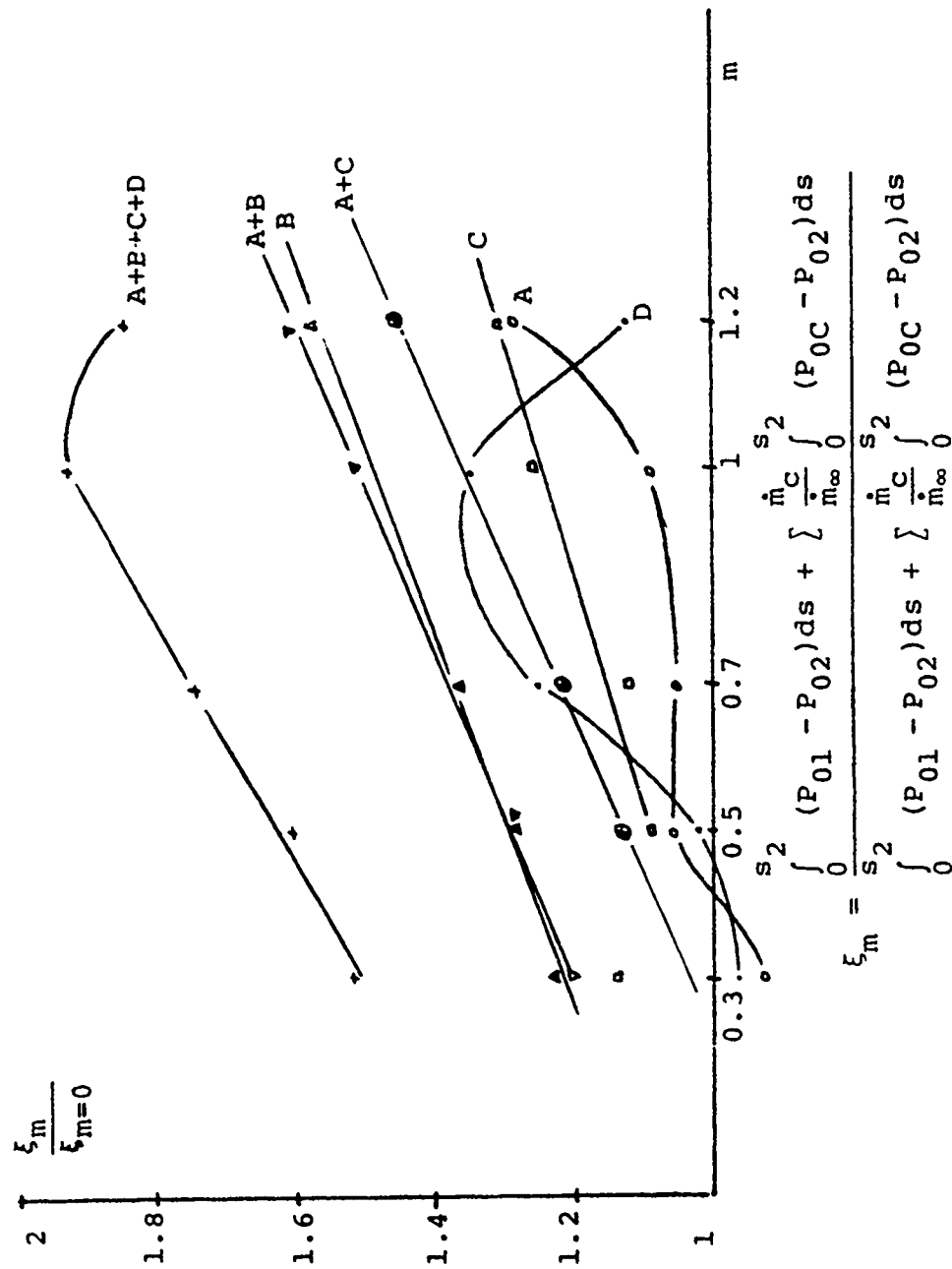Figure 60. Variation of η for Full Injection.

Figure 61. Correlation of η with A_0.

105

$$\xi_m = \dfrac{\displaystyle\int_0^{s_2}(P_{01}-P_{02})\,ds + \sum \dfrac{\dot{m}_C}{\dot{m}_\infty}\displaystyle\int_0^{s_2}(P_{0C}-P_{02})\,ds}{\displaystyle\int_0^{s_2}(P_{01}-P_{02})\,ds + \sum \dfrac{\dot{m}_C}{\dot{m}_\infty}\displaystyle\int_0^{s_2}(P_{0C}-P_{02})\,ds}$$

Figure 62.   Loss Coefficient Versus the Blowing Parameter.

$$\xi_m = \frac{\displaystyle\int_0^{s_2}(P_{01}-P_{02})\,ds + \sum \frac{\dot{m}_c}{\bar{m}_\infty}\displaystyle\int_0^{s_2}(P_{0C}-P_{02})\,ds}{\displaystyle\int_0^{s_2}(P_{01}-P_2)\,ds + \sum \frac{\dot{m}_c}{\dot{m}_\infty}\displaystyle\int_0^{s_2}(P_{0C}-P_2)\,ds}$$
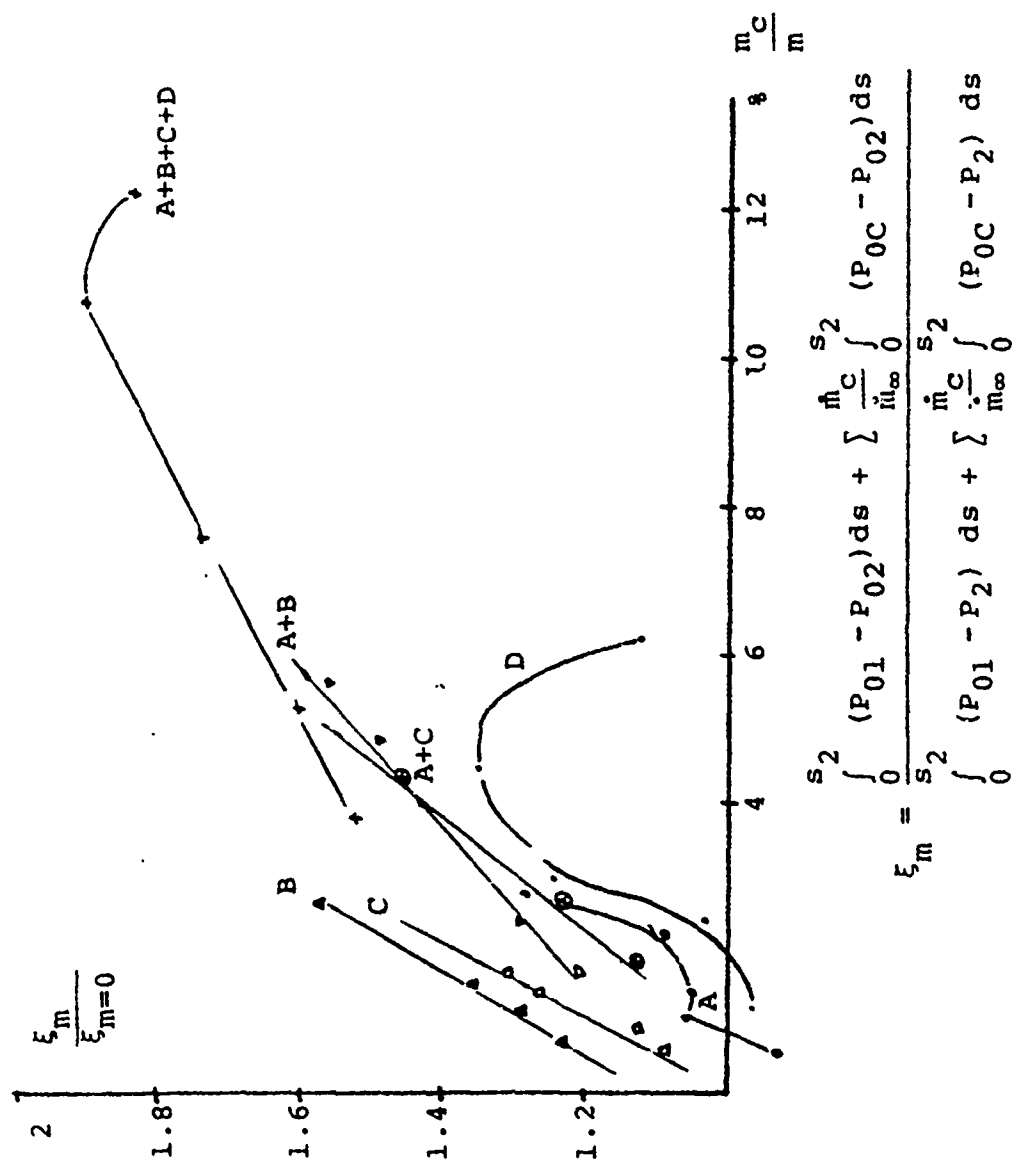
Figure 63. Loss Coefficient Versus Percentage of Injected Coolant.

107